Contents

1 Introduction **1**

2 Bayesian Estimation and Hypothesis Tests for a Circular GLM **3**

2.1 Introduction . . . 3
2.2 Bayesian circular GLM . . . 6
2.2.1 Likelihood . . . 7
2.2.2 Priors . . . 8
2.3 MCMC sampling . . . 10
2.3.1 Sampling β_0 . . . 10
2.3.2 Sampling κ . . . 10
2.3.3 Sampling $\boldsymbol{\beta}$ . . . 12
2.3.4 Sampling $\boldsymbol{\delta}$ . . . 12
2.4 Hypothesis tests . . . 12
2.4.1 Equality constrained hypotheses . . . 13
2.4.2 Inequality constrained hypotheses . . . 14
2.5 Simulation study . . . 15
2.5.1 Simple regression . . . 16
2.5.2 Factorial ANOVA . . . 17
2.5.3 ANCOVA with four covariates . . . 18
2.5.4 Bayes factors and posterior model probabilities . . . 19
2.6 Example . . . 19
2.6.1 ANOVA model . . . 21
2.6.2 ANCOVA model . . . 23
2.6.3 Inequality constrained hypothesis . . . 24
2.7 Discussion . . . 25
2.8 Acknowledgements . . . 26

A Bayesian Tests for Circular Uniformity **29**

A.1 Introduction . . . 29
A.2 Frequentist tests of circular uniformity . . . 30

A.3 A Bayesian test for circular uniformity with a von Mises alternative . . . 31
A.3.1 Choosing priors . . . 32
A.3.2 Priors based on the conjugate prior . . . 33
A.3.3 Jeffreys prior . . . 35
A.3.4 Simulation . . . 36
A.4 A Bayesian test for circular uniformity against a Kernel Density alternative . . . 38
A.4.1 Simulation . . . 39
A.5 Examples . . . 40
A.5.1 Homing pigeon example 1 . . . 41
A.5.2 Homing pigeon example 2 . . . 42
A.6 Discussion . . . 43
A.7 Acknowledgements . . . 45

B Mixtures of Peaked Power Batschelet Distributions for Circular Data With Application to Saccade Directions 47
B.1 Introduction . . . 47
B.2 Family of Batschelet Distributions . . . 50
B.2.1 Inverse Batschelet distribution . . . 50
B.2.2 Power Batschelet distribution . . . 53
B.2.3 Measures of circular dispersion . . . 55
B.3 Inference for Batschelet mixtures . . . 56
B.3.1 EM Algorithm . . . 56
B.3.2 Bayesian inference . . . 58
B.3.3 Model identifiability . . . 60
B.3.4 Model selection and hypothesis testing . . . 61
B.4 Illustration . . . 63
B.4.1 Synthetic data . . . 63
B.4.2 Free-viewing data . . . 65
B.5 Discussion . . . 68
B.6 Acknowledgements . . . 70

A Bayesian inference for mixtures of von Mises distributions using the reversible jump MCMC sampler 71
A.1 Introduction . . . 71
A.2 Von Mises Mixture Model . . . 74
A.2.1 Von Mises mixture density . . . 74
A.2.2 Likelihood . . . 75
A.2.3 Prior distributions . . . 75
A.3 Reversible jump MCMC for von Mises Mixtures . . . 76

A.3.1 Updating the weights w . . . 77
A.3.2 Updating component parameters μ and κ . . . 77
A.3.3 Updating the allocation z . . . 78
A.3.4 Dimensionality changing moves . . . 78
A.3.5 Label switching . . . 83
A.4 Simulation study . . . 83
A.4.1 Simulation scenarios . . . 83
A.4.2 Starting values . . . 84
A.4.3 Convergence . . . 84
A.4.4 Results . . . 84
A.5 Illustration . . . 86
A.5.1 Dataset . . . 86
A.5.2 Results . . . 87
A.6 Discussion . . . 88

B Dealing With Partially Observed Crime Times 97
B.1 Introduction . . . 97
B.2 Aoristic data . . . 99
B.3 Aoristic Fraction method . . . 102
B.4 Statistical models for aoristic data . . . 105
B.4.1 Circular data models . . . 105
B.4.2 Aoristic Likelihood . . . 106
B.4.3 Data augmentation . . . 108
B.5 Nonparametric models . . . 109
B.5.1 Dirichlet Process Mixture models . . . 110
B.6 Applications . . . 112
B.6.1 Ashby & Bowers data . . . 112
B.6.2 Montgomery Crime data . . . 114
B.6.3 Montly crime time trends . . . 115
B.7 Discussion . . . 116
B.8 Acknowledgements . . . 118

A Appendix 119
.1 Conditional distribution of β_0 . . . 119
.2 Properties of the Power Batschelet Distribution . . . 120
.3 Proof of variance overestimation using the aoristic fraction method . . . 121
.3.1 Data on the real line . . . 121
.3.2 Aoristic data . . . 124
.4 Von Mises based Dirichlet Process Mixture model . . . 127
.5 Rejection sampling aoristic data . . . 129

.6 Prior independent of μ_0 130

Chapter 1

Introduction

Chapter 2

Bayesian Estimation and Hypothesis Tests for a Circular GLM

2.1 Introduction

Circular data are measured in angles or directions, and are frequently encountered in scientific fields as diverse as life sciences (Mardia, 2011), behavioural biology (Bulbert et al., 2015), cognitive psychology (Kaas & Van Mier, 2006), bioinformatics (Mardia et al., 2008), political science (J. Gill & Hangartner, 2010) and environmental sciences (Lagona, 2016; Lagona et al., 2015; Arnold & SenGupta, 2006). In psychology, circular data occur often in motor behaviour research (Mechsner et al., 2001, 2007; Postma et al., 2008; Baayen et al., 2012), as well as in the application of circumplex models (Leary, 1957; Gurtman & Pincus, 2003; Gurtman, 2009). Circular data differ from linear data in the sense that circular data are measured in a periodical sample space. For example, an angle of 1° is quite close to an angle 359°, although linear intuition suggests otherwise.

Therefore, linear models may not properly describe the process that has generated the circular data of interest. Circular data analysis has been developed to deal with this, although attention to this type of analysis has been limited. Only slightly more than a handful of in-depth books on circular data analysis have been published (Fisher, 1995; Mardia & Jupp, 1999; Pewsey et al., 2013; Jammalamadaka & Sengupta, 2001), and in general, statistical methods for circular data are somewhat limited.

Here, attention is turned to analysis of datasets with a circular outcome, predicted by covariates that can be continuous (linear) or categorical. This

leads to a structure similar to the Generalized Linear Model (GLM), which has both multiple regression and ANCOVA as special cases.

Three main approaches to circular data analysis might be distinguished. First, the intrinsic approach employs distributions directly defined on the circle (Fisher & Lee, 1992; Artes, 2008). Second, the wrapping approach 'wraps' a univariate distribution around the circle by taking the modulus of data on the real line (Ferrari, 2009; Coles, 1998). Third, the embedding approach projects points from a bivariate distribution to the circle (Nuñez-Antonio et al., 2011; Nuñez-Antonio & Gutiérrez-Peña, 2014; Wang & Gelfand, 2014; **?**; Maruotti, 2016). While the wrapping and embedding approach provide promising avenues of study in their own right, here attention is restricted to the intrinsic approach, as it might provide the most natural analysis of circular data.

Within the intrinsic approach, the circular analogue to the Normal distribution is the von Mises distribution (Von Mises, 1918). This symmetric unimodal distribution is given by

$$\mathcal{M}(\theta \mid \mu, \kappa) = [2\pi I_0(\kappa)]^{-1} \exp\left(\kappa \cos\left[\theta - \mu\right]\right), \tag{2.1}$$

where $\theta \in (-\pi, \pi)$ represents an angular measurement, $\mu \in (-\pi, \pi)$ represents the mean direction, $\kappa \in \mathbb{R}^+$ is a concentration parameter, and $I_0(\cdot)$ represents the modified Bessel function of the first kind and order zero. Some examples of frequentist methods that employ the von Mises distribution are a circular ANOVA (Watson & Williams, 1956), circular ANCOVA (Artes, 2008) and circular regression (Fisher & Lee, 1992). Here, a Bayesian analysis of such models will be developed.

Early approaches to Markov chain Monte Carlo (MCMC) sampling for the von Mises distribution provide a method for sampling μ when κ is known (Mardia & El-Atoum, 1976) and sampling both parameters for a single group of data (Damien & Walker, 1999). Guttorp & Lockhart (1988) present a conjugate prior for the von Mises model. Recent theoretical work has much improved the efficiency of the sampling of the concentration parameter of the von Mises distribution (Forbes & Mardia, 2015).

Some development has also taken place in the field of semiparametric inference for circular data models, often using Dirichlet process priors (Bhattacharya & Sengupta, 2009; Ghosh et al., 2003; George & Ghosh, 2006; McVinish & Mengersen, 2008). In particular, Ghosh et al. (2003) provide Bayes factors for the simple hypothesis test of equality of two means. However, these methods are generally complex, which makes it hard to extend these models, for example to include covariates. Therefore, we will focus on parametric models, with residuals following the von Mises distribution.

A Bayesian circular regression analysis has been developed by J. Gill & Hangartner (2010), using starting values from a frequentist iterative reweighted least squares (IRLS) algorithm, which is similar to that used by Fisher & Lee (1992). J. Gill & Hangartner (2010) note that the likelihood function of the regression coefficients from their model is not globally logarithmically concave, which might cause the algorithm to converge to a local maximum. To combat this, J. Gill & Hangartner (2010) advise careful inspection of the likelihood surface of the regression coefficients. Drawbacks of the approach taken by J. Gill & Hangartner (2010) are that a prior is not specified, the algorithm is slow, categorical predictors are not treated separately and for larger models it may be unclear whether the regression coefficients have converged to the global maximum.

Recent work has provided a multivariate extension of the von Mises distribution (Mardia et al., 2008; Mardia & Voss, 2014), which offers a promising new way of thinking about circular covariate models. The multivariate von Mises was applied in this context by Lagona (2016) within a Generalized Linear Model (GLM) setting, applying MCMC likelihood approximation as in Geyer & Thompson (1992) to compute maximum likelihood estimates. This approach is not Bayesian, but it is a promising approach because of its flexibility, allowing both the mean and concentration to be dependent on an arbitrary set of covariates, as well as allowing observations to be dependent.

There are three main drawbacks of the circular GLM approach to circular data analysis currently. First, the GLM approach is not free from the lack of concavity as described in J. Gill & Hangartner (2010), although this has not yet been investigated in detail. Second, the current approach does not have separate parameters for differences in group mean direction, which precludes the popular ANCOVA model to some extent. Third, Bayesian hypothesis tests for this model are not available, which limits its applicability.

The structure of this paper is as follows. The circular data GLM model is developed in a fully Bayesian setting in Section 2.2. The lack of concavity in the likelihood function will be examined, and suggestions will be formulated on how to deal with this issue. Details on the MCMC sampler are provided in Section 2.3. Section 2.4 outlines Bayesian hypothesis tests for this model, both for equality and inequality constrained hypotheses. Then, a simulation study for the method is provided in Section 2.5. Section 2.6 provides an application of our method to empirical data from cognitive psychology. Finally, Section B.7 provides a short discussion.

2.2 Bayesian circular GLM

Consider a dataset $\{\theta_i, \boldsymbol{x}_i, \boldsymbol{d}_i\}, (i = 1, \ldots, n)$, where θ_i is a circular outcome variable, $\boldsymbol{x}_i \in \mathbb{R}^K$ is a column vector of continuous linear covariates which are assumed to be standardized, and $\boldsymbol{d}_i \in \{0, 1\}^J$ is a column vector of dichotomous variables indicating group membership. Assume that each observed angle θ_i is generated independently from a von Mises distribution $\mathcal{M}(\theta_i \mid \mu_i, \kappa)$. Then, μ_i is chosen to be

$$\mu_i = \beta_0 + \boldsymbol{\delta}^T \boldsymbol{d}_i + g(\boldsymbol{\beta}^T \boldsymbol{x}_i), \tag{2.2}$$

where $\beta_0 \in [-\pi, \pi)$ is an offset parameter which serves as a circular intercept, $\boldsymbol{\delta} \in [-\pi, \pi)^J$ is a column vector of circular group difference parameters, $g(\cdot) : \mathbb{R} \to (-\pi, \pi)$ is a twice differentiable link function, and $\boldsymbol{\beta} \in \mathbb{R}^K$ is a column vector of regression coefficients. Jammalamadaka & Sengupta (2001) and Fisher & Lee (1992) discuss the choice of the link function. A common and natural choice for the link function is $g(x) = 2\tan^{-1}(x)$, which we will focus on here.

This model specification differs from the usual approach to circular regression models, as these generally set $\mu_i = \beta_0 + g(\boldsymbol{\beta}^T \boldsymbol{x}_i)$ (Fisher & Lee, 1992; J. Gill & Hangartner, 2010; Lagona, 2016). However, we view this model as unsatisfactory when including dichotomous predictors in $\boldsymbol{x}$, which we will illustrate in Figure 2.1. Consider a single dichotomous predictor d added to a model with a single continuous predictor x. The dichotomous predictor might be added into the model as $\mu = \beta_0 + g(\beta x + \delta d)$. Adding δ in the link function shifts the location of the prediction line, but also its shape. Therefore, the shape for $d = 0$ is fixed, but for $d = 1$ the shape is dependent on a free parameter, δ. This makes the shape of the prediction line (and therefore the analysis) depend on the arbitrary choice of reference group, which can be seen in Figure 2.1a. To solve this, we advocate setting $\mu = \beta_0 + \delta d + g(\beta x)$, the resulting prediction lines of which are shown in Figure 2.1b.

A comparable approach is taken in Artes (2008), where a separate intercept is estimated for each group. However, having a separate intercept for each group means that a factorial design with main effects only can not be specified. In many applications, especially in psychology, this is problematic. The approach here is more flexible in that it allows a researcher to either fit a model with main effects only, to fit a model with specific interactions, or to compare these models. In addition, Artes (2008) also describes a non-parallel case where the regression parameters are estimated separately for each group. This model can be obtained as a special case of the model provided here by including appropriate interaction terms in the model.

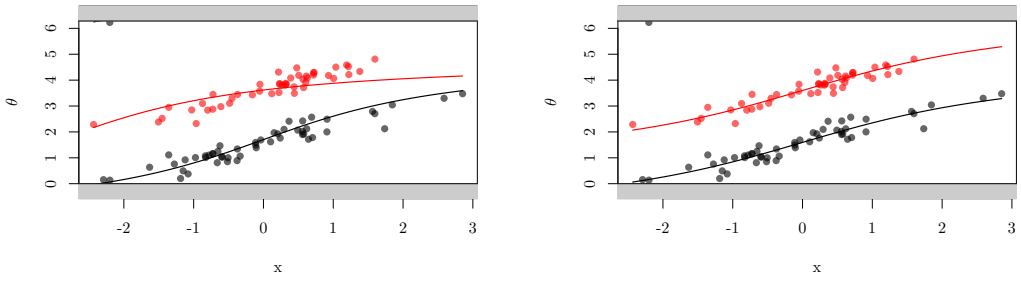

(a) $\mu_i = \beta_0 + g(\beta x_i + \delta d_i)$ (b) $\mu_i = \beta_0 + \delta d_i + g(\beta x_i)$

Figure 2.1: Prediction lines from two different models, which were fitted to a dataset with $n = 100$, and true parameters $\delta = 2, \beta_0 = \pi/2, \beta = 0.4, \kappa = 20$. The two models have (a) dichotomous predictors placed in the link function, and (b) dichotomous predictors treated separately.

2.2.1 Likelihood

Denote the set of parameters by $\boldsymbol{\phi} = \{\beta_0, \kappa, \boldsymbol{\delta}, \boldsymbol{\beta}\}$. The joint likelihood for the GLM-type model is then given by

$$f(\boldsymbol{\theta}, \boldsymbol{X}, \boldsymbol{d} \mid \boldsymbol{\phi}) = \prod_{i=1}^{n} \mathcal{M}(\theta_i \mid \mu_i, \kappa) \tag{2.3}$$

$$= \{2\pi I_0(\kappa)\}^{-n} \exp\left\{\kappa \sum_{i=1}^{n} \cos\left[\theta_i - \left(\beta_0 + \boldsymbol{\delta}^T \boldsymbol{d}_i + g(\boldsymbol{\beta}^T \boldsymbol{x}_i)\right)\right]\right\}. \tag{2.4}$$

If we let $\psi_i = \theta_i - \boldsymbol{\delta}^T \boldsymbol{d}_i - g(\boldsymbol{\beta}^T \boldsymbol{x}_i)$, $(i = 1, \ldots, n)$, then we can recognize the conditional likelihood $f(\beta_0, \kappa \mid \boldsymbol{\delta}, \boldsymbol{\beta}, \boldsymbol{\theta}, \boldsymbol{X}, \boldsymbol{d})$ as the likelihood of the parameters of a von Mises distribution with mean direction β_0 and concentration κ, as shown in Appendix .1.

The conditional distribution of β_0 is $\mathcal{M}(\bar{\psi}, R_\psi \kappa)$, where $\bar{\psi}$ and R_ψ are the mean direction and resultant length of the vector $\boldsymbol{\psi}$, given by

$$\bar{\psi} = \operatorname{atan2}\left(\sum_{i=1}^{n} \sin\psi_i, \sum_{i=1}^{n} \cos\psi_i\right), \quad R_\psi = \sqrt{\left(\sum_{i=1}^{n} \cos\psi_i\right)^2 + \left(\sum_{i=1}^{n} \sin\psi_i\right)^2}.$$

Conditionals for κ, $\boldsymbol{\beta}$ and $\boldsymbol{\delta}$ are not of simple form and require special attention.

2.2.2 Priors

The next step in the model specification is setting prior distributions for the parameters $\boldsymbol{\phi}$. We will focus on uninformative, default priors where possible. The joint prior is factored as

$$p(\boldsymbol{\phi}) \propto p(\beta_0, \kappa \mid \boldsymbol{\delta}, \boldsymbol{\beta}) p(\boldsymbol{\delta}) p(\boldsymbol{\beta}) \tag{2.5}$$

so that $\boldsymbol{\beta}$ and $\boldsymbol{\delta}$ are independent. Furthermore,

$$p(\boldsymbol{\delta}) \propto \prod_{j=1}^{J} p(\delta_j), \quad p(\boldsymbol{\beta}) \propto \prod_{k=1}^{K} p(\beta_k). \tag{2.6}$$

Next, the choice of each of these priors is discussed.

$p(\delta_j)$

For each δ_j, the circular uniform distribution is a natural and uninformative default prior, so that

$$p(\delta_j) = \frac{1}{2\pi}, \ \forall j = 1, \ldots, J. \tag{2.7}$$

This prior indicates that given a mean direction for some reference group, there is no knowledge on the mean direction of group j.

$p(\beta)$

For each β_k there is no natural uninformative prior. A constant prior $p(\beta_k) \propto 1$ could be employed. However, as noted by Fisher (1995) and J. Gill & Hangartner (2010), this leads to a posterior of irregular form, including local maxima and non-zero asymptotes, as shown in Figure 2.2a.

However, because the linear predictors are standardized, the interpretation of the size of β is equal across studies. Therefore, we can determine a priori which values of β_k would be probable in practical research scenarios. In this case, if $\sum_{k=1}^{K} |\beta_k| > 1.5$, the majority of the probability mass of the data is on the semi-circle opposite of the group intercept ($\beta_0 + \boldsymbol{\delta}^T \boldsymbol{d}$), which is not likely in practice. This expectation can be translated to a weakly informative prior distribution. Here, this was done by setting the prior as

$$\beta_k \sim N(0, \sigma^2), \ \forall k = 1, \ldots, K, \tag{2.8}$$

where $N(\mu, \sigma^2)$ denotes the Normal distribution with mean μ and variance σ^2. For a Normal prior with any finite σ^2, there are no non-zero asymptotes

in the conditional posterior of β for any values of $\beta_0, \kappa, \boldsymbol{\delta}$, because $\log f_N(x \mid 0, \sigma^2) \to -\infty$ as $|x| \to \infty$. As $\sigma^2 \to 0$, the prior becomes more informative and the posterior for β_k centers on 0. As $\sigma^2 \to \infty$, the prior becomes less informative, but the posterior becomes more irregular, with large plateaus and more local maxima. By default, we choose $\sigma^2 = 1$ so that the prior is the standard Normal distribution, which represents the weakly informative prior mentioned previously, for which values of $|\beta_k| > 1.5$ are a priori unlikely.

To illustrate this, the resulting posterior is compared to the posterior resulting from the constant prior in Figure 2.2. The posterior is based on a synthetic data set of 7 observations with a single predictor $\boldsymbol{x} = -3, \ldots, 3$, which is standardized and the outcome is then computed as $\theta_i = 2\tan^{-1}(x_i) + \varepsilon_i$ where $\varepsilon_i \sim N(0, 1/10)$, so the true β is 1. In Figure 2.2, the conditional posterior of β is displayed given $\beta_0 = 0, \kappa = 1$. Figure 2.2a gives a zoomed-out view of the posterior resulting from the constant prior, where the asymptotes are clearly visible. Figure 2.2b shows a zoomed-in view of the resulting conditional posterior from a prior with $\sigma^2 = 1/5$ (dashed), $\sigma^2 = 1$ (dashed), $\sigma^2 = 5$ (dotted). It can be seen that the $N(0, 5)$ prior takes a shape not unlike the one seen in Figure 2.2a, although the asymptote is avoided. The $N(0, 1/5)$ prior can be seen to have a strong influence on the posterior estimate for this data where the true $\beta = 1$. The $N(0, 1)$ prior represents a balance for which the asymptotes are solved, but the posterior estimates are very close to the maximum likelihood estimates. In practical settings generally $|\beta| << 1$, so that the influence of the prior will often be minimal. For these priors the posterior is not necessarily logarithmically concave, which might make optimization difficult, but which MCMC methods handle well.

$p(\beta_0, \kappa)$

For the von Mises part of the model we follow the conjugate prior provided by Guttorp & Lockhart (1988), given by

$$p(\beta_0, \kappa \mid \boldsymbol{\delta}, \boldsymbol{\beta}) \propto I_0(\kappa)^{-c} \exp\left[R_0 \kappa \cos(\beta_0 - \mu_0)\right]. \tag{2.9}$$

The prior hyperparameters $\{c, R_0, \mu_0\}$ can be interpreted as the prior sample size c, prior resultant length R_0 and prior mean direction μ_0 respectively of a hypothetical set of angles $\psi = \theta - \boldsymbol{\delta}^T \boldsymbol{d} - g\left(\boldsymbol{\beta}^T \boldsymbol{x}\right)$. Setting informative prior expectations for the parameters of the distribution of a random angle ψ might be difficult, because conditioning on $\boldsymbol{\beta}$ and $\boldsymbol{\delta}$ makes ψ hard to interpret. However, an uninformative prior is easily obtained by setting $c = 0, R_0 = 0$, which is the approach taken here. Note that this does induce an improper (constant) prior on κ.

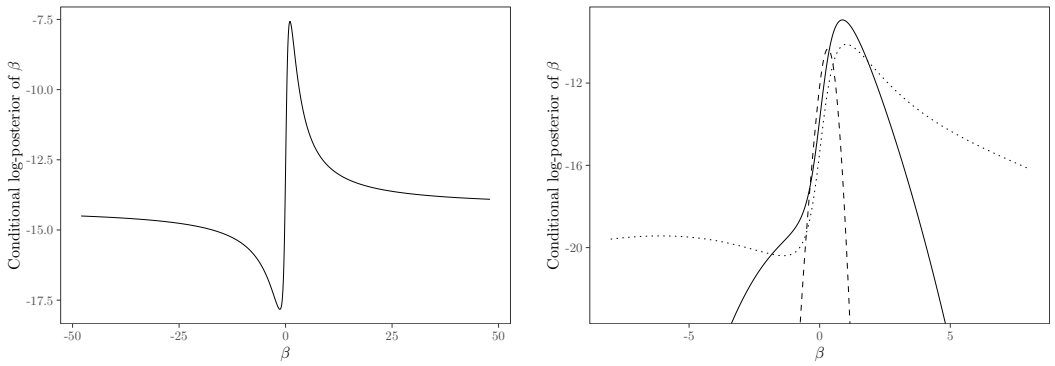

(a) $p(\beta_k) \propto 1$

(b) $p(\beta_k) \propto N(0,\ 1/5)$ (dashed)
$p(\beta_k) \propto N(0,\ 1)$ (solid)
$p(\beta_k) \propto N(0,\ 5)$ (dotted)

Figure 2.2: Comparison of the conditional log-posterior of β_k when using (a) a constant prior, which means the log-posterior is equal to the log-likelihood, and (b) a Normal prior with three different values for σ^2.

2.3 MCMC sampling

In this section, details will be discussed for the MCMC sampling procedure, given below as Algorithm 1. Usually, the algorithm converges fast and mixes rapidly, at least for smaller models. The following sections provide further details on sampling $\beta_0, \kappa, \boldsymbol{\beta}$ and $\boldsymbol{\delta}$.

2.3.1 Sampling β_0

Using the likelihood discussed in Section 2.2.1 and the uninformative prior from Section 2.2.2, it can be seen that the conditional posterior distribution of β_0 is $\mathcal{M}(\bar{\psi}, R_\psi \kappa)$. To draw from this distribution, a new vector $\boldsymbol{\psi}$ is computed in each iteration, using the current values of $\{\boldsymbol{\beta}, \boldsymbol{\delta}\}$. Then, the corresponding values of $\bar{\psi}$, and R_ψ are computed. In this case, a Gibbs step can be applied, because it is straightforward to sample from the von Mises distribution, for example as in Best & Fisher (1979).

2.3.2 Sampling κ

Sampling κ is performed by employing a fast rejection sampler described by Forbes & Mardia (2015). This algorithm takes inputs $\{m, \zeta\}$ and returns a new value from the conditional distribution of κ. Here, with an uninformative

Algorithm 1 MCMC algorithm for circular GLM

Set $\boldsymbol{\phi}^{(1)} \leftarrow \{\beta_0^{(1)}, \kappa^{(1)}, \boldsymbol{\beta}^{(1)}, \boldsymbol{\delta}^{(1)}\}$, which are the given starting values.
for q $= 2, \ldots,$ Q **do**
  $\psi_i \leftarrow \theta_i - \boldsymbol{\delta}^T \boldsymbol{d}_i - g(\boldsymbol{\beta}^T \boldsymbol{x}_i),\ \forall\ i = 1, \ldots, n.$
  $R_\psi \leftarrow \sqrt{\left(\sum_{i=1}^n \cos\psi_i\right)^2 + \left(\sum_{i=1}^n \sin\psi_i\right)^2}.$
  $\bar{\psi} \leftarrow \text{atan2}\left[\sum_{i=1}^n \sin\psi_i, \sum_{i=1}^n \cos\psi_i\right].$
  Sample $\beta_0 \sim \mathcal{M}\left(\bar{\psi}, R_\psi \kappa\right).$
  $\zeta \leftarrow -n^{-1} R_\psi \cos\left(\beta_0 - \bar{\psi}\right).$
  Sample κ with `sampleKappa`(n, ζ) as in Forbes & Mardia (2015).
  for $j = 1, \ldots, J$ **do**
    Sample a candidate $\delta_j^* \sim \mathcal{M}\left(\delta_j, R_\psi \kappa\right).$
    $\alpha_{\delta_j} \leftarrow \log p\left(\delta_j^*, \boldsymbol{\phi}_{(-\delta_j)} \,\middle|\, \boldsymbol{\theta}, \boldsymbol{X}, \boldsymbol{d}\right) - \log p\left(\delta_j, \boldsymbol{\phi}_{(-\delta_j)} \,\middle|\, \boldsymbol{\theta}, \boldsymbol{X}, \boldsymbol{d}\right).$
    Sample $u_1 \sim U[0, 1].$
    if $\alpha_{\delta_j} > \log u_1$ **then**
      $\delta_j \leftarrow \delta_j^*$
    end if
  end for
  for $k = 1, \ldots K$ **do**
    Sample $u_2 \sim U[-w, w]$ and $u_3 \sim U[0, 1].$
    $\beta_k^* \leftarrow \left(\beta_k + \tan(u_2\pi/2)\right) / \left(1 - \beta_k \tan(u_2\pi/2)\right).$
    $\alpha_{\beta_k} \leftarrow \log p\left(\beta_k^*, \boldsymbol{\phi}_{(-\beta_k)} \,\middle|\, \boldsymbol{\theta}, \boldsymbol{X}, \boldsymbol{d}\right) + \log f_{tc}\left(\beta_k^* \mid w\right) -$
      $\log p\left(\beta_k, \boldsymbol{\phi}_{(-\beta_k)} \,\middle|\, \boldsymbol{\theta}, \boldsymbol{X}, \boldsymbol{d}\right) - \log f_{tc}\left(\beta_k \mid w\right),$
    where $f_{tc}\left(x \mid w\right) = 1 / \left(w\pi\left[1 + x^2\right]\right).$
    if $\alpha_{\beta_k} > \log u_3$ **then**
      $\beta_k \leftarrow \beta_k^*$
    end if
  end for
  $\boldsymbol{\phi}^{(q)} \leftarrow \boldsymbol{\phi}$
end for

prior on the von Mises model, $m = n$ and $\zeta = -R_\psi \cos(\beta_0 - \bar{\psi})/n$. For further details, see Forbes & Mardia (2015).

2.3.3 Sampling $\boldsymbol{\beta}$

Sampling $\boldsymbol{\beta}$ is performed by a Metropolis-Hastings step (Metropolis et al., 1953; Hastings, 1970). However, because of the irregular shape of the posterior, a random walk on β_k may cause slow convergence. If the current value for β_k is further from zero, we might prefer to propose candidates that are further away from the current value.

Therefore, motivated by the circular nature of the parameter space, candidates are generated by

$$\beta_k^* = \frac{\beta_k^{(cur)} + \tan(u\pi/2)}{1 - \beta_k^{(cur)} \tan(u\pi/2)}, \tag{2.10}$$

where u is a random variate from the uniform distribution $U(-w, w)$, with w a tuning parameter. Here, we choose $w = .05$. This procedure can be shown to be equivalent to drawing a proposal from the truncated Cauchy distribution $f\left(\beta_k^* \,\middle|\, \beta_k^{(cur)}, w\right) = 1/\left(w\pi\left[1 + \beta_k^{*2}\right]\right)$ with bounds

$$\left[\frac{\beta_k^{(cur)} + \tan(-\pi w/2)}{1 - \beta_k^{(cur)} \tan(-\pi w/2)}, \frac{\beta_k^{(cur)} + \tan(\pi w/2)}{1 - \beta_k^{(cur)} \tan(\pi w/2)}\right].$$

Note that this proposal is not symmetric, although the Metropolis-Hastings ratio corrects for this lack of symmetry in the usual way.

2.3.4 Sampling $\boldsymbol{\delta}$

It can be seen that the conditional posterior of each δ_j is a convolution of two von Mises distributions, which itself is not von Mises. Mardia & Jupp (1999, p. 44) provide an approximation for such a convolution. Here, a slightly simpler approach is taking employing another Metropolis-Hastings step with von Mises proposals such that

$$\delta_j^* \sim \mathcal{M}\left(\delta_j^{(cur)}, R_\psi^{(cur)} \kappa^{(cur)}\right). \tag{2.11}$$

2.4 Hypothesis tests

In order to make decisions on a researcher's hypotheses, it is useful to consider hypothesis testing. A Bayesian approach to testing two discrete hypotheses

against each other is by updating the prior odds of the hypotheses by multiplying them by the Bayes factor (Kass & Raftery, 1995; Jeffreys, 1961), in order to produce the posterior odds of the two hypotheses. From the posterior odds, we can obtain the posterior model probability of H_1 compared to H_0, $p(H_1 \mid D)$, where D represents the data, in this case $\{\boldsymbol{\theta}, \boldsymbol{X}, \boldsymbol{d}\}$. This is an intuitive probability of interest, because it represents our current belief that H_1 is true rather than H_0, and this probability might further be used to make decisions.

Two types of hypothesis tests are considered here. First, we consider traditional equality constrained hypotheses, comparing a null hypothesis to an alternative. Second, we consider inequality constrained hypotheses (Hoijtink et al., 2008; Hoijtink, 2011), where we test whether a parameter is larger than some other parameter, which can be a function of the parameters in the model or a fixed value.

2.4.1 Equality constrained hypotheses

Consider two hypotheses about some model parameter γ,

$$H_0 : \gamma = \gamma_0, \quad H_1 : \gamma \in \Omega_\gamma, \tag{2.12}$$

where Ω_γ is the sample space of γ. The associated Bayes factor is given by

$$BF_{01} = \frac{p(D \mid H_0)}{p(D \mid H_1)}. \tag{2.13}$$

To obtain the Bayes factor, we must compute the quantity

$$p(D \mid H_s) = \int p(D, \boldsymbol{\phi}_s \mid H_s) d\boldsymbol{\phi}_s, \tag{2.14}$$

where $\boldsymbol{\phi}_s$ denotes the set of parameters in the model for hypothesis H_s. In general, this integral is not easy to compute, although special cases admit closed-form solutions. Here we will apply the Savage-Dickey method (Dickey et al., 1970; O'Hagan & Forster, 2004), following Wagenmakers et al. (2010). This method is based upon the result that, under some assumptions,

$$\frac{p(D \mid H_0)}{p(D \mid H_1)} = \frac{p(\gamma = \gamma_0 \mid D, H_1)}{p(\gamma = \gamma_0 \mid H_1)}, \tag{2.15}$$

which is a ratio of the posterior and prior probability of γ_0 under model H_1. In practice, this means that the probability of γ_0 under H_1 must be evaluated, both in the prior and the posterior. Although trivial in some conjugate

situations, for the circular GLM this needs to be addressed separately for each parameter to which we wish to compute the Bayes factor.

In this study, this type of hypothesis test will be applied to both δ and β. For some β_k, the hypotheses under evaluation are

$$H_0 : \beta_k = 0, \quad H_1 : \beta_k \in \mathbb{R}. \tag{2.16}$$

Taking a Normal prior on β_k as before, $p(\beta_k = 0 \mid H_1) = p_N(0 \mid \mu = 0, \sigma^2 = 1) \approx .399$.

For some δ_j, the hypothesis under evaluation is

$$H_0 : \delta_j = 0, \quad H_1 : \delta_j \in [-\pi, \pi). \tag{2.17}$$

With a uniform prior on δ_j, $p(\delta_j = 0 \mid H_1) = 1/2\pi \approx .159$.

For $p(\beta_k = 0 \mid D, H_1)$ and $p(\delta_j = 0 \mid D, H_1)$, a simple estimate is obtained by computing the height of the histogram bar that would contain 10% of the observations and which would have γ_0 as its midpoint. A more sophisticated approach could employ log-spline distributions on the real line (Stone et al., 1997) and on the circle (Ferreira et al., 2008).

We note that if γ_0 is far from the posterior samples of γ, this estimate will not be stable. However, Wagenmakers et al. (2010) note that evidence for H_1 is overwhelming by that point, which means that accuracy is much less important.

Another remark to be made is that this method is only valid if the nuisance parameters between the two hypotheses serve the same purpose. For a discussion, see Consonni et al. (2008).

2.4.2 Inequality constrained hypotheses

In practice, researchers often have directed (one-sided) hypotheses, which may be specified by using inequality constraints. Bayesian analysis of inequality constrained hypotheses has been studied by Klugkist et al. (2005) and Wetzels et al. (2010).

For some model parameter γ, a simple hypothesis to evaluate could be

$$H_0 : \gamma > \gamma_0, \quad H_1 : \gamma < \gamma_0.$$

In order to quantify our belief in these hypotheses, we employ an encompassing hypothesis $H_{unc} : \gamma \in \Omega_\gamma$, from which an MCMC sample $\boldsymbol{\gamma} = \{\gamma^{(1)}, \ldots, \gamma^{(Q)}\}$ is obtained (Klugkist et al., 2005). Then, assuming the encompassing prior does not favor either hypothesis, it can be shown that the

Bayes factor for H_0 versus H_1 is given by

$$BF_{01} = \frac{p(D \mid H_0)}{p(D \mid H_1)} = \frac{p(D \mid H_0)/p(D \mid H_{unc})}{p(D \mid H_1)/p(D \mid H_{unc})} = \frac{\sum_{s=1}^{Q} I\left(\gamma^{(s)} \in \Omega_{\gamma|H_0}\right)}{\sum_{s=1}^{Q} I\left(\gamma^{(s)} \in \Omega_{\gamma|H_1}\right)}, \tag{2.18}$$

where $I(\cdot)$ is an indicator function, $\gamma^{(s)}$ is a sample from the unconstrained model H_{unc}, and $\Omega_{\gamma|H_s}$ is the admitted sample space for γ under hypothesis H_s.

This is a flexible approach, because it allows evaluation of any combination of inequality constrained hypotheses against each other. For example, consider a model with three groups, where we denote the mean directions by $\{\mu_1, \mu_2, \mu_3\}$. Then, a major advantage of the inequality constrained hypothesis approach is that it becomes easy to assess the model

$$\mu_1 > \mu_2 > \mu_3 \tag{2.19}$$

2.5 Simulation study

A simulation study was performed to assess the effectiveness of the proposed method. The sampler was implemented in Rcpp (Eddelbuettel & François, 2011), and analyzed in R (R Core Team, 2016). Generally, the method converges fast and mixes well for each cell in the simulation, so that a burn-in of 1000 and a number of iterations of 20000 was deemed sufficient, with no thinning. Three different models are considered. First, a circular regression scenario with a single linear predictor. Second, a 2×2 factorial ANOVA model with main effects only. Third, an ANCOVA model with a single grouping variable and four linear covariates. For all models, the artificial data featured (total) sample sizes $n = \{20, 100\}$, concentrations $\kappa = \{2, 10\}$ and circular intercept $\beta_0 = \pi/2$. Additional simulations were performed with $n = 50$, $\kappa = 5$ and $\beta, \delta = 0.2$, which are not shown here for brevity's sake, as they provided similar results to the other scenarios.

For each scenario, 5000 datasets were generated and subsequently analyzed. Point estimates obtained from the MCMC sampler are $\hat{\beta}_0$, the posterior mean direction of β_0, $\hat{\kappa}$, the posterior mode of κ, $\hat{\beta}$, the posterior mean of β, and $\hat{\delta}$, the posterior mean direction of δ. In addition, credible intervals are obtained from the posterior samples as well, by taking the circular quantiles of β_0, the Highest Posterior Density (HPD) interval of κ, the regular quantiles of $\boldsymbol{\beta}$, and the circular quantiles of $\boldsymbol{\delta}$. Circular quantiles of a set of angles $\boldsymbol{\theta}$ are obtained by computing the set of angles $(\boldsymbol{\theta} + \bar{\theta} - \pi)$, obtaining the linear quantiles, and finally subtracting $(\bar{\theta} - \pi)$ from the computed lower and upper bound.

Table 2.1: Results of the simulation study for the simple regression scenario. 'Cov.' denotes the 95% coverage for a specific parameter, while 'Acc.' denotes the acceptance probability. MCT denotes the mean computation time in seconds.

True			β_0		κ		β_1			
β	κ	n	Bias	Cov.	$\hat{\kappa}$	Cov.	$\hat{\beta}_1$	Cov.	Acc.	MCT
0.05	2	20	-0.00	0.95	2.09	0.97	0.05	0.94	0.84	0.58
		100	-0.00	0.95	1.99	0.98	0.05	0.95	0.66	2.26
	20	20	-0.00	0.94	22.70	0.95	0.05	0.94	0.47	0.59
		100	-0.00	0.95	20.36	0.95	0.05	0.94	0.23	2.37
0.80	2	20	-0.00	0.94	2.08	0.97	0.81	0.95	0.86	0.58
		100	0.00	0.96	2.00	0.98	0.81	0.95	0.72	2.33
	20	20	-0.00	0.94	22.37	0.95	0.80	0.95	0.55	0.60
		100	0.00	0.95	20.37	0.95	0.80	0.94	0.29	2.44

In order to assess bias, point estimates were averaged over the datasets. For β_0, and $\boldsymbol{\delta}$, this means computation of the mean direction, for other values this refers to the regular linear mean. In addition, a coverage was obtained for each parameter by computing the proportion of the appropriate credible intervals that contained the true value. Finally, acceptance probabilities refer to the proportion of proposals for this parameter that were accepted by the Metropolis-Hastings step, which is applicable only for δ and β.

The three different scenarios for the predictors will be discussed separately in the following sections. The section will be concluded with a discussion of the behavior of the Bayes factors for these three scenarios.

2.5.1 Simple regression

For the simple regression data were simulated by first generating a vector $\boldsymbol{x}_r$ independently from the standard normal distribution $N(0, 1)$. This vector is then standardized by $\boldsymbol{x} = (\boldsymbol{x}_r - \bar{\boldsymbol{x}}_r)/\text{var}(\boldsymbol{x}_r)$. Then, the circular outcome is computed by

$$\theta_i = \pi/2 + g\left(\beta_1 x_i\right) + \varepsilon_i, \tag{2.20}$$

where β takes values $\{0.05, 0.8\}$, and $\varepsilon_i \sim \mathcal{M}(0, \kappa)$.

Table 2.1 shows the results of this simulation study. Performance is quite good, providing unbiased estimates and great coverage, which shows that the weakly informative prior on β_1 does not strongly harm the frequency

Table 2.2: Results of the simulation study for the factorial ANOVA scenario. 'Cov.' denotes the 95% coverage for a specific parameter, while 'Acc.' denotes the acceptance probability. MCT denotes the mean computation time in seconds.

True			β_0		κ		δ_1			
δ	κ	n	Bias	Cov.	$\hat{\kappa}$	Cov.	$\hat{\delta}_1$	Cov.	Acc.	MCT
0.05	2	20	-0.00	0.95	2.10	0.97	0.06	0.95	0.78	0.70
		100	-0.00	0.95	1.99	0.98	0.05	0.95	0.78	2.63
	20	20	-0.00	0.93	22.75	0.95	0.05	0.93	0.79	0.71
		100	0.00	0.95	20.35	0.95	0.05	0.94	0.78	2.71
0.80	2	20	-0.00	0.95	2.10	0.97	0.80	0.96	0.79	0.69
		100	0.00	0.95	2.00	0.98	0.80	0.95	0.78	2.62
	20	20	-0.00	0.94	22.65	0.95	0.80	0.93	0.78	0.71
		100	-0.00	0.95	20.35	0.95	0.80	0.95	0.78	2.71

properties of our Bayesian estimation procedure. Acceptance rates decline slightly for more concentrated data, which could be ameliorated in practice by tuning the proposals. The sampler runs quite fast, as the longest time a single analysis took was 2.44 seconds.

2.5.2 Factorial ANOVA

For the factorial ANOVA scenario, data were simulated by first generating two vectors, $\boldsymbol{d}_1$ and $\boldsymbol{d}_2$, by randomly drawing either 0 or 1 with probability .5. This means that we generally create unbalanced designs, and the number of subjects in each group differs between the simulated datasets. This reflects a realistically broad range of possible research designs. The outcome is computed by

$$\theta_i = \pi/2 + \delta_1 d_{1i} + \delta_2 d_{2i} + \varepsilon_i, \tag{2.21}$$

where $\delta_1 = \delta_2$ takes values $\{0.05, 0.8\}$, and $\varepsilon_i \sim \mathcal{M}(0, \kappa)$.

Table 2.2 shows the results of the simulation study. Once again, the sampler performs well in all situations. In contrast with β in the regression model, the acceptance rate of δ does not depend on n, κ, or true δ, because its proposal adapts itself to these parameters.

Table 2.3: Results of the simulation study for the ANCOVA scenario. 'Cov.' denotes the 95% coverage for a specific parameter, while 'Acc.' denotes the acceptance probability. MCT denotes the mean computation time in seconds.

True			β_0		κ		δ_1			β_1			
β, δ	κ	n	Bias	Cov.	$\hat{\kappa}$	Cov.	$\hat{\delta}_1$	Cov.	Acc.	$\hat{\beta}_1$	Cov.	Acc.	MCT
0.05	2	20	0.01	0.95	1.96	0.94	0.04	0.96	0.79	0.01	0.96	0.85	1.24
		100	-0.00	0.95	1.99	0.98	0.05	0.95	0.78	0.05	0.95	0.67	4.11
	20	20	0.00	0.93	22.88	0.96	0.05	0.94	0.79	0.05	0.94	0.47	1.21
		100	0.00	0.95	20.36	0.95	0.05	0.95	0.78	0.05	0.95	0.23	4.11
0.80	2	20	-0.01	0.95	1.95	0.94	0.73	0.96	0.79	0.58	0.95	0.86	1.24
		100	0.00	0.87	1.78	0.88	0.79	0.82	0.78	0.60	0.88	0.73	4.32
	20	20	0.00	0.93	17.43	0.92	0.80	0.74	0.79	0.69	0.93	0.56	1.25
		100	-0.00	0.70	13.18	0.69	0.80	0.82	0.78	0.40	0.70	0.46	4.31

2.5.3 ANCOVA with four covariates

Here, a single grouping variable was generated as in Section 2.5.2, while the linear covariates were generated as in Section 2.5.1. Then, the outcome is computed by

$$\theta_i = \pi/2 + \delta_1 d_{1i} + g(\beta_1 x_{i1} + \beta_2 x_{i2} + \beta_3 x_{i3} + \beta_4 x_{i4}) + \varepsilon_i, \tag{2.22}$$

where we have chosen the true values $\delta_1 = \beta_1 = \beta_2 = \beta_3 = \beta_4$ in all simulations, taking values $\{0.05, 0.8\}$, and $\varepsilon_i \sim \mathcal{M}(0, \kappa)$.

Table 2.3 shows the results of the simulation study. Only the results for β_1 and δ_1 are shown, because results the other regression parameters are almost identical. For most scenarios, the results are once again adequate. It can be seen that the scenario with strong effects ($\beta = \delta = 0.8$), estimates are often unsatisfactory. It should be noted that in these scenarios, the data show high variance. In general, if $\sum_{k=1}^{K} |\beta_k| > 1.5$, the data are spread all over the circle, such that many estimates of $\boldsymbol{\beta}$ are somewhat plausible, which results in an irregular posterior. Therefore, the sampler performs quite badly. Note that this is a property of the GLM approach to circular regression, rather than this specific model or implementation. In practice, however, we expect that this kind of dataset will almost never occur, although it might be advisable to monitor obtained estimates for this situation.

2.5.4 Bayes factors and posterior model probabilities

For hypothesis testing, Bayes factors and posterior model probabilities were obtained as detailed in Section 2.4. Figure 2.3 depicts boxplots of the posterior probability of the correct model for the inequality and equality hypotheses, for the three different models, where in each case all true $\beta = \delta = 0.05$. This means that in all cases H_1 is true, so values close to 1 indicate that in a given scenario greatly prefers the correct model. The hypotheses given are listed below.

- Regression
  - Test for equality: $H_0 : \beta_1 = 0$ vs. $H_1 : \beta_1 \neq 0$,
  - Test for inequality: $H_0 : \beta_1 < 0$ vs. $H_1 : \beta_1 > 0$,
- ANOVA and ANCOVA
  - Test for equality: $H_0 : \delta_1 = 0$ vs. $H_1 : \delta_1 \neq 0$,
  - Test for inequality: $H_0 : \delta_1 < 0$ vs. $H_1 : \delta_1 > 0$,

Generally, the correct hypothesis becomes favored as the sample size increases, as expected. In addition, there is less simulation variability when n increases, shown by a smaller range in the boxplot. Compared to the inequality hypothesis, the equality hypothesis is more prone to pick up group differences in δ (ANOVA and ANCOVA model), as well as in the regression model when $\kappa = 2$.

2.6 Example

In this section, our method will be applied to data from van Dijk et al. (2013). In this study, an experiment was conducted to assess whether deafness enhances haptic perception. Haptic perception is assessed here by means of a haptic parallel setting task, where subjects are required to set two bars parallel, so that errors are measured in an angular differece to the reference direction. In this task, errors generally fall in the counterclockwise direction, which produces a positive score on the deviation from the target. Therefore, groups that are less apt at this task are expected to have stronger positive deviations, counterclockwise from the reference direction.

Three groups are distinguished: deaf subjects, sign language interpreters and a control group. Table 2.4 shows some summary statistics of background variables for the three groups, as well as the main outcome, deviation. Note

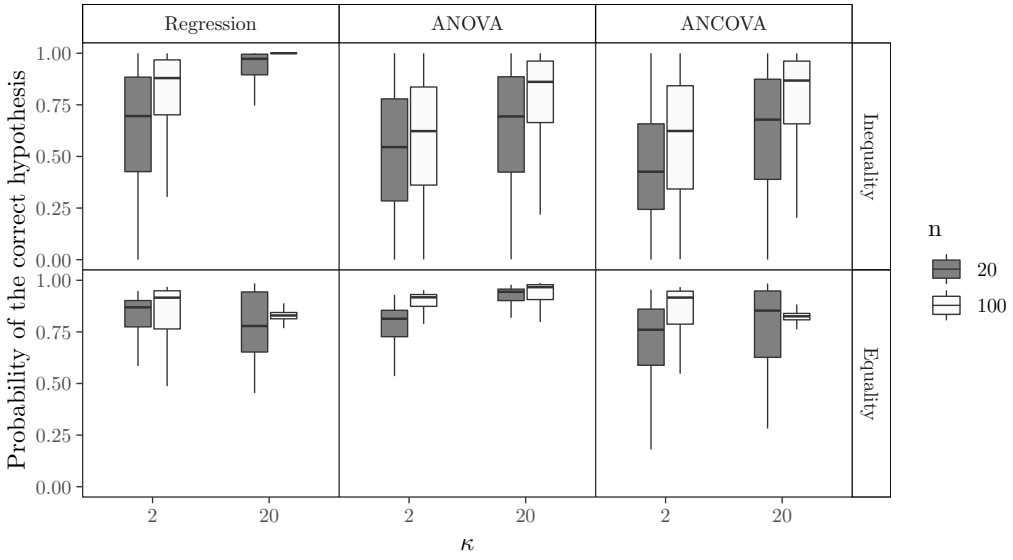

Figure 2.3: Boxplot of the posterior model probability assigned to the correct model in 5000 simulations with $\beta = \delta = 0.05$ for the inequality (top) and equality (bottom) hypotheses. For the regression scenario, inequality tests $\beta_1 > 0$ vs. $\beta_1 < 0$ and equality tests $\beta_1 \neq 0$ vs. $\beta_1 = 0$. For the ANOVA and ANCOVA models inequality tests $\delta_1 > 0$ vs. $\delta_1 < 0$ and equality tests $\delta_1 \neq 0$ vs. $\delta_1 = 0$.

Table 2.4: Summary statistics of the mean age (years), mean education (years) and mean direction of deviation (degrees).

	Age		Education		
	Mean	SD	Mean	SD	Deviation
Deaf	41.20	13.48	16.60	1.55	14.73
Interpreter	38.44	8.60	16.88	1.50	25.22
Control	44.75	9.73	17.06	1.44	28.82

that the original study examines two different conditions in a repeated measures design, an "immediate" and a "delayed" condition, of which we only show the "immediate" outcome for illustration purposes. Therefore, the data under consideration are made independent.

The analysis will proceed as follows. First, a basic ANOVA model will be fitted to this dataset. Then, an ANCOVA model is examined. Lastly, informative inequality constrained hypotheses based on theory are evaluated.

2.6.1 ANOVA model

The goal in the ANOVA model is to assess whether the three groups differ. For this and all following models, the control group will be used as the reference group. The outcome in the ANOVA model is given by $\theta_i \sim \mathcal{M}(\mu_i, \kappa)$, where $\mu_i = \beta_0 + \delta_{df} d_{df} + \delta_{in} d_{in}$, where d_{df} and d_{in} are dummy variables for the deaf and interpreter group, respectively, and each δ is labeled appropriately. The main hypothesis is that the deaf group performs better than the control group, which could manifest itself as $\delta_{df} < 0$. Second, interpreters might also outperform the control group, which would mean $\delta_{in} < 0$.

A burn-in of 1000 was used, and the MCMC sampler was run for 100000 iterations. Figure 2.4 shows convergence plots for the four model parameters, where it can be seen that the sampler converges well.

Results are shown in Table 2.5. Estimates are given by the posterior mean direction of $\beta_0, \delta_{df}, \delta_{in}$ and the posterior mode of κ. The credible interval of δ_{df}, the difference between the deaf group mean direction and the control group mean direction, is given by (-0.42, -0.08), which can be seen as evidence for a non-zero group difference, as zero is not in this interval. The credible interval for the interpreter group mean direction is (-0.24, 0.11), which can be seen as evidence against a non-zero group difference.

A more sophisticated approach is to employ the hypothesis tests that were developed. Employing the equality constrained hypotheses, a mild amount of

Table 2.5: Results for the ANOVA model. LB and UB respectively represent lower and upper bound of the 95% credible interval of the given parameter.

	Estimate	LB	UB
β_0	0.51	0.38	0.63
κ	17.77	11.26	26.16
δ_{df}	-0.25	-0.42	-0.08
δ_{in}	-0.07	-0.24	0.11

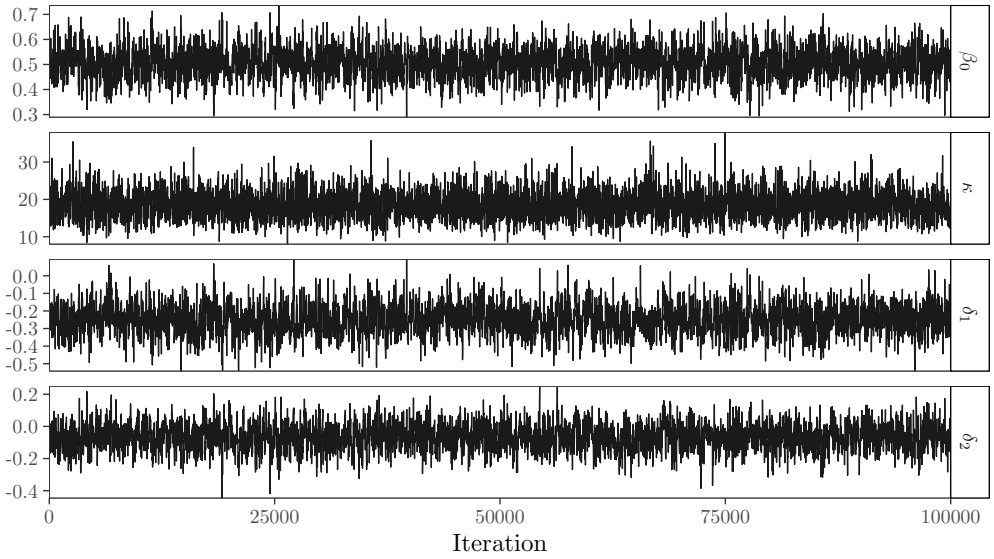

Figure 2.4: Convergence plots for the ANOVA model.

Table 2.6: Results for the ANCOVA model.

	Estimate	LB	UB
β_0	0.50	0.38	0.62
κ	18.30	11.54	27.19
δ_{df}	-0.21	-0.39	-0.04
δ_{in}	-0.08	-0.24	0.09
β_{age}	-0.02	-0.06	0.01
β_{hand}	0.03	-0.01	0.06

support was found in favor of the hypothesis that deaf participants differ from the controls ($BF_{\mu_{cn}\neq\mu_{df}:\mu_{cn}=\mu_{df}} = 2.69$), while a mild amount of support was found against the hypothesis that deaf participants differ from sign language interpreters ($BF_{\mu_{in}\neq\mu_{df}:\mu_{in}=\mu_{df}} = 0.34$).

This highlights that this method is conservative in supporting alternative hypotheses such as $H_1 : \mu_{in} \neq \mu_{df}$. This is a result of the circular uniform prior on δ, which suggests that more subjective approach could be less conservative and more likely to pick up on group differences. For example, a von Mises prior on δ with $\kappa > 0$ could be used. This subjective prior represents the knowledge that mean directions of different groups are usually somewhat close together. In this case, selection of the κ to be used becomes a core issue, which represents a trade-off between the amount additional power for the hypothesis test and the amount of (potentially unwanted) prior information included in the analysis.

The inequality hypothesis tests show a large amount of support for the hypothesis that deaf participants perform better than the controls ($BF_{\mu_{cn}>\mu_{df}:\mu_{cn}<\mu_{df}} = 267.82$), and for the hypothesis that deaf participants perform better than sign language interpreters ($BF_{\mu_{in}>\mu_{df}:\mu_{in}<\mu_{df}} = 52.28$).

2.6.2 ANCOVA model

In order to properly assess the effects found, it is useful to take into account theoretically relevant covariates. Here, we include age and handedness (that is, strength of hand preference) as covariates, and investigate the effect this has on previous conclusions. Table 2.6 shows the output of the ANCOVA model, with age and handedness as linear covariates.

From the results, it seems that the covariates do not have an effect on performance. Under equal prior odds, the Bayes factors for the predictors indeed indicate 29.35 times more support for the hypothesis $\beta_{age} = 0$ compared to the alternative $\beta_{age} \neq 0$, and 19.08 times more support for the hypothesis

$\beta_{hand} = 0$ than the alternative $\beta_{hand} \neq 0$. While controlling for covariates, the evidence for a negative δ_{df} is still substantive, indicating superior performance of deaf individuals over controls ($BF_{\mu_{df}<\mu_{cn} \,:\, \mu_{df}>\mu_{cn}} = 96.75$). As there is little support for the inclusion of covariates, they are omitted in subsequent analyses.

2.6.3 Inequality constrained hypothesis

Although van Dijk et al. (2013) do not evaluate inequality constrained hypotheses directly, the theories stated by the authors can be interpreted as such. First, they state:

> "On the basis of a greater proneness in visuospatial processing, we could expect a better developed haptic orientation processing ability in deaf individuals."

Then, with regards to sign language interpreters, they state:

> "The relative positions of the signer's hands are used to map spatial relations in the real world. We may speculate here that experienced signers can also do the reverse more easily: interpret the hand positions forced by inspecting the bars in the parallel setting task in absolute world reference frames. If so we would expect both deaf and hearing signers to outperform non-signing hearing controls but not to differ from each other."

These expectations can be mapped to hypotheses about the mean directions of the three groups, which are given by

$$\text{(Deaf) } \mu_{df} = \beta_0, \quad \text{(Interpreter) } \mu_{in} = \beta_0 + \delta_1, \quad \text{(Control) } \mu_{cn} = \beta_0 + \delta_2.$$

Following for example Rueda et al. (2009) and Baayen & Klugkist (2014), it is important to specify inequality constraints on circular data as either isotropic, or non-isotropic. Isotropic orderings are defined on the circle, and denote in which order the parameters are encountered as we move around the circle, relative to one another. Non-isotropic orderings are orderings relative to a fixed point on the circle. In this case, a type of non-isotropic orderings are considered where the hypothesis states that one parameter lies in the semi-circle counterclockwise of another parameter. In this case, we have chosen to translate the expectations to the following hypotheses:

$$H_1 : \mu_{df} < (\mu_{in}, \mu_{cn}) < \mu_{df} + \pi, \quad H_2 : \mu_{cn} - \pi < (\mu_{df}, \mu_{in}) < \mu_{cn}. \quad (2.23)$$

Using the inequality constrained framework as described in Section 2.4.2, the support for either hypothesis can be quantified.

Following this method, we find that H_1 is true in 97.9% of the MCMC iterations, while H_2 occurs in 78% of the iterations, so both hypotheses are likely. From this, we find no conclusive evidence for either H_1 or H_2 ($BF_{H_1:H_2} = 1.25$). This means that although the study provides useful insight in the performance of deaf subjects, there is not enough evidence yet to decide on these two competing hypotheses.

2.7 Discussion

We developed a Bayesian circular GLM, with appropriate priors, proper treatment of dichotomous variables, and Bayesian hypothesis tests. Our method forms a middle ground between two veins of research into Bayesian analysis of circular data. On one hand, analysis of complex data shapes (Ghosh et al., 2003; Ferreira et al., 2008; Fernández-Durán & Mercedes Gregorio-Domínguez, 2016) provides modeling for a broad class of datasets but few possibilities for prediction and covariate models. On the other hand, circular regression models (Fisher & Lee, 1992; J. Gill & Hangartner, 2010; Lagona, 2016) provide prediction and covariates, but encounter problems with likelihood shapes and a lack of available hypothesis tests. The GLM aproach is promising because of its flexibility to allow for many different kinds of models, while also allowing straightforward extensions. Our method brings three main contributions to the literature.

First, we have shown that the irregular log-likelihood surface of the regression parameters $\boldsymbol{\beta}$ in a circular GLM can be dealt with naturally by employing a weakly informative prior that encapsulates our actual belief that extreme values for $\boldsymbol{\beta}$ are unlikely in applied research, while we still let the data overpower the prior. This is analogous to the widely accepted idea that very large effect sizes, say, Cohen's $d > 1$, are improbable in most scientific disciplines where empirical research is necessary, in particular the social sciences. If the method would indicate support for such large values of $|\beta|$, a researcher would not believe that the model is correct, and reassess it. Our prior simply represents the lack of belief in large values of $|\beta|$.

Second, we have separated the group difference parameters from linear covariates, in order to allow modeling of a large array of ANOVA designs, including factorial and ANCOVA designs. This provides researchers with a straightforward way to map their hypotheses to a design. In addition, model comparison can easily be made possible through the DIC or WAIC (Gelman et al., 2003, Ch. 7).

Third, we have developed Bayesian hypothesis tests based on the Bayes factor for the circular data case. The tests employed here are pbased on the Savage-Dickey method advocated by Wagenmakers et al. (2010) and the inequality constrained aproach of Hoijtink (2011). Many Bayesian approaches to circular data analysis lack any form of hypothesis testing, which we view as limiting their ability to be applied in practice. In order to create statistical methods that are employed in practice, we must accomodate the desire for hypothesis testing, and compute posterior model probablities. Therefore, we have taken a step in this direction as well, showing how Bayesian hypothesis tests can be developed easily in the circular data context by using MCMC output.

Although the computational methods employed here are stable and allow for useful inferences, further consideration of useful hypotheses and their associated Bayes factors will be important for the applicability of the Bayesian paradigm to circular data analysis, in particular in behavioural research. Here, we have not provided Bayes factors based on estimation of the marginal likelihood as in Chib (1995) and subsequent work in this field, although this approach might be more flexible than the methods applied here. Another approach might be to attempt to develop priors that allow for closed-form Bayes factors in a similar vein as the g-prior in the linear case (Zellner, 1986; Liang et al., 2012). The computational simplicity of such Bayes factors is useful in many scenarios, although the complexity of the designs for such Bayes factors are usually limited.

In the broader scope of circular data analysis, our method can be seen as a Bayesian extension of the approaches of Artes (2008) and Lagona (2016). Further extensions of this model might ease the assumption of i.i.d. observations taken here by applying properties of the multivariate von Mises distribution (Mardia et al., 2008; Mardia & Voss, 2014), as in Lagona (2016).

In sum, the Bayesian approach provides a promising way to draw inference from circular data. Usual approaches are based on large sample or high concentration approximations (Artes, 2008) or bootstrap approaches for simple models (Baayen et al., 2012; Baayen & Klugkist, 2014). Our approach does not need such approximations, and provides a new direction for circular data analysis of GLM-type models.

2.8 Acknowledgements

This work was supported by a Vidi grant awarded to I. Klugkist from NWO, the Dutch Organization for Scientific Research (NWO 452-12-010).

The authors are grateful to two reviewers for helpful comments.

The authors are grateful to A. Postma for providing the illustrative data.

User-friendly code for the main analyses of the paper can be found in a GitHub package at https://github.com/keesmulder/CircGLMBayes.

All code for both the statistical tools, the simulation study and the paper is available online at https://github.com/keesmulder/BayesMultCircCovariates.

Appendix A

Bayesian Tests for Circular Uniformity

A.1 Introduction

Circular data are measured in angles or directions. They are frequently encountered in scientific fields as diverse as life sciences (Mardia, 2011), behavioural biology (Bulbert et al., 2015), cognitive psychology (Kaas & Van Mier, 2006), bioinformatics (Mardia et al., 2008), political sciences (J. Gill & Hangartner, 2010) and environmental sciences (Arnold & SenGupta, 2006). In psychology, circular data occur often in motor behaviour research (Mechsner et al., 2001, 2007; Postma et al., 2008; Baayen et al., 2012), as well as in the application of circumplex models (Gurtman & Pincus, 2003; Gurtman, 2009; Leary, 1957). Circular data differ from linear data in the sense that circular data are measured in a periodical sample space. For example, an angle of 1° is quite close to an angle 359°, although linear intuition suggests otherwise.

A fundamental hypothesis of interest is that of circular uniformity. A test for circular uniformity can be used to assess a hypothesis of theoretical interest by itself, but can also be used as a preliminary assessment, because most tests performed in circular statistics are only valid if the data is non-uniform. Several methods for assessing circular uniformity exist in the frequentist framework. These will be reviewed in Section A.2.

In the rest of this paper, Bayesian hypothesis tests will be added to this arsenal. In order to create a Bayesian test of circular uniformity, the Bayes factor will be employed, which is often hailed as the standard way of performing a Bayesian hypothesis test (Kass & Raftery, 1995; Jeffreys, 1961). A major advantage of this Bayesian method is that through specifying the

alternative hypothesis and the associated prior, we can precisely quantify support for either the null hypothesis or the alternative hypothesis. Methods based on null hypothesis significance testing only signify whether or not the null hypothesis can be rejected, but never provide support in favor of the null hypothesis. In practice, failure to reject the null hypothesis in a frequentist test is often taken as evidence for the null. However, a failure to reject the null might just as well be caused by a lack of power, so that the evidence in the data is indifferent to circular uniformity. In contrast, the Bayesian hypothesis test developed here is able to provide support for the null hypothesis. This alleviates some of the well-described issues with null hypothesis significance testing, and is particularly useful for tests that are used as a preliminary assessment, such as circular uniformity tests.

To compute the Bayes factor, the so-called marginal likelihood must be obtained for each hypothesis. The marginal likelihood is the normalizing constant of the posterior, and the key ingredient of the Bayes factor. To obtain the marginal likelihood one must specify the prior distribution of the parameters in each hypothesis. The null hypothesis (circular uniformity) has no parameters, so no prior is needed for it. The alternative hypothesis, however, requires specification of both a model for the data, would they be non-uniform, and second, a prior for the parameters in this model. This paper will investigate two alternative hypotheses, one based on the von Mises distribution and one based on a kernel density alternative. In addition, several priors will be investigated that can be used with each model.

The rest of the paper is structured as follows. A short review of frequentist tests of circular uniformity is provided in Section A.2. The Bayesian circular uniformity test for a von Mises alternative is discussed in Section A.3. The Bayesian circular uniformity test for a kernel density alternative, which functions as an omnibus test, is discussed in Section A.4. The methods are applied to example datasets in Section A.5. Section B.5 provides a discussion.

A.2 Frequentist tests of circular uniformity

Here, we will shortly review frequentist tests of circular uniformity. Four commonly used tests are Kuiper's test (Kuiper, 1960), Rayleigh's test (Mardia & Jupp, 2000; Brazier, 1994), Rao's test of equal spacing (Rao, 1976) and Ajne's test (Ajne, 1968). Perhaps the most common of these is the Rayleigh test. Let $\boldsymbol{\theta} = (\theta_i = 1, \ldots, \theta_n)$ denote a set of data consisting of angles, and let the mean resultant length $\bar{R} = n^{-1}\sqrt{(\sum_{i=1}^{n} \cos\theta_i)^2 + (\sum_{i=1}^{n} \sin\theta_i)^2}$. Then the Rayleigh test statistic can be computed simply as $2n\bar{R}^2$, which has

approximately a χ^2_2 distribution. It can be shown that the Rayleigh test is the most powerful test against von Mises alternatives, as well as Projected Normal (PN) alternatives (Bhattacharyya & Johnson, 1969). Although the Rayleigh test is consistent against unimodal alternatives, it is not consistent against alternatives that have resultant length $\rho = 0$, in particular distributions with antipodal symmetry (Mardia & Jupp, 2000).

Another test is Kuiper's test (Kuiper, 1960), which is based on the maximum difference between the theoretical and empirical distribution function. It is consistent against all alternatives to uniformity (Mardia & Jupp, 2000). A similar test uses Watson's U^2 statistic (Watson, 1961), which is instead based on the *mean* difference between the theoretical and empirical distribution function.

Several other tests for circular uniformity exist, among which Rao's equal spacing test (Rao, 1976), the range test (Laubscher & Rudolph, 1968), the Hodges-Ajne test (Hodges, 1955; Ajne, 1968), Ajne's A_n test (Ajne, 1968), and the Hermans-Rasson test (Hermans & Rasson, 1985). Somewhat more recently, a smooth test for circular uniformity was developed by Bogdan et al. (2002). A test specifically targeting multimodal alternatives was developed by Pycke (2010).

A.3 A Bayesian test for circular uniformity with a von Mises alternative

In this section, a Bayesian hypothesis test for circular uniformity against a von Mises alternative will be developed. The von Mises distribution is a natural distribution on the circle, given by

$$\mathcal{M}(\theta \mid \mu, \kappa) = [2\pi I_0(\kappa)]^{-1} \exp\{\kappa \cos(\theta - \mu)\}, \tag{A.1}$$

where $\theta \in [0, 2\pi)$ is an angle, $\mu \in [0, 2\pi)$ is the mean direction, $\kappa \in \mathbb{R}^+$ is a concentration parameter and $I_0(\cdot)$ is the modified Bessel function of the first kind and order zero.

The test will be based on the Bayes factor, which is the ratio of two marginal likelihoods, given by

$$BF_{10} = \frac{m_1(\boldsymbol{\theta})}{m_0(\boldsymbol{\theta})} = \frac{\int_{\boldsymbol{\phi}} p(\boldsymbol{\phi}, \boldsymbol{\theta} \mid H_1) d\boldsymbol{\phi}}{\int_{\boldsymbol{\phi}} p(\boldsymbol{\phi}, \boldsymbol{\theta} \mid H_0) d\boldsymbol{\phi}}, \tag{A.2}$$

where $\boldsymbol{\theta} = \theta_1, \ldots, \theta_n$ is a data set consisting of angles, and $\boldsymbol{\phi}$ is a vector of parameters belonging to the chosen model. For the von Mises distribution

$\boldsymbol{\phi} = (\mu, \kappa)^T$. Because the null hypothesis does not feature parameters and assigns equal probability to each data point, $m_0(\boldsymbol{\theta})$ depends only on the sample size. The circular uniform distribution has $p(\theta) = (2\pi)^{-1} \forall\, \theta \in [0, 2\pi)$, so the marginal likelihood for H_0 is obtained by

$$m_0(\boldsymbol{\theta}) = \prod_{i=1}^{n} p(\theta_i) = (2\pi)^{-n}. \tag{A.3}$$

The marginal likelihood of H_1 is given by

$$m_1(\boldsymbol{\theta}) = \int_{\boldsymbol{\phi}} f(\boldsymbol{\phi}, \boldsymbol{\theta} \mid H_1) d\boldsymbol{\phi} = \int_0^{\infty} \int_0^{2\pi} f(\mu, \kappa, \boldsymbol{\theta} \mid H_1) d\mu d\kappa, \tag{A.4}$$

where

$$f(\mu, \kappa, \boldsymbol{\theta} \mid H_1) \propto p(\mu, \kappa \mid H_1) f(\boldsymbol{\theta} \mid \mu, \kappa, H_1) \tag{A.5}$$

is the kernel of the posterior, where the prior $p(\mu, \kappa \mid H_1)$ must still be chosen, and $f(\mu, \kappa \mid \boldsymbol{\theta}, H_1)$ is the likelihood. The likelihood of the von Mises distribution is given by

$$f(\boldsymbol{\theta} \mid \mu, \kappa, H_1) = \prod_{i=1}^{n} \mathcal{M}(\theta_i \mid \mu, \kappa) = [2\pi I_0(\kappa)]^{-n} \exp\left\{R\kappa \cos(\bar{\theta} - \mu)\right\}, \tag{A.6}$$

where R is the resultant length and $\bar{\theta}$ is the mean direction.

For any prior $p(\mu, \kappa)$ that does not depend on μ, the Bayes factor simplifies to

$$\begin{aligned} BF_{10} &= (2\pi)^n \int_0^{\infty} p(\mu, \kappa) \int_0^{2\pi} [2\pi I_0(\kappa)]^{-n} \exp\left\{R\kappa \cos(\bar{\theta} - \mu)\right\} d\mu d\kappa & \text{(A.7)} \\ &= \int_0^{\infty} I_0(\kappa)^{-n} p(\mu, \kappa) \int_0^{2\pi} \exp\left\{R\kappa \cos(\bar{\theta} - \mu)\right\} d\mu d\kappa & \text{(A.8)} \\ &= 2\pi \int_0^{\infty} p(\mu, \kappa) \frac{I_0(R\kappa)}{I_0(\kappa)^n} d\kappa, & \text{(A.9)} \end{aligned}$$

where the last step uses the fact that $I_0(x) = [2\pi]^{-1} \int_0^{2\pi} \exp\{x \cos\theta\}\, d\theta$. Thus, computation of the Bayes factor requires only univariate integration.

A.3.1 Choosing priors

Choosing the prior for this hypothesis test is not trivial. In principle, the prior for $\{\mu, \kappa\}$ should capture our actual belief about the possible values of the parameters, given that the alternative hypothesis is true. Although

researchers are free to determine their own prior for this test, we propose some general guidelines for the set of possible priors to be considered here.

First, it should be noted that choosing improper priors generally do not result in useful Bayesian hypothesis tests. Therefore, proper priors will be used.

Second, if a test for circular uniformity is considered, the researcher will generally not already have an idea about the mean direction of the data if H_1 is true, because they are investigating whether there even is a preferred (mean) direction. Therefore, we suggest taking a circular uniform prior on μ. This is done by taking $p(\mu) = [2\pi]^{-1}$ and independent of κ, so that $p(\mu, \kappa) = p(\mu)p(\kappa) = p(\kappa)/(2\pi)$ and we can concern ourselves only with choosing the prior for κ.

Finally, a researcher that considers circular uniformity to be a reasonable hypothesis rarely expects strongly concentrated distributions, even if the alternative hypothesis were true. Therefore, we suggest setting a prior for κ that gives most of its probability to fairly low values of κ. Should the data follow a concentrated distribution anyway, the test will be powerful regardless.

In practice, whether these expectations are reasonable should be assessed by the researcher themselves. However, taking this approach allows us to build default methods that work well in most research scenarios in which the test would be applied. In the following sections, different choices for priors are considered, and for each the resulting test is assessed.

A.3.2 Priors based on the conjugate prior

A conjugate prior for the von Mises distribution was suggested by Guttorp & Lockhart (1988), and is given by

$$p(\mu, \kappa) \propto I_0(\kappa)^{-c} \exp\left\{R_0 \kappa \cos(\mu - \mu_0)\right\}, \tag{A.10}$$

where μ_0, R_0, and c are the prior mean, prior resultant length, and prior 'sample size', respectively. As discussed previously, we would like to remove the necessity to choose a prior mean μ_0. This can be done by putting a circular uniform prior on μ_0 and integrating it out so that

$$p(\mu, \kappa) \propto \int_0^{2\pi} [2\pi]^{-1} I_0(\kappa)^{-c} \exp\left\{R_0 \kappa \cos(\mu - \mu_0)\right\} d\mu_0 = \frac{I_0(R_0\kappa)}{I_0(\kappa)^c}, \tag{A.11}$$

which only depends on κ. Then, all that remains is choosing values for R_0 and c. It can easily be seen seen that imagining a single datapoint on the circle results in $R_0 = 1$ and $c = 1$, producing the constant prior on κ. Because

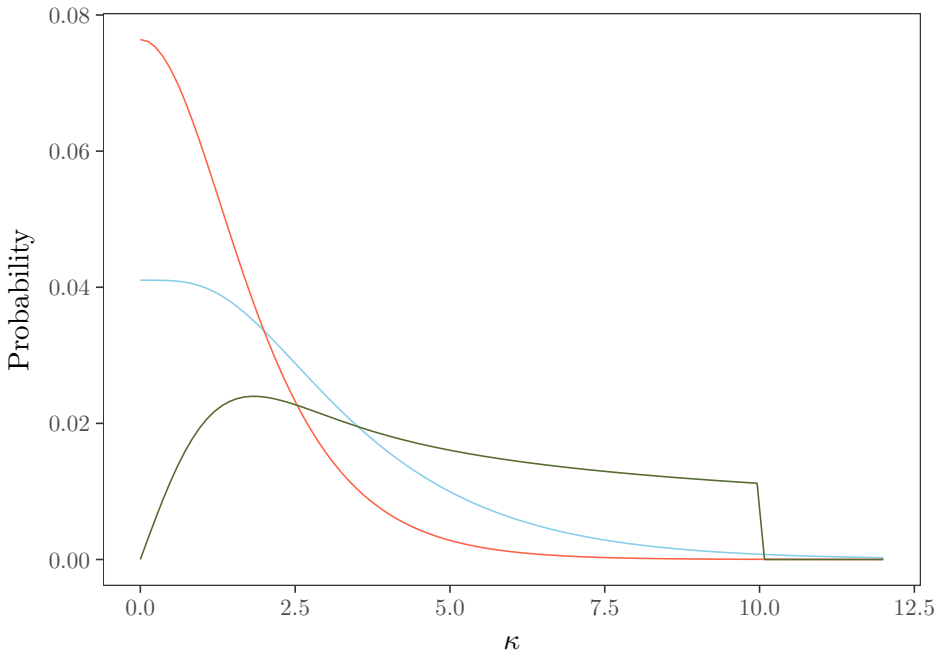

Figure A.1: Graphs of three different choices of priors for κ: Prior A.12 (red) has $R_0 = 0, c = 1$, prior A.13 (blue) has $R_0 = \sqrt{2}, c = 2$, and the Jeffreys prior (green) has $\kappa_u = 10$.

the constant prior is improper and therefore invalid for hypothesis testing, we examine two valid options instead.

First, the prior used by McVinish & Mengersen (2008) has $R_0 = 0, c = 1$, so that we obtain

$$p(\mu, \kappa) \propto I_0(\kappa)^{-1}. \tag{A.12}$$

This prior will be referred to as prior A.12, and is displayed in Figure A.1, in red.

Second, the prior could be taken to be proportional to the likelihood of an imagined dataset $\{a, a + \pi/2\}$, with a any angle. This imagined dataset has two angles at 90° from one another. This results in $R_0 = \sqrt{2}, c = 2$, so we obtain

$$p(\mu, \kappa) \propto I_0\left(\sqrt{2}\kappa\right) I_0(\kappa)^{-2}. \tag{A.13}$$

This prior will be referred to as prior A.13, and is displayed in Figure A.1, in blue. It can be seen that this prior has more mass at higher values of κ.

Denoting the normalizing constant of either prior by $g = 2\pi \int_0^\infty I_0(R_0\kappa) I_0(\kappa)^{-c} d\kappa$,

the marginal likelihood for H_1 for these priors is

$$m_1(\boldsymbol{\theta}) = \int_0^{\infty} \int_0^{2\pi} p(\mu, \kappa) f(\boldsymbol{\theta} \mid \mu, \kappa) d\mu d\kappa \tag{A.14}$$

$$= g\,[2\pi]^{-n} \int_0^{\infty} \frac{I_0(R_0\kappa)}{I_0(\kappa)^c} I_0(\kappa)^{-n} \int_0^{2\pi} \exp\left\{R\kappa \cos\left(\bar{\theta} - \mu\right)\right\} d\mu d\kappa \tag{A.15}$$

$$= g\,[2\pi]^{-(n+1)} \int_0^{\infty} I_0(R_0\kappa) I_0(R\kappa) I_0(\kappa)^{-(n+c)} d\kappa. \tag{A.16}$$

The Bayes factor in favor of the alternative is then

$$BF_{10} = \frac{m_1(\boldsymbol{\theta})}{m_0(\boldsymbol{\theta})} = [2\pi]^n m_1(\boldsymbol{\theta}) = g\,[2\pi]^{-1} \int_0^{\infty} I_0(R_0\kappa) I_0(R\kappa) I_0(\kappa)^{-(n+c)} d\kappa. \tag{A.17}$$

This can be computed by univariate numerical integration.

A.3.3 Jeffreys prior

The Jeffreys prior is a common choice for non-informative priors, especially in low-dimensional parameter spaces as is the case here. The Jeffreys prior is proportional to the square root of the determinant of the Fisher Information Matrix $\mathcal{I}(\boldsymbol{\phi})$ for a single observation, so that for the von Mises distribution it is given by

$$p(\boldsymbol{\phi}) \propto \sqrt{\det\left[\mathcal{I}(\boldsymbol{\phi})\right]} = \sqrt{\kappa A(\kappa) A'(\kappa)}, \tag{A.18}$$

where $A(\kappa) = I_1(\kappa)/I_0(\kappa)$ and $A'(\kappa) = \frac{d}{d\kappa} A(\kappa)$.

An attractive property of this prior is that it has $p(\kappa = 0) = 0$. However, this prior is improper, which means it can not be used directly in hypothesis testing. Therefore, we suggest to take a truncation of this prior from above at some value κ_u. A proper prior based on the Jeffreys prior is then given by

$$p(\mu, \kappa \mid \kappa_u) = \frac{I(\kappa < \kappa_u)\sqrt{\kappa A(\kappa) A'(\kappa)}}{2\pi \int_0^{\kappa_u} \sqrt{\kappa A(\kappa) A'(\kappa)} d\kappa}, \tag{A.19}$$

where $I(\cdot)$ is an indicator function. This prior with $\kappa_u = 10$ is shown in Figure A.1, in green.

To choose κ_u, it might be thought of as an upper bound for the values of κ for which we will be able to find support. If the data favors a value of κ higher than κ_u, the marginal likelihood of the alternative hypothesis H_1 will be underestimated, although H_1 will still be preferred. Conversely, it should be noted that even if the likelihood strongly suggests $\kappa < \kappa_u$, the

resulting Bayes Factor will still depend on κ_u through the integral in the normalizing constant. The concern that a somewhat arbitrary choice must be made can be alleviated somewhat by performing a sensitivity analysis. In Section A.3.4, it will be shown that the hypothesis test using this prior performs well even for some fixed values of κ_u.

The Bayes Factor is given by

$$BF_{10} = (2\pi)^n \int_0^\infty \int_0^{2\pi} p(\mu, \kappa) f(\boldsymbol{\theta} \mid \mu, \kappa) d\mu d\kappa \tag{A.20}$$

$$= \int_0^\infty p(\mu, \kappa) I_0(\kappa)^{-n} \int_0^{2\pi} \exp\left\{R\kappa \cos(\bar{\theta} - \mu)\right\} d\mu d\kappa \tag{A.21}$$

$$= 2\pi \left[\int_0^{\kappa_u} \sqrt{\kappa A(\kappa) A'(\kappa)} d\kappa\right]^{-1} \int_0^{\kappa_u} \sqrt{\kappa A(\kappa) A'(\kappa)} I_0(R\kappa) I_0(\kappa)^{-n} d\kappa. \tag{A.22}$$

A.3.4 Simulation

In order to assess the performance of the Bayesian hypothesis tests with a von Mises alternative and the three priors discussed previously, a simulation study was performed. One million datasets were sampled from the von Mises distribution with κ set to $\{0, 0.5, 1, 2, 5\}$, where $\kappa = 0$ was used three times more often as it represents H_0. Samples sizes were randomly selected from $\{2, \ldots, 15, 20, 30, \ldots, 190, 200\}$.

Figure A.2 shows the performance of $BF_{10} > 1$ as a decision criterion for all priors, as well as a plot of the obtained log Bayes factors. In general, all three tests perform well, and are particularly good at correctly classifying data generated under the null hypothesis. Prior A.12 and prior A.13 show very similar performance, although prior A.13 is more prone to select H_0. The Jeffreys prior with $\kappa_u = 20$ is even more prone to select H_0. When data is almost uniform with $\kappa = 0.5$, the tests need a large sample size to select H_1 more than half of the time (around $n > 50$ for prior A.12 and prior A.13, and $n > 100$ for the Jeffreys prior with $\kappa_u = 20$).

Compared to the error rates of the Rayleigh test, the current test has better power in all situations but those with $\kappa = .5, n > 30$ and $\kappa = 0, n < 30$. For those cases, it can be seen in the plots on the right of Figure A.2 that the Bayes factors that are produced are somewhat indecisive, so they may not be taken as evidence in favor of either hypothesis at all. Also, it can be seen that if H_0 is true, $p(H_0 \mid \boldsymbol{\theta}) \to 1$ as $n \to \infty$, which is not the case for the Rayleigh test.

It can be seen that in some cases, such as in A.2a with $\kappa = 0.5$, increasing the sample size from 1 to 10 actually decreases the probability of selecting

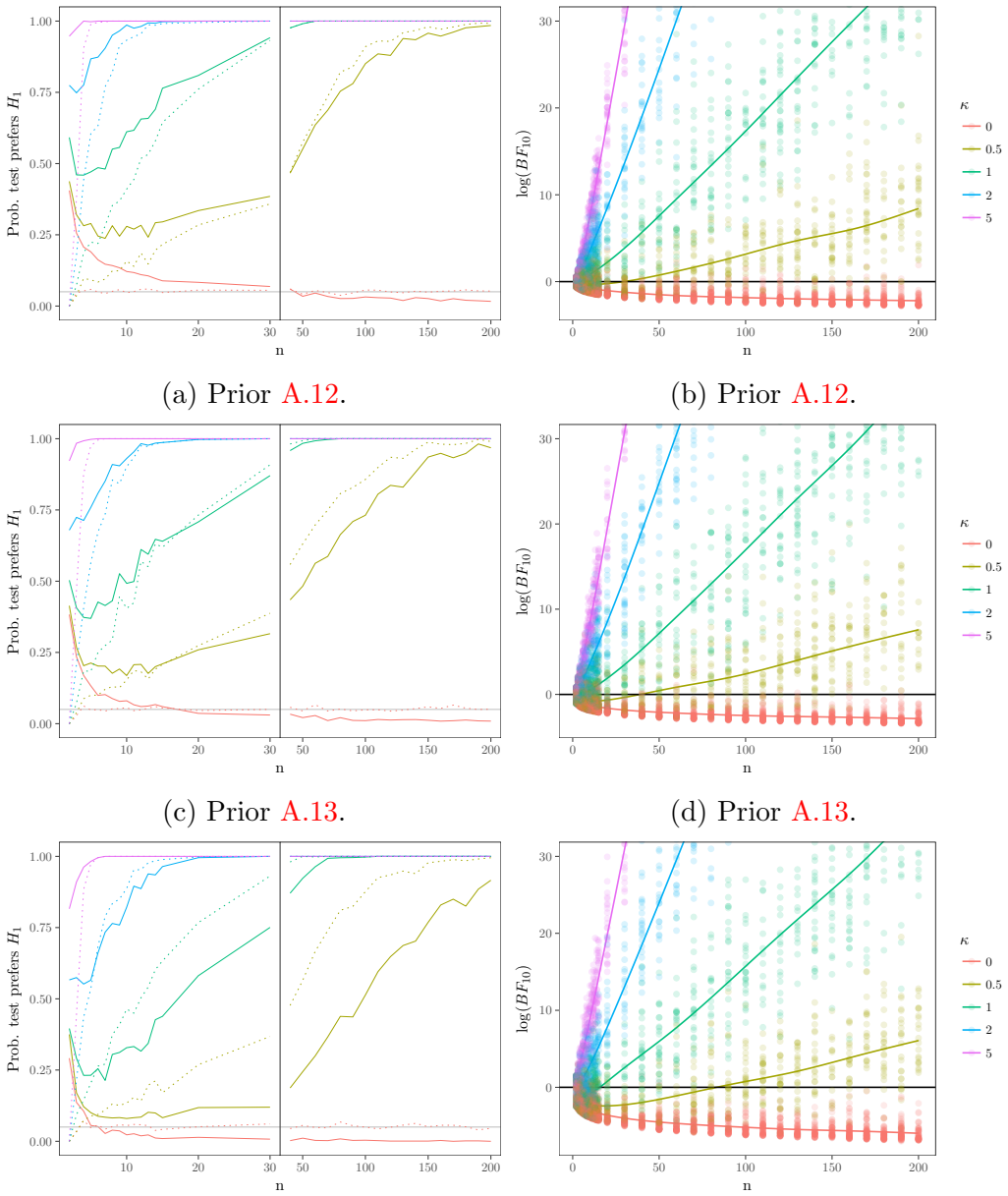

(a) Prior A.12. (b) Prior A.12.

(c) Prior A.13. (d) Prior A.13.

(e) Jeffreys prior with $\kappa_u = 20$. (f) Jeffreys prior with $\kappa_u = 20$.

Figure A.2: Results of the simulation study for prior A.12 (top), prior A.13 (middle) and the Jeffreys prior (bottom) with $\kappa_u = 20$. The left plots show the proportion of simulations which obtained a Bayes factor in favor of the alternative hypothesis ($BF_{10} > 1$). Error rates for the Rayleigh test with $\alpha = .05$ are provided as dotted lines, with the nominal significance displayed as a gray line at .05. The right plots show a subsample of the log-Bayes factors obtained for different sample sizes n and κ, as well as a solid trendline computed from the full simulation showing the average log Bayes factor for each sample size.

H_1, even though it is the true hypothesis. This is a known property of some Bayesian hypothesis tests. It should be noted that in these cases, the Bayes factor is shows indecision.

A.4 A Bayesian test for circular uniformity against a Kernel Density alternative

If the von Mises alternative is insufficient, the correct alternative distribution to test against is often unknown. A pure Bayesian approach could be to formulate a set of possible models, and choose between this set of alternatives. However, this requires attempting to fit an infinite set of models which might be hard to do in practice.

Instead, it may be useful to fit a very flexible model as the alternative, which can mimic the true distribution well, so as to provide an omnibus test against many possible models. A kernel density fulfills this role, being able to approximate any density given enough data. Recent developments of kernel density methods for circular data have focused on kernel density bandwith selection and kernel regression (Di Marzio et al., 2009; Oliveira et al., 2012; Di Marzio et al., 2013; Oliveira et al., 2014).

Here, we will build a test for circular uniformity which uses a von Mises kernel density as the alternative. The pdf of the kernel density based on a dataset $\mathbf{\Theta} = \Theta_1, \ldots, \Theta_n$ is given by

$$f(\theta \mid \mathbf{\Theta}, \kappa) = \frac{1}{n} \sum_{i=1}^{n} \mathcal{M}(\theta \mid \Theta_i, \kappa). \tag{A.23}$$

Our interest is to obtain a posterior for the bandwith κ, which is the only free parameter. However, if the likelihood is specified as

$$f(\mathbf{\Theta} \mid \kappa) = \prod_{j=1}^{n} f(\theta_j \mid \mathbf{\Theta}, \kappa) = \prod_{j=1}^{n} \sum_{i=1}^{n} \mathcal{M}(\theta_j \mid \Theta_i, \kappa). \tag{A.24}$$

then $\mathcal{M}(\theta_j \mid \Theta_i, \kappa) \to \infty$ if $i = j, \kappa \to \infty$. Therefore, following Hall et al. (1987), we specify the likelihood in a Leave-one-out cross-validation sense, by setting

$$f(\mathbf{\Theta} \mid \kappa) = \prod_{j=1}^{n} \sum_{i \neq j} \mathcal{M}(\theta_j \mid \Theta_i, \kappa). \tag{A.25}$$

This leads to the posterior

$$p(\kappa \mid \mathbf{\Theta}) \propto f(\kappa \mid \mathbf{\Theta}) p(\kappa) \tag{A.26}$$

where the prior for $p(\kappa)$ must still be set. Note that for this model, κ has a different interpretation than in the von Mises, so a different prior is in order. Specifically, in the von Mises model κ refers to the concentration of the full dataset, while in the kernel density model κ refers to the concentration around each separate data point. Therefore, higher values of κ should be considered likely a priori.

The Bayes factor is given by

$$BF_{10} = [2\pi]^n \int_0^\infty p(\kappa) \prod_{j=1}^{n} \sum_{i \neq j} [2\pi I_0(\kappa)]^{-1} \exp\{\kappa \cos(\theta_j - \Theta_i)\}\, d\kappa \tag{A.27}$$

$$= \int_0^\infty \frac{p(\kappa)}{I_0(\kappa)^n} \prod_{j=1}^{n} \sum_{i \neq j} \exp\{\kappa \cos(\theta_j - \Theta_i)\}\, d\kappa, \tag{A.28}$$

which is once again computed by univariate numerical integration.

For priors of the type discussed in Section A.3.2, the Bayes factor for some R_0 and c can be written as

$$BF_{10} = \left[\int_0^\infty I_0(R_0\kappa) I_0(\kappa)^{-c} d\kappa\right]^{-1} \int_0^\infty I_0(R_0\kappa) I_0(\kappa)^{-(n+c)} \prod_{j=1}^{n} \sum_{i \neq j} \exp\{\kappa \cos(\theta_j - \Theta_i)\}\, d\kappa. \tag{A.29}$$

Another good option for the kernel density model specifically is the Jeffreys prior discussed in A.3.3, as it allows tuning κ_u to accomodate reasonably high values for the concentration. For this prior, the Bayes factor can be written as

$$BF_{10} = \left[2\pi \int_0^{\kappa_u} \sqrt{\kappa A(\kappa) A'(\kappa)} d\kappa\right]^{-1} \int_0^{\kappa_u} \frac{\sqrt{\kappa A(\kappa) A'(\kappa)}}{I_0(\kappa)^{n+1}} \prod_{j=1}^{n} \sum_{i \neq j} \exp\{\kappa \cos(\theta_j - \Theta_i)\}\, d\kappa. \tag{A.30}$$

A.4.1 Simulation

We assess the performance of the kernel based circular uniformity test for antipodal von Mises. The antipodal von Mises is an antipodally symmetric mixture of two von Mises distributions, where data was obtained by drawing from the pdf

$$f(\theta \mid \mu, \kappa) = \frac{1}{2}\mathcal{M}(\theta \mid \mu, \kappa) + \frac{1}{2}\mathcal{M}(\theta \mid \mu + \pi, \kappa). \tag{A.31}$$

This alternative hypothesis is chosen to be especially hard for the von Mises based tests developed in Section A.3. The setup in terms of sample sizes and chosen true values for κ is the same as in Section A.3.4.

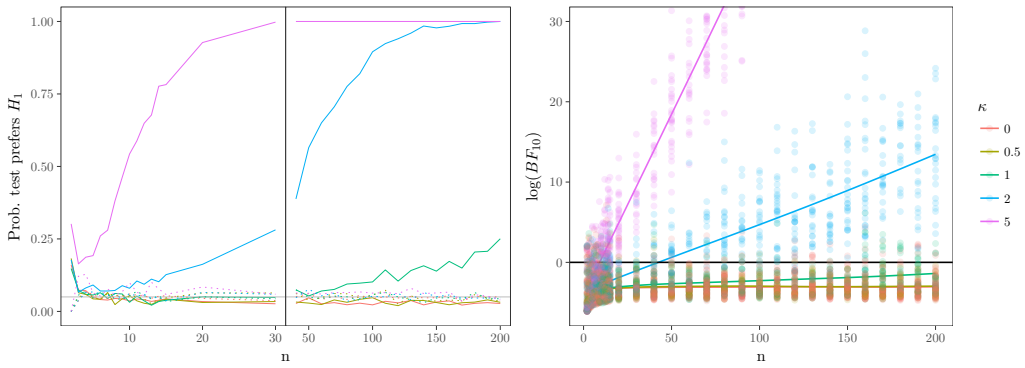

(a) (b)

Figure A.3: Performance for data from the antipodal von Mises distribution with various true values for κ. The left plot shows the proportion of simulations which obtained a Bayes factor in favor of the alternative hypothesis ($BF_{10} > 1$). Error rates for the Rayleigh test with $\alpha = .05$ are provided as dotted lines, with that nominal significance displayed as a gray line at .05. The right plot shows a subsample of the log Bayes factors obtained for different sample sizes n and κ, as well as a solid trendline computed from the full simulation showing the average log Bayes factor for each sample size.

Results for data generated from the antipodal von Mises distribution are displayed in Figure A.3. It can be seen that the Rayleigh test performs abysmally, which is expected, because it is based on rejection of H_0 for large values of the resultant length, which for the antipodal von Mises is zero on average. Our method picks up the difference with reasonable power when data was generated with $\kappa > 2$. In order to detect nonuniformity for antipodal von Mises data with $\kappa = 1$, a very large sample is needed, but it must be noted that antipodal data with small κ is almost uniform. Evidence in favor of H_0 is collected slowly, but with larger sample sizes, H_0 is selected more and more.

A.5 Examples

In this section, the method will be applied to two examples.

In a classic experiment on pigeon homing (Schmidt-Koenig, 1963), the vanishing angles of homing pigeons were measured, with the initial question of whether the vanishing direction is circular uniform or follows some other circular distribution. Two datasets from this experiment are depicted in Figure A.4. In one experiment, also provided in Fisher (1995), fifteen homing

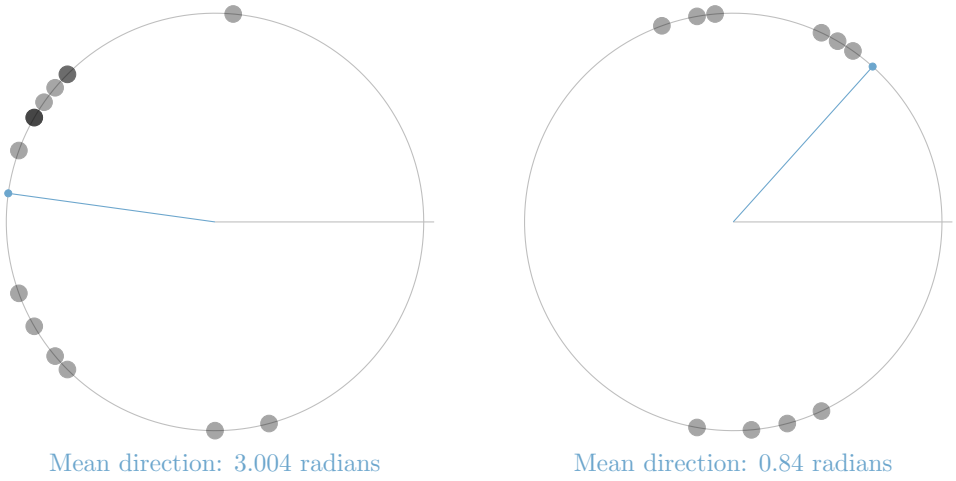

(a) Example data 1. (b) Example data 2.

Figure A.4: The two example datasets. For each subfigure, the blue line between the center and the circle depicts the mean direction, while the gray line depicts 0°.

pigeons were measured to have vanishing directions given by

$$\{85°, 135°, 135°, 140°, 145°, 150°, 150°, 150°, 160°, 285°, 200°, 210°, 220°, 225°, 270°\}$$

(Figure A.4a). In another dataset, provided in Mardia & Jupp (2000), ten pigeons were measured to have vanishing directions $\{55°, 60°, 65°, 95°, 100°, 110°, 260°, 275°, 285°, 295°\}$ (Figure A.4b).

A.5.1 Homing pigeon example 1

The results for the first dataset are given in Table A.1. For this dataset, reasonable hypotheses are that the data are either circular uniform (which we call H_0), or that the data follow a symmetric unimodal distribution, where we pick the von Mises distribution (which we call $H_{\mathcal{M}}$ here). These two hypotheses are evaluated as discussed in Section A.3.2, using prior A.12 given by $p(\kappa) \propto I_0(\kappa)^{-1}$ because a low concentration is expected. Table A.1 denotes the results of our hypothesis test, as well as the Rayleigh test for comparison. The log marginal likelihood of H_0 is -27.57, while the log marginal likelihood of $H_{\mathcal{M}}$ is -23.92, so $H_{\mathcal{M}}$ is most supported by the data. In fact, the Bayes factor in favor of $H_{\mathcal{M}}$ is 38.54, so that the posterior probability of $H_{\mathcal{M}}$ is 0.975, which constitutes strong support for this hypothesis.

A.5.2 Homing pigeon example 2

For the second dataset, the hypothesis that the data is bimodal is also reasonable, although we might not want to assume antipodal symmetry. To demonstrate the flexibility of the Bayesian approach, we evaluate three hypotheses jointly. The hypotheses are circular uniformity (H_0), the von Mises distribution ($H_{\mathcal{M}}$), and the kernel density alternative (H_k) described in Section A.4. For the von Mises distribution, the same conjugate prior is used as before, $p(\kappa) \propto I_0(\kappa)^{-1}$. For the kernel density alternative, higher concentrations are more plausible than for the von Mises hypothesis, because dispersion in the final kernel density model is not exclusively determined by κ, but also by the spread of the data. Therefore, we pick the Jeffreys prior here, truncated above at 40. In a small sensitivity analysis for the truncation value (not reported further), the Bayes factor was robust to truncation values above 20, although setting the value extremely high will influence the marginal likelihood, and the inference as a result.

In order to compare the relative probability of each hypothesis, posterior model probabilities were computed. When choosing between a set of p models, we can compute the posterior model probability of model i, assuming equal prior model probabilities, as

$$p(H_i \mid \boldsymbol{\theta}) = \frac{m_i(\boldsymbol{\theta})}{\sum_{j=1}^{p} m_j(\boldsymbol{\theta})}, \tag{A.32}$$

where $m_a(\boldsymbol{\theta})$ denotes the marginal likelihood of model H_a. This will provide the relative probabilities of the models that are assessed.

Results are displayed in Table A.2. The Rayleigh test is not significant ($p = 0.62$), suggesting no departure from uniformity. In contrast, our comparison of hypotheses shows a preference for the kernel density alternative, giving it a posterior model probability of 0.954. This can be seen as evidence that the data generation distribution is likely neither the circular uniform distribution nor the von Mises distribution. Rather, the correct model was likely not included in the set of models that were assessed, which should motivate the researcher to further investigate possible models. This result is easy to interpret and understand, and provides a more complete picture than the usual frequentist test.

Table A.1: Results of example 1.

Bayes Factor	$p(H_0 \mid \boldsymbol{\theta})$	$p(H_{\mathcal{M}} \mid \boldsymbol{\theta})$	Rayleigh Statistic	Rayleigh p-value
38.542	0.025	0.975	0.637	0.001

Table A.2: Results of example 2.

$p(H_0 \mid \boldsymbol{\theta})$	$p(H_{\mathcal{M}} \mid \boldsymbol{\theta})$	$p(H_k \mid \boldsymbol{\theta})$	Rayleigh Statistic	Rayleigh p-value
0.034	0.012	0.954	0.223	0.620

A.6 Discussion

Bayesian hypothesis tests for assessing circular uniformity were developed in this paper. The Bayesian approach provides three major advantages for this type of hypothesis. First, the hypothesis of circular uniformity is precisely the type of hypothesis which might be true in reality, so that we would want to choose H_0 if the data supports it. The available frequentist tests do not support this, as an insignificant p-value does not allow us to draw conclusion on whether H_0 is true. Second, the Bayesian hypothesis test allows us to quantify the strength of the evidence, either in an odds ratio in the Bayes factor, or in an intuitive probability in the posterior model probability, which is more informative than the simple dichotomous decisions provided by null hypothesis tests. Third, the Bayesian framework allows us to add additional hypotheses to the comparison quite easily. In example 2 in Section A.5.2, this is used by having the kernel density alternative effectively act as a "none of the above" category, motivating the researcher to search for a model that fits the data better.

Among the most central critiques of the Bayesian method (and Bayesian testing in particular) lies the difficulty in choosing priors, as this seemingly requires us to know in advance what distribution the data may have should the alternative hypothesis be true. Moreover, the conclusions drawn in Bayesian hypothesis tests are often highly dependent on seemingly arbitrary quantities, most notably the parameters of the prior distribution. However, when choosing a frequentist test for circular uniformity, one is faced with a plethora of tests (see Section A.2) which are each most powerful against different alternatives. This choice closely mirrors the choice of the prior in the alternative hypothesis of a Bayesian hypothesis test. For example, this can be seen in Landler et al. (2018), where different tests are recommended for different expected alternative distributions. In either case, we must use our expectations of the distribution of the data, should the alternative hypothesis be true. Furthermore, in Section A.3.1 it was shown how the selection of priors can be dealt with to circumvent the concerns about their influence on the results.

Beyond circular uniformity, previously Bayesian analyses of circular models have been investigated from several viewpoints. Bayesian model assessment has been investigated for wrapped models (Ravindran & Ghosh, 2011),

projected normal models (Nuñez-Antonio et al., 2015) and semiparametric intrinsic models (Bhattacharya & SenGupta, 2009; George & Ghosh, 2006). However, the only previously discussed Bayesian test for circular uniformity the authors are aware of is in McVinish & Mengersen (2008), where the alternative hypothesis is a Dirichlet process mixture of triangular distributions. Compared to that work, our focus is on adding parametric alternatives, simplifying computation, assessing performance of the Bayes factor, developing accessible computational tools and comparison of this method to frequentist methods, both conceptually and in a simulation study. Computation involved in evaluating the marginal likelihood of our models has been reduced to simple univariate numerical integration, which makes running these tests more straightforward and markedly faster. Also, the tools used in this paper are easily available from R through the package `BayesCircIsotropy`, available on GitHub.

Assessing the performance of the method, it was shown that the test is often powerful in selecting the correct model, both for the data from the null hypothesis as well as the alternative. The main difficulty in practice, as is often the case in Bayesian analyses, is selecting a prior. In general, choosing a prior with larger variance will allow us to find support for a larger set of true models, but required sample size to find this support will increase. As is shown in the simulation, some default options perform quite well in common research settings. In practice, it is often advisable to perform a prior sensitivity analysis.

Although the philosophical underpinnings of Bayesian hypothesis testing are not the focus of this paper, we will shortly connect the current work with the ongoing discussion. The Bayesian framework is sometimes touted as inductive, which would suggest Bayesian model comparison is sufficient to draw scientific conclusions from data. Recently, Gelman & Shalizi (2013) refute this claim outright and advocate model checking, as models are usually wrong. We generally follow the view of Morey et al. (2013) and note that tools developed here are useful to give preference between models, but do not necessarily provide inductive evidence in favor of the model assessed, such as the von Mises model. The kernel density alternative presented in Section A.4 functions as a form of model checking, circumventing the step of deciding on test statistics to be used in a posterior predictive check, or deciding on a specific alternative hypothesis to test against.

Finally, the approach of this paper is to apply Bayesian hypothesis testing to basic circular data analyses. Future work might attempt to obtain easily computable marginal likelihoods for more complex models. In circular data analysis, model selection is an important avenue that requires more attention.

A.7 Acknowledgements

This work was supported by a —— grant awarded to —— from —— (——).

Appendix B

Mixtures of Peaked Power Batschelet Distributions for Circular Data With Application to Saccade Directions

B.1 Introduction

Eye movements are commonly used to study aspects of cognition and its development (Itti & Koch, 2001; Henderson, 2003). Eye movements consist of point fixations and movements between fixations called saccades. In particular, eye movements are of paramount importance in studying the top-down division of attention. For a review, see Rayner (2009).

In eye movement research, a major quantity of interest is the *saccade direction*, the angle between two consecutive fixations. For example, one topic of interest using saccade directions investigates the existence of general directional biases (Tatler & Vincent, 2009), such as a preference for saccades along the horizontal axis (Foulsham et al., 2008) or a preference for leftward saccades (Foulsham et al., 2013). Another topic of interest is eye movement behaviour when reading (Rayner, 2009). Furthermore, distributions of eye movement directions are used to assess the closeness of algorithms to human performance on a variety of eye movement tasks, such as visual search (Najemnik & Geisler, 2008) and saccadic decision making (Tatler et al., 2017; Engbert et al., 2015; Le Meur & Coutrot, 2016).

Previously, it has been difficult to directly analyze a sample of saccade directions. One pragmatic solution to the difficulty of analyzing saccade directions is categorizing the angles in a number of general directions, such

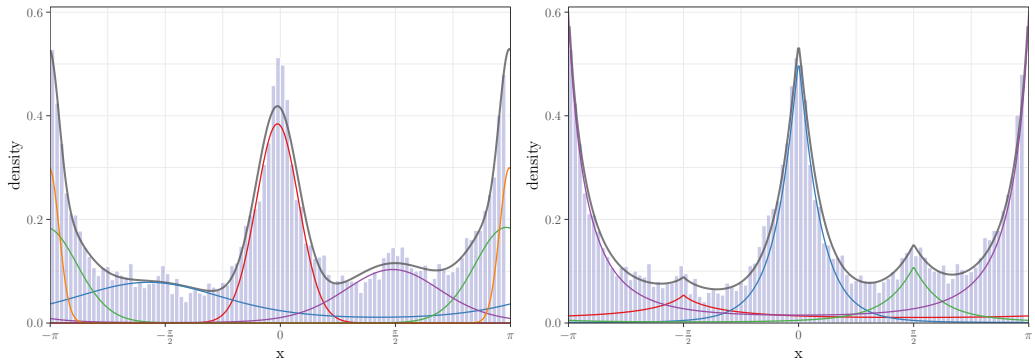

(a) Von Mises mixtures through `movMF`. (b) Proposed method.

Figure B.1: A comparison of two approaches of analyzing saccade direction. Each colored distribution represents a single component of the mixture model.

as in Foulsham et al. (2008). However, such analyses have reduced power, provide less precise interpretation, and require arbitrary selection of a method of categorization.

A natural model of saccade directions can be obtained by viewing saccade directions as circular data, that is, data measured in angles. Circular data differ from linear data in the sense that circular data are measured in a periodical sample space. For example, an angle of 1° is quite close to an angle 359°, although linear intuition suggests otherwise. Circular data are frequently encountered in scientific fields as diverse as life sciences (Mardia, 2011), behavioural biology (Bulbert et al., 2015), cognitive psychology (Kaas & Van Mier, 2006), bioinformatics (Mardia et al., 2008), political sciences (J. Gill & Hangartner, 2010) and environmental sciences (Arnold & SenGupta, 2006). In this study, a model will be developed that leans on the field of circular statistics (Fisher, 1995; Mardia & Jupp, 2000; Pewsey et al., 2013) to provide satisfying inference for saccade direction data.

Previously, Van Renswoude et al. (2016) used mixtures of von Mises distributions to model saccade direction data, using the R package `movMF` (Hornik & Grün, 2014). The `movMF` package was developed in the more general case for von Mises-Fisher mixtures of distributions on $p-$dimensional hyperspheres, with circular mixtures resulting as a special case. The van Renswoude saccade direction data and the von Mises mixture fit are displayed in Figure B.1a. It can be seen that the peakedness of the data is not captured well. The peaked mixture model in Figure B.1b is the final model to be introduced in this work. It naturally incorporates peakedness

and requires fewer parameters. It can clearly be seen that using the von Mises mixture approach for saccade direction data is not a natural fit, and as such has major drawbacks.

In this paper, four major drawbacks of analyzing saccade directions using the von Mises mixture method of Hornik & Grün (2014) will be addressed. First, the `movMF` approach provides estimates for the parameters of the model by using the Expectation-Maximization (EM) algorithm, but no measure of their uncertainty, such as confidence intervals or standard errors. Second, it can be seen that saccade direction distributions are very often sharp-peaked or flat-topped distributions, which are not directly modeled by this approach. Instead, the mixture model will deal with peaked data by fitting multiple components on a single mode, which precludes interpretation of the component parameters. Third, because the mixture model deals with peakedness by fitting multiple components for a single mode, it is impossible to compare variances of components, which is something of interest in many saccade direction studies, such as in Van Renswoude et al. (2016). Fourth, there is often a desire to fix component means (or other parameters) to pre-specified values, in order to improve power, which is not possible currently.

The model that will be developed in this paper for saccade direction data has two main characteristics. First, it will be a mixture of circular distributions. Second, it will employ flexible distributions in order to naturally model sharp-peaked and flat-topped components. Inference will be developed in a frequentist framework through an EM-algorithm and the bootstrap, and in a Bayesian framework through MCMC sampling. In order to speed up the required computations, a new distribution will be introduced that mimics the behaviour of the symmetric density introduced in Jones & Pewsey (2012).

As a motivating example, this study will rely on saccade direction data which was previously published on in Van Renswoude et al. (2016). The main interest in this work is in describing behavioural differences in free-viewing between adults and infants (see also Aslin (2007)). The data consists of 12367 saccades from adults and 4832 saccades from infants. For details on data collection, see Van Renswoude et al. (2016). This data is plotted in Figure B.2. Because the hypotheses of interest inform the development of the model, they will be revisited here. First, the researchers are interested in reaffirming a horizontal bias, that is, there are more saccade directions along the horizontal axis than the vertical axis. Second, infants are expected to have larger variance in their saccade directions. Third, the researchers are interested in the difference in the horizontal bias of infants and adults. For all of these hypotheses, currently one would be limited to descriptive analyses. The methods developed in this paper will allow full statistical inference. The methods are available in the `R` package `flexcircmix`, freely

available on GitHub.

The structure of this paper will proceed as follows. In Section B.2, the base distribution of the mixture model will be discussed, and the Power Batschelet distribution will be introduced. Inference for the resulting mixture model will be discussed in Section B.3. The method will be illustrated on both synthetic data and the van Renswoude data in Section B.4. Finally, some concluding remarks will be given in Section B.5.

B.2 Family of Batschelet Distributions

In this section, we will introduce Batschelet-type distributions. First, the Inverse Batschelet distribution of Jones & Pewsey (2012) will be recapped. Then, this approach will be adapted into the Power Batschelet distribution. Lastly, a note on computing the circular variance for such distributions will be given.

B.2.1 Inverse Batschelet distribution

The Inverse Batschelet distribution is a peaked or flat-topped circular distribution. It is constructed by modifying a base distribution, for which the von Mises distribution will be used. The von Mises distribution can be seen as a circular analogue to the normal distribution. In the following, it will be introduced shortly.

Denote the unit circle by $\mathbb{S}^1$, and the set of observed angles (in radians) by $\boldsymbol{\theta} = \theta_1, \ldots, \theta_n$, with $\theta_i \in \mathbb{S}^1$. For notational simplicity, we assume $\theta \in [-\pi, \pi)$. The von Mises distribution is given by

$$\mathcal{M}(\theta \mid \mu, \kappa) = [2\pi I_0(\kappa)]^{-1} \exp\left\{\kappa \cos(\theta - \mu)\right\}, \tag{B.1}$$

where θ is the observed angle, $\mu \in [-\pi, \pi)$ is the mean direction, $\kappa \in \mathbb{R}^+$ is a concentration parameter and $I_0(\cdot)$ is the modified Bessel function of the first kind and order zero. Note that this density is periodic, so $\mathcal{M}(\theta \mid \mu, \kappa) = \mathcal{M}(\theta + 2k\pi \mid \mu, \kappa)$, $\forall\ k \in \mathbb{Z}$. Various von Mises densities are displayed in Figure B.1a as the separate components of the mixture.

Clearly, saccade directions tend to follow more peaked densities than the von Mises density. Two approaches to incorporate peakedness in the model are the Jones-Pewsey distribution (Jones & Pewsey, 2005) and the Inverse Batschelet distribution (Jones & Pewsey, 2012). Both options have the von Mises distribution as a special case. However, the latter is of somewhat simpler form and allows for more peaked distributions, so it will be employed here.

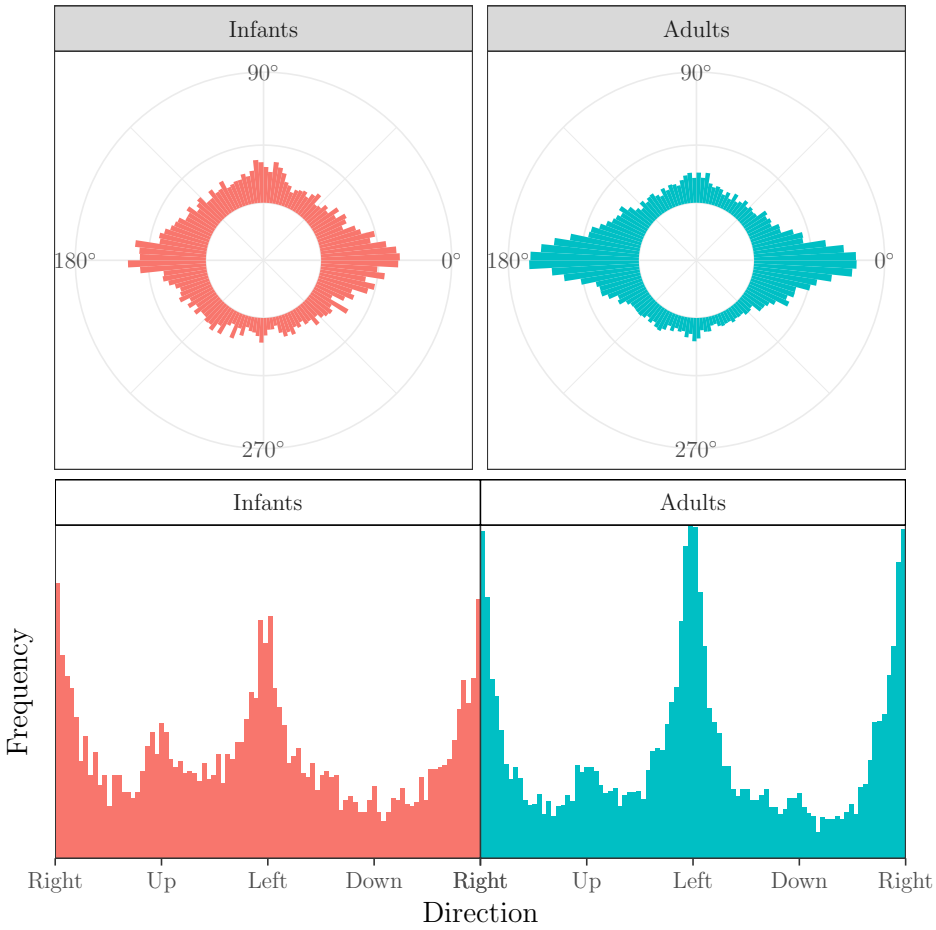

Figure B.2: Plots of the example data. The top plot provides the data in polar coordinates. The bottom plot shows the data on the real line, where the left and right sides of the plot represent the same point on the circle.

The core idea of the peaked densities developed in Batschelet (1981) is that given a circular density $f(\theta)$, a new distribution emerges if we take $f(\tau(\theta))$ for some bijective function τ which maps the circle onto itself. We will refer to all distributions obtained by this construction as **Batschelet distributions**, possibly with a prefix relating to the specific bijective function τ used. Attention will be limited to using the von Mises density as the base distribution f, such that we will work in practice with $f_\kappa(\tau(\theta-\mu))$, with κ the concentration parameter of the von Mises distribution.

The function originally used by Batschelet (1981) is given by

$$\tau(\theta) = \theta + \lambda \sin\theta, \tag{B.2}$$

where the peakedness parameter $\lambda \in [-1, 1]$ can be used to obtain a family of flat-topped densities. Using the inverse of $\tau(\theta)$ instead results in a family of peaked densities (Abe et al., 2010; Pewsey et al., 2011). A family of densities incorporating both flat-topped and peaked members was developed in Jones & Pewsey (2012) and will be employed here.

The von Mises based symmetric Inverse Batschelet density is given by

$$f(\theta \mid \mu, \kappa, \lambda) = [2\pi I_0(\kappa) K_{\kappa,\lambda}]^{-1} \exp\{\kappa \cos t_\lambda(\theta - \mu)\} \tag{B.3}$$

where

$$t_\lambda(\theta) = \frac{1-\lambda}{1+\lambda}\theta + \frac{2\lambda}{1+\lambda} s_\lambda^{-1}(\theta) \tag{B.4}$$

with $s_\lambda^{-1}(\theta)$ being the inverse of $s_\lambda(\theta) = \theta - \frac{1}{2}(1+\lambda)\sin(\theta)$, and

$$K_{\kappa,\lambda} = \frac{1+\lambda}{1-\lambda} - \frac{2\lambda}{1-\lambda} \int_{-\pi}^{\pi} [2\pi I_0(\kappa)]^{-1} \exp\left\{\kappa \cos\left(\theta - (1-\lambda)\sin(\theta)/2\right)\right\} d\theta. \tag{B.5}$$

Note that $t_\lambda(\theta)$ is not available analytically because $s_\lambda^{-1}(\theta)$ is not. Therefore, evaluation of the density requires both numerical integration and numerical inversion. The density is plotted with various values of λ in Figure B.3a. It can be seen that the peaked distribution observed for the saccade data can be obtained from this distribution when $0 < \lambda \leq 1$.

Although for many applications the computational burden of numerically inverting a function for each density evaluation is acceptable, such computations quickly become burdensome upon incorporation of the density into a larger model, such as a mixture model. This same can occur when using certain methods for uncertainty quantification, such as MCMC or the bootstrap. Therefore, in order to be able to employ Batschelet distributions in a broader context of models, an alternative to $t_\lambda(\theta)$ will be introduced in the following section. The major advantage will be that the alternative will not require numerical inversion.

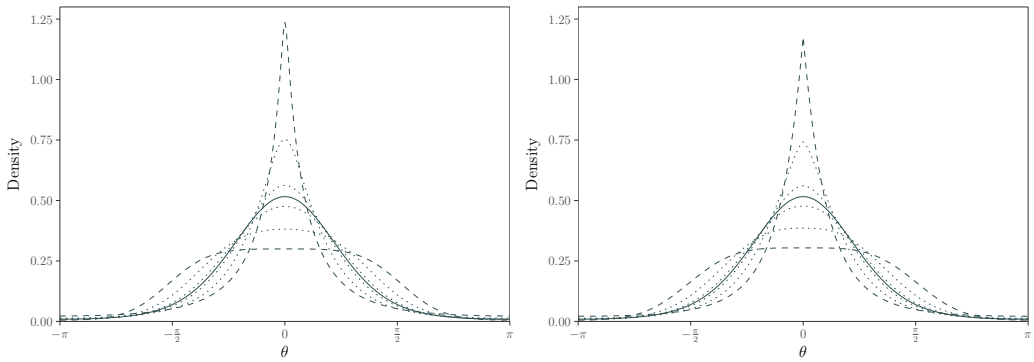

(a) Inverse Batschelet distribution. (b) Power Batschelet distribution.

Figure B.3: Two types of Batschelet distributions, based on the von Mises distribution with $\mu = 0, \kappa = 2$. In order of increasing height at $\theta = 0$, the peakedness parameter $\lambda = \{-.8, -.4, -.1, 0, .1, .4, .8\}$. In each figure, $\lambda = \{-.8, .8\}$ are dashed, while $\lambda = 0$ is a solid black line, with all others dotted. It can be seen that the densities are extraordinarily similar.

B.2.2 Power Batschelet distribution

In order to improve computational efficiency in more complex models, $t_\lambda(\theta)$ can be replaced by a function of similar shape, but more appealing computational properties. We propose

$$t^*_\lambda(\theta) = \text{sign}(\theta)\pi \left(\frac{|\theta|}{\pi} \right)^{\gamma(\lambda)}, \tag{B.6}$$

with $\gamma(\lambda) \in \mathbb{R}^+$, which has the basic properties required of it, namely to be a mapping of the circle onto itself, so long as $-\pi \leq \theta \leq \pi$ is assumed. In practice, this property is generally forced upon the original data θ_o by taking $\theta = [(\theta_o + \pi) \mod 2\pi] - \pi$. Note this does not change the angle, merely its numerical representation.

Next, the function $\gamma(\lambda)$ should be chosen such that changing λ mimics the behaviour of parameter λ of the Inverse Batschelet distribution in Equation B.3. First, in order to keep the parametrization where $-1 \leq \lambda \leq 1$ with negative values corresponding to flat-topped densities, take

$$\gamma(\lambda) = \frac{1 - c\lambda}{1 + c\lambda}, \tag{B.7}$$

where c is some fixed constant, chosen such that t^*_λ closely approximates t_λ. In order to choose c, the difference between t^*_λ and t_λ was numerically minimized

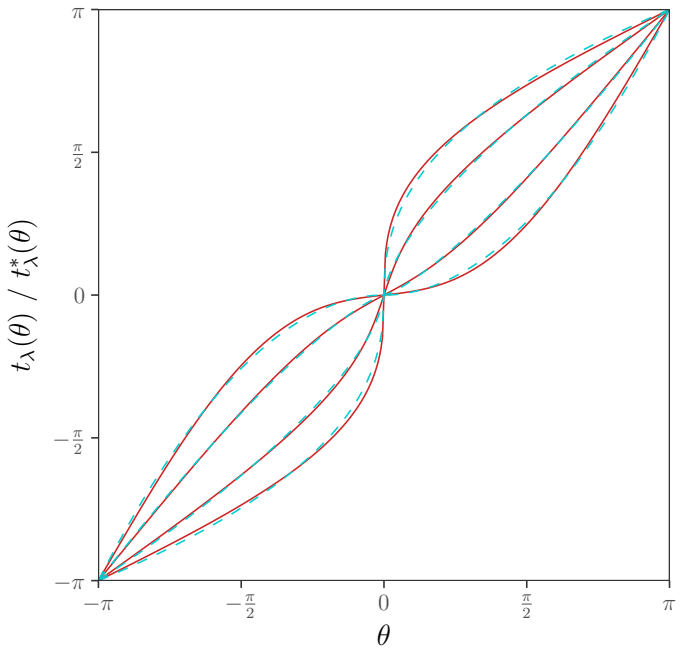

Figure B.4: Comparison of t^*_λ (blue, dashed) used for the Power Batschelet distribution and t_λ (red, solid) used for the Inverse Batschelet distribution, with, in order of increasing height at $\pi/2$, peakedness parameter $\lambda = \{-.8, -.3, .5, 1\}$.

over values of c,[1] resulting in $c = 0.4052284$. The two functions t^*_λ and t_λ, are plotted together in Figure B.4. It is clear that the functions, although they do not exactly coincide, are strongly comparable. In practical use, the resulting density of the Power Batschelet distribution was found to be evaluated more than several hundred times faster than the Inverse Batschelet distribution. The resulting density is shown in Figure B.3b, where again, we conclude that the densities are strongly similar.

The new continuous function $t^*_\lambda(\theta)$ is trivial to compute and has several attractive properties. For example, note that the we simply have $t^{*-1}_\lambda(\theta) = t^*_{-\lambda}(\theta)$.

[1] To be precise, c was chosen such that for a specific λ, the mean absolute difference between $t_\lambda(\theta)$ and $t^*_\lambda(\theta)$ evaluated at 100 points evenly spread on the circle was minimized. The final $c = 0.4052284$ is the average between the optimal c for $\lambda = 1$ and $\lambda = -1$. The two functions do not have coincide exactly, as being able to directly compare values for λ is only used for interpretability.

Using this function, the Power Batschelet distribution is then defined as

$$f_{PB}(\theta \mid \mu, \kappa, \lambda) = [K^*_{\kappa,\lambda}]^{-1} \exp\{\kappa \cos t^*_\lambda(\theta - \mu)\}, \tag{B.8}$$

where

$$t^*_\lambda(\theta) = \text{sign}(\theta)\pi \left(\frac{|\theta|}{\pi}\right)^{\frac{1-0.4052284\lambda}{1+0.4052284\lambda}}, \tag{B.9}$$

and the inverse of the normalizing constant is

$$K^*_{\kappa,\lambda} = \int_{-\pi}^{\pi} \exp\{\kappa \cos t^*_\lambda(\theta - \mu)\} d\theta, \tag{B.10}$$

which must still be numerically integrated. The Power Batschelet distribution generally shares the properties of the Inverse Batschelet distribution, in that it is symmetric around μ and unimodal. Several further properties of this distribution are discussed in Appendix .2.

A possible problem is that if $0 < \lambda \leq 1$, we have $0 < \gamma(\lambda) < 1$, and thus $\frac{dt^*_\lambda(\theta)}{d\theta}\Big|_{\theta=0} = \infty$, so the function is not twice differentiable for that range of λ, nor smooth. That is, the probability density is continuous, and so is $t^*_\lambda(\cdot)$, but its derivative is not, nor is $\frac{df_{PB}(\theta|\mu,\kappa,\lambda)}{d\theta}$. As a result, not all regularity conditions for maximum likelihood estimation are not met, in very similar fashion to the commonly used Laplace (double exponential) distribution. In addition, due to the role of this distribution as a close approximation to the Inverse Batschelet, results for the Power Batschelet distribution can be seen as an approximation to the results of the Inverse Batschelet distribution.

If one is concerned about the regularity conditions for the Power Batschelet distribution, the Inverse Batschelet distribution is an alternative which is also implemented in the package `flexcircmix`. However, any analysis with that method may several orders of magnitude longer. In practice, we have not run into any issues related to this, so we prefer the computational efficiency of the Power Batschelet distribution.

B.2.3 Measures of circular dispersion

While for the von Mises distribution the circular variance is known to decrease monotonically with increasing κ regardless of the other parameters, this does not hold true for Batschelet distributions, because the peakedness parameter λ also exerts strong influence on the circular variance. However, it is desirable to compare the circular variance across components in the mixture model discussed in the following sections. Therefore, we compute the circular variance v, given by $v = 1 - \rho$, where ρ is the population resultant

length associated with the circular density $f(\theta \mid \boldsymbol{\phi})$, where $\boldsymbol{\phi}$ denotes a vector of parameters. In the general case, it is given by

$$\rho = E[\cos\Theta] = \int_{-\pi}^{\pi} \cos\theta \; p(\theta \mid \boldsymbol{\phi}) d\theta. \tag{B.11}$$

If the data has the von Mises distribution, it is known that $\rho = \frac{I_1(\kappa)}{I_0(\kappa)}$ (Mardia & Jupp, 2000), but in general, computing ρ will require numerical integration. Denoting the normalizing constant by $C(\kappa, \lambda) = \left[\int_{-\pi}^{\pi} \exp\{\kappa \cos t_\lambda(\theta)\} d\theta\right]^{-1}$, we have

$$\rho(\kappa, \lambda) = E[\cos\Theta] = \int_{-\pi}^{\pi} \cos\theta \; p(\theta \mid \mu, \kappa, \lambda) d\theta \tag{B.12}$$

$$= C(\kappa, \lambda) \int_{-\pi}^{\pi} \cos\theta \;\; \exp\{\kappa \cos t_\lambda(\theta)\} d\theta. \tag{B.13}$$

This means we should need at most two numerical integrations. Lastly, the circular standard deviation can be computed by $\sigma_c = \sqrt{-2 \log \rho}$ (Fisher, 1995).

B.3 Inference for Batschelet mixtures

The mixture of Batschelet distributions is given by

$$f(\theta \mid \boldsymbol{\mu}, \boldsymbol{\kappa}, \boldsymbol{\lambda}, \boldsymbol{\alpha}) = \sum_{j=1}^{J} \alpha_j f_B(\theta \mid \mu_j, \kappa_j, \lambda_j), \tag{B.14}$$

where j indexes the J components in the mixture, α_j are component weights, and $f_B(\cdot)$ is the chosen density, either Inverse Batschelet or Power Batschelet.

First, in Section B.3.1, an EM algorithm will be presented. Second, in Section B.3.2, a method for inference through MCMC is presented. A note on identifiability is given in B.3.3. Note that the number of components will be assumed to be known initially. In Section B.3.4, model selection and hypothesis testing will be discussed, which can be used to select the number of components as well evaluate many types of hypotheses. For a discussion of direct inference on mixtures with an unknown number of components, see Richardson & Green (1997).

B.3.1 EM Algorithm

Directly maximizing the observed data log-likelihood of a mixture model is generally difficult. Therefore, the EM-algorithm will be employed, which

exploits the fact that the complete data maximum likelihood, that is, with observed labels, is easier to maximize.

The EM-algorithm consists of the following steps:

(Initialization) Define an $n \times J$ matrix $\boldsymbol{W} = \{\boldsymbol{w}_1, \ldots, \boldsymbol{w}_J\}^T$, where $\boldsymbol{w}_j$ are n-vectors. Initialize the parameters $\boldsymbol{\mu}, \boldsymbol{\kappa}, \boldsymbol{\lambda}, \boldsymbol{\alpha}$ at some user-specified values.

(E-step) Compute, for all i, j, the elements of $\boldsymbol{W}$ as

$$w_{i,j} = \frac{\alpha_j f_B(\theta_i \mid \mu_j, \kappa_j, \lambda_j)}{\sum_{s=1}^{J} \alpha_s f_B(\theta_i \mid \mu_s, \kappa_s, \lambda_s)}. \tag{B.15}$$

(M-step) For each component k, maximize

$$\ell(\mu_j, \kappa_j, \lambda_j, w_j \mid \boldsymbol{\theta}) = \sum_{i=1}^{n} w_{i,j} \log f_B(\theta_i \mid \mu_j, \kappa_j, \lambda_j). \tag{B.16}$$

The maximization of this log-likelihood of the parameters of a Batschelet distribution may proceed through the Nelder-Mead simplex (Nelder & Mead, 1965), as was done in Jones & Pewsey (2012).

Note that the EM algorithm is not guaranteed to find a global maximum. Therefore, reasonable (or multiple) starting values should be used, in order to assess the validity of the final results. If avoiding convergence to local maxima is of particular importance, one could consider implementing a stochastic version of the EM algorithm (Diebolt & Ip, 1996; Nielsen et al., 2000). However, the Bayesian MCMC approach described in Section B.3.2 shares the advantages of such methods.

In addition to obtaining estimates of the mixture model, it is essential to infer the uncertainty around these estimates. For mixture models, asymptotic standard errors obtained from inverting the Fisher Information generally require very large datasets in order to have desirable properties (McLachlan & Peel, 2004). Therefore, parameter uncertainty will need to be assessed either through bootstrapping, or through MCMC.

Bootstrapping was implemented through a non-parametric bootstrap (Efron & Tibshirani, 1994). In order to reduce computational burden, the EM algorithm of each bootstrap sample was given the full data estimates as starting values.

B.3.2 Bayesian inference

A Bayesian analysis of the finite mixture of von Mises-based Batschelet distributions is available through MCMC sampling (Chib & Greenberg, 1995; Gilks et al., 1995). For an introduction focused on mixture models, see Frühwirth-Schnatter (2006). Besides providing uncertainty quantification naturally by performing inference on the posterior distribution rather than a set of estimates, the Bayesian paradigm also provides computational advantages in this case. In particular, the MCMC algorithm is less likely to converge to local maxima.

As is common for Bayesian sampling for mixture models , the parameter space is augmented by a vector of latent variables $\boldsymbol{z} \in \{1, \ldots, J\}^n$ which contains a group label for each observation. By randomly assigning each observation to a group during every iteration, the problem simplifies to MCMC sampling for each component separately. First, in Section B.3.2, priors for this model will be discussed. Then, the MCMC algorithm will be provided in Section B.3.2.

Priors

Although subjective priors can be chosen in practical use, attention here will be restricted to (somewhat) non-informative priors. Priors are required for $\alpha_j, \mu_j, \kappa_j$ and λ_j, either jointly or separately. In principle, priors could even be set for the group assignments.

The component weights α_j are given the conjugate Dirichlet prior distribution, with vector prior parameter $\boldsymbol{n}_0 \in [\mathbb{R}^+]^J$. If $\boldsymbol{n}_0 = \mathbf{1}_J$, this prior is uninformative.

The mean directions μ_j are given a circular uniform prior, $p(\mu_j) = [2\pi]^{-1}, \mu_j \in [-\pi, \pi)$, which is proper.

The concentration parameters κ_j are given a constant prior $p(\kappa_j) \propto 1$, which is improper. In principle, the Jeffreys prior for the von Mises distribution could also be used. The Jeffreys prior is proportional to the square root of the determinant of the Fisher Information Matrix $\mathcal{I}(\boldsymbol{\phi})$, so that for the von Mises distribution it is given by

$$p(\boldsymbol{\phi}) \propto \sqrt{\det\left[\mathcal{I}(\boldsymbol{\phi})\right]} = \sqrt{\kappa A(\kappa) A'(\kappa)}, \tag{B.17}$$

where $A(\kappa) = I_1(\kappa)/I_0(\kappa)$ and $A'(\kappa) = \frac{d}{d\kappa} A(\kappa)$. However, note that this is *not* the Jeffreys prior for the Inverse Batschelet distribution (as the given $\mathcal{I}(\boldsymbol{\phi})$ is the Fisher information of the von Mises), nor for a mixture of any circular distributions, nor proper. However, it can be used as a relatively diffuse default prior for cases in which very large values of κ are deemed

unlikely. For the case of the von Mises distribution, Hornik & Grün (2013) show that the resulting posterior is almost surely proper if $n \geq 2$. A final alternative is to use a relatively diffuse non-conjugate proper prior, such as one from the gamma family of distributions.

The peakedness parameter λ can be given a proper uniform prior $p(\lambda_j) = 1/2, \lambda_j \in [-1, 1)$. However, Jones & Pewsey (2012) note that in maximum likelihood estimation of the Inverse Batschelet model, estimates often fall on the boundary of the parameter space. Boundary avoiding priors can be used here to prevent this behaviour of the estimates. In particular, one may posit that large values of $|\lambda_j|$ are a priori unlikely. This belief can be captured in a rescaled Beta(a, b) prior, so that $p(\lambda_j) \propto f_{Beta}\left(\frac{\lambda+1}{2} \mid a, b\right)$. If $a = 1, b = 1$, this results in the uniform prior on $[-1, 1]$, while $1 < a, b \leq 2$ gives a range of priors which favor smaller values for $|\lambda_j|$, and thus less peaked and less flat-topped densities.

MCMC algorithm

In the application of MCMC sampling, only the group assignments in latent variable $\boldsymbol{z}$ and the mixture weights $\boldsymbol{\alpha}$ have known full conditional distributions. All other parameters are updated using the Metropolis-Hastings algorithm (Metropolis et al., 1953; Hastings, 1970). After selecting starting values, the algorithm will be performed for $m = 1, \ldots, M$ iterations, which will constitute a sample from the posterior distribution. One iteration m of the algorithm proceeds as follows:

(Sample z_i) For each observation θ_i, sample $z_i \in 1, \ldots, J$ with group probabilities

$$P(z_i = j) = \frac{\alpha_j f_B(\theta_i \mid \mu_j, \kappa_j, \lambda_j)}{\sum_{s=1}^{J} \alpha_s f_B(\theta_i \mid \mu_s, \kappa_s, \lambda_s)}.$$

This represents assigning this observation to one of the possible mixture components.

(Sample $\boldsymbol{\alpha}$) Sample the vector of mixture weights

$$\boldsymbol{\alpha} = \alpha_1, \ldots, \alpha_J \sim \text{Dirichlet}(\boldsymbol{n} + \boldsymbol{n}_0),$$

where $\boldsymbol{n} = \{\sum_{i=1}^{n} I(z_i = 1), \ldots, \sum_{i=1}^{n} I(z_i = J)\}^T$, with $I(\cdot)$ the indicator function, and $\boldsymbol{n}_0$ the vector prior parameter for the Dirichlet, which is set to $\boldsymbol{n}_0 = \mathbf{1}_n$ by default for an uninformative prior. Note that the definition of $\boldsymbol{n}$ means that all we need to do to sample the mixture weights is counting the number of observations assigned to each group.

(Sample $\mu_j, \kappa_j, \lambda_j$) For each mixture component $j \in 1, \ldots, J$, sample parameters $\mu_j, \kappa_j, \lambda_j$. Note that none of these parameters have known distributions, so we resort to Metropolis-Hastings throughout.

(a) Sample μ_j using an MH-step. As for the proposal μ_j^*, we make use of the fact that the distribution reduces to the von Mises distribution if $\lambda = 0$. Therefore, we can draw from the known distribution of the mean of the von Mises distribution, because it will be somewhat close to the desired distribution. We can take either the previously sampled μ, by sampling from $\mu_j^* \sim \mathcal{M}\left(\mu_j^{(m-1)}, R_j\kappa\right)$, or use the current sample mean direction $\bar{\theta}$, by sampling from $\mu_j^* \sim \mathcal{M}\left(\bar{\theta}_j, R_j\kappa\right)$, where $\bar{\theta}_j$ and R_j are computed from the sample assigned to component j.

(b) Sample κ_j using a MH-step, using a gamma distribution with mean $\kappa^{(m-1)}$ as the proposal distribution. The variance of this gamma distribution is a tuning parameter, which can be changed to improve computational efficiency of the algorithm. If the variance is $\kappa^{(m-1)}$, the proposal is the χ^2-distribution with $\kappa^{(m-1)}$ degrees of freedom. In practice, setting the variance to $.05\kappa^{(m-1)}$ seems to work well.

(c) Sample λ_j using a MH-step, using a uniform proposal

$$U\left[\max(-1, \lambda_j^{(m-1)} - \varepsilon),\ \ \min(1, \lambda_j^{(m-1)} + \varepsilon)\right]. \tag{B.18}$$

Note that although the proposal distribution seems symmetric, this is not the case if the current value is less than ε from the boundary. Because the proposal is not symmetric, the proposal distribution must be included in the MH ratio. Again, ε is a tuning parameter, and we will set $\varepsilon = 0.01$.

It is well known that if parameters are strongly correlated, MCMC sampling can benefit from joint proposals for the correlated parameters. The parameters κ and λ are correlated, although not in an extreme fashion. Therefore, κ and λ may be sampled jointly, although this did not always prove beneficial in practice.

B.3.3 Model identifiability

In general, mixture models may not be identifiable (Teicher, 1963), a property which manifests itself most often through label switching, where component

k represents a different unobserved subpopulation in different bootstrap or MCMC samples from the model. However, forcing an ordering on the means may be sufficient for identification (Everitt, 2004).

For the case of Batschelet mixtures on the circle, means are sometimes fixed by design, because this can be a reasonable assumption for saccade data. If the means are fixed, the model is identifiable as long as $\{\kappa_j = 0, \lambda = 0\}$ in no more than one component. If this assumption is violated, any convex combination of mixture weights α_j of components where $\{\kappa_j = 0, \lambda = 0\}$ gives the same probability density, so the model is not identified. This is unlikely in practice and can simply be checked in the output.

If the means are not fixed but estimated, label switching may occur. In practical inference, if label switching has occurred, this would be evident in bootstrap or MCMC samples. If label switching has occurred, a post-processing step may be used to solve this issue (Stephens, 2000; Jasra et al., 2005). However, care must be taken in ensuring a circular ordering rather than a linear ordering.

B.3.4 Model selection and hypothesis testing

It is often relevant to compare several models and select the best among them, for example to select the required number of mixture components. The most common approach to model selection is through information criteria such as AIC (Akaike, 1987) and BIC (Schwarz et al., 1978) in frequentist settings, and DIC (Spiegelhalter et al., 2002) and WAIC (Watanabe, 2010) in Bayesian settings (for an overview, see Wagenmakers & Waldorp (2006)). Such tools are provided in the `R` package `flexcircmix` accompanying this paper and provide an approximate comparison of the fit of various models.

However, the Bayesian approach also allows us to perform more sophisticated model comparisons naturally by comparing the models on their posterior model probability. Consider a set of Q models $\mathcal{M}_1, \ldots, \mathcal{M}_Q$ each indexed by a set of free parameters $\boldsymbol{\phi}$, that are to be compared on their probability after observing data. This set of models can also be hypotheses to be compared. For example, one could compare a 3-component model with a 4-component model, a model with mean directions fixed at the cardinal directions versus a model where mean directions can vary freely, or a model that allows peaked distributions (ie. $\lambda \in (-1, 1)$) versus a von Mises mixture model (ie. $\lambda = 0$).

In order to obtain the posterior model probability, the prior probability of the models under consideration must first be assessed. Here, and throughout the rest of this work, the models will be assumed to have equal prior probability, so $p(\mathcal{M}_s) = 1/Q$. As a result, the prior probability drops out of

the rest of the formulae.

Then, regardless of the set of models under consideration, we can compute the posterior model probability

$$\text{pmp}(\mathcal{M}_s) = \frac{p(\mathcal{M}_s \mid \boldsymbol{x})}{\sum_{q=1}^{Q} p(\mathcal{M}_q \mid \boldsymbol{x})} \tag{B.19}$$

where $p(\mathcal{M}_s \mid \boldsymbol{x})$ is the *marginal likelihood*, given by

$$p(\mathcal{M}_s \mid \boldsymbol{x}) = \int_{\Omega_{\boldsymbol{\phi}}} p(\boldsymbol{x} \mid \boldsymbol{\phi}) d\boldsymbol{\phi}, \tag{B.20}$$

where $\Omega_{\boldsymbol{\phi}}$ is the sample space of the parameter vector for the model $\mathcal{M}_s$. This integral is in general not easy to compute and has sparked a wealth of methods for computing it (for an overview, see Ardia et al. (2012) and Friel & Wyse (2012)). Perhaps the most promising and stable sampling-based solution is found in bridge sampling (Meng & Wong, 1996), which was recently made more easily applicable as a post-processing step on MCMC output through the `R` package `bridgesampling` (Gronau et al., 2017). Broadly speaking, bridge sampling produces an estimate of the marginal likelihood by evaluating additional samples from a known density that approximates the posterior. For details, see Gronau et al. (2017) and Meng & Wong (1996).

Two issues arise for this specific application. First, the sample of mean direction parameters $\boldsymbol{\mu}_j$ lie on a circular parameter space. Bridge sampling will find a known density that approximates the posterior by using the linear mean and the covariance matrix of the MCMC samples, for example by using the multivariate normal density with the same mean vector and covariance matrix. The approximation need only be roughly correct, which is not necessarily the case for our model. For example, if we have a circular parameter with a mean direction near zero, some sampled values will lie in both intervals $[0, .1]$ and $[2\pi - .1, 2\pi)$. The linear mean will then incorrectly lie near π, and the linear variance will be far too large. To solve this, we will change the numerical representation of the mean direction sample of $\boldsymbol{\mu}_j$ such that it lends itself better to the linear approximation. To do this, first the posterior mean direction $\bar{\mu}_j$ is computed from the sample of mean directions $\boldsymbol{\mu}_j$. Then, by taking $\boldsymbol{\mu}_j^* = [(\boldsymbol{\mu}_j - \bar{\mu}_j + \pi) \bmod 2\pi] - \pi + \bar{\mu}_j$, a numerical representation is obtained that does not have any 'gaps' on the real line, but corresponds to the same set of angles $\boldsymbol{\mu}_j$.

The second issue is that the sample of component weight parameters $\alpha_j \in [0, 1]$ lie on a simplex, that is, they are constrained to sum to one. The bridge sampling usually lies on the real line, such as the aforementioned multivariate normal distribution, which means the constrained parameter space

is ignored, so that almost surely invalid proposals are sampled. Therefore, these parameters are given a stick-breaking representation and are then logit-transformed, in a similar manner as in Stan (Carpenter et al., 2017). For details on the transformation, its inverse and associated Jacobian, see the Stan reference manual (Stan Development Team, 2017). The solutions for both circular and simplex parameters were contributed to the latest version of the `bridgesampling` package.

B.4 Illustration

In order to illustrate the methods presented in this work, they will be applied to two examples.

First, the method is applied to a synthetic dataset in Section B.4.1, where it is shown that the true parameters of a data generating process can be recovered. Then, in Section B.4.2, the method is shown to provide new insights in the saccade direction data from Van Renswoude et al. (2016).

B.4.1 Synthetic data

Here, the methods developed in this paper will be applied to a synthetic data set for which parameter values are known. In order to sample from the Inverse Batschelet distribution, the sampling algorithm from Jones & Pewsey (2012) was applied. A data set consisting of 1000 angles was sampled with parameters $\boldsymbol{\mu} = \{-1, 1, 2\}$, $\boldsymbol{\kappa} = \{20, 4, 15\}$, $\boldsymbol{\lambda} = \{-.7, 0, .7\}$, and $\boldsymbol{\alpha} = \{.25, .25, .5\}$.

The results are shown in Table B.1 and Figure B.5. First, it is clear that the method is able to recover mean direction. Also, it can be seen that both the bootstrapped confidence intervals and the credible intervals generally include the true value, and cases in which this is not true can be attributed to sampling error.

As mentioned previously, the joint likelihood of $\{\kappa, \lambda\}$ is correlated. Because of this, it can be seen in Table B.1 that neither κ nor λ can be estimated precisely, with both having confidence intervals that are quite wide. A remarkable property of this method is that while neither of the variance-related parameters is estimated very precisely, the circular standard deviation, computed as in Section B.2.3, has tighter confidence intervals and is estimated more precisely, so inference on it will be more powerful than inference directly on κ or λ.

The components weights are estimated adequately in all cases.

Table B.1: Synthetic data fits using the Power Batschelet distribution.

		EM	Boot. CI		Bayes (MCMC)		
	Truth	Est.	2.5%	97.5%	Median	2.5%	97.5%
μ_1	-1.00	-1.00	-1.09	-0.91	-1.00	-1.04	-0.96
κ_1	20.00	24.92	8.67	63.37	27.67	8.91	59.99
λ_1	-0.70	-0.81	-1.00	-0.47	-0.85	-0.99	-0.51
α_1	0.25	0.26	0.23	0.28	0.26	0.23	0.29
σ_{c1}	0.52	0.55	0.51	0.60	0.56	0.51	0.60
μ_2	1.00	0.98	0.95	1.01	1.00	0.97	1.03
κ_2	4.00	3.26	3.17	3.94	3.52	2.80	5.17
λ_2	0.70	0.89	0.66	1.00	0.81	0.54	0.98
α_2	0.25	0.26	0.23	0.29	0.27	0.23	0.31
σ_{c2}	0.34	0.42	0.33	0.44	0.38	0.27	0.53
μ_3	2.00	1.97	1.95	2.00	1.98	1.96	2.00
κ_3	15.00	16.29	10.87	44.57	25.08	11.37	67.42
λ_3	0.00	-0.09	-0.36	0.08	-0.22	-0.47	0.06
α_3	0.50	0.48	0.45	0.51	0.48	0.44	0.51
σ_{c3}	0.26	0.28	0.26	0.30	0.28	0.25	0.30

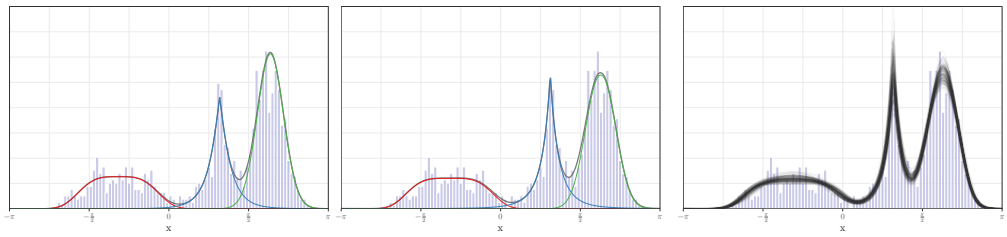

(a) True density. (b) Fit from EM algorithm. (c) MCMC fit.

Figure B.5: Synthetic data plots using the power Batschelet distibution. The sample of synthetic data, plotted along with a sample of 200 densities of which the parameters were sampled in the MCMC. That is, the spread of probability density functions provides a rough uncertainty bound for the true probability at each point.

B.4.2 Free-viewing data

Here, the method will be applied to a real world example, the free-viewing dataset that was originally published in Van Renswoude et al. (2016), shown again in Figure B.6. As discussed in Section B.1, there are several hypotheses one might wish to learn about using this dataset. One hypothesis of interest is whether infants have a larger circular variance for each of their mixture components. Another is whether the horizontal bias, that is, the preference for left-right movements, is weaker for infants than for adults. These hypotheses will be assessed here.

Because the mixture model has a fairly large number of parameters, it can be fruitful to consider fixing parameters about which we do not need to learn. For free-viewing data, modes are always observed oriented exactly in the cardinal directions, which will simplify our modeling problem somewhat. The mean directions can be chosen to be fixed at $\mu_1 = -\pi/2$ (upward), $\mu_2 = 0$ (rightward), $\mu_3 = \pi/2$ (downward), $\mu_4 = \pi$ (leftward). Because fewer components are needed in the Batschelet mixture and because the means are fixed, the model actually has fewer parameters than the von Mises mixture model. It is also possible to loosen this assumption slightly by placing a strong prior on the mean directions centered on the aforementioned cardinal directions.

For Bayesian inference, the priors were chosen according to the consideration in Section B.3.2. To be specific, the prior for μ_j was circular uniform, for κ_j the Jeffreys prior of the von Mises distribution, for λ_j the prior was the rescaled beta distribution proportional to $f_{Beta}\left(\frac{\lambda+1}{2} \mid \sqrt{2}, \sqrt{2}\right)$, and finally the prior for α_j was Dirichlet($\boldsymbol{\alpha} = \{\sqrt{2}, \ldots, \sqrt{2}\}^T$). The MCMC algorithm was run for 46000 iterations, split into 46 parallel chains each having a burn in of 1000.

A bootstrap was run with 10000 bootstrap replications. For both adults and infants, the results from the EM algorithm with bootstrapped standard errors will be displayed together with the Bayesian approach in Table B.2.

Adults

Results for the adult sample are displayed in Figures B.6a and B.6b. Visually, the model fit seems excellent, and it can be seen that observed distributions are generally quite peaked. For adults, it can be seen that all four components contribute to the overall shape of the overall shape of the model.

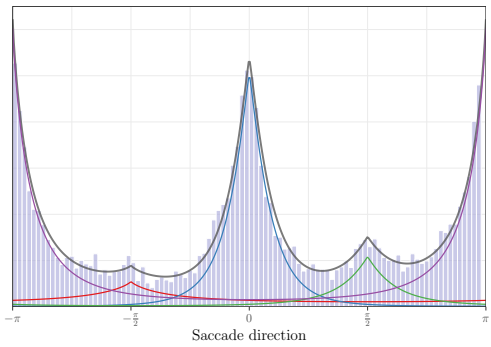

(a) EM fit for adults.

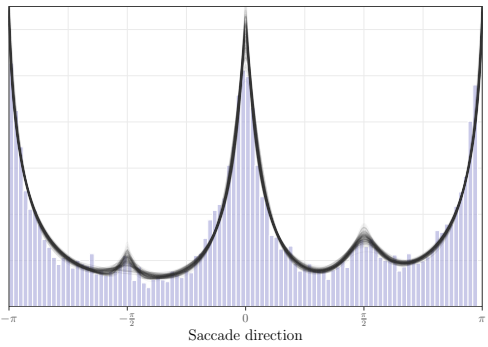

(b) MCMC fit for adults.

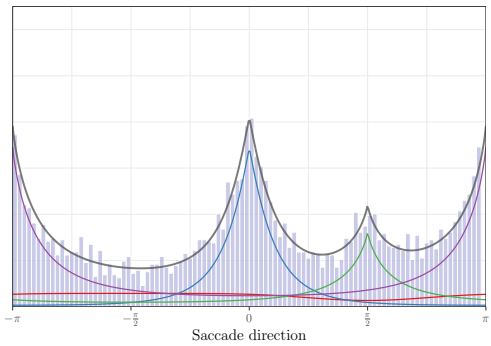

(c) EM fit for infants.

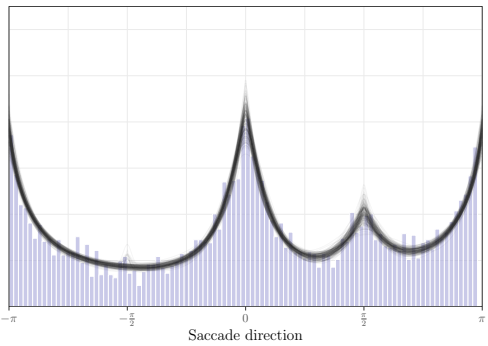

(d) MCMC fit for infants.

Figure B.6: Free-viewing data fit for adults (top) and infants (bottom) using the power Batschelet distibution. The x-axis is given in radians, where 0 corresponds to the rightward direction, while $\pi/2$ corresponds to the downward direction. In the left plot, it can be seen that a third component is estimated for adults, while this is not the case for infants. In the right plot, the densities are plotted that result from sampled parameter sets from the MCMC.

Infants

For infants, judging from the convergence plots in Figure B.7, there might be grounds to assume that fewer than four components may suffice. Specifically, we can see that component 1 (upward) has component weight α that tends to zero. This can also be seen in Figure B.6c, where the red (upward) component 1 is taken as almost completely flat.

Horizontal Bias comparison

The main question of whether the horizontal bias of adults and infants differ can be addressed by comparing the circular standard deviation in Table B.2, as well as compare the component weights $\boldsymbol{\alpha}$.

The horizontal components are component 2 and 4. For the rightward component 2, with ($\mu_2 = 0$), the estimates are generally somewhat similar between adults and infants, as the confidence and credible intervals overlap.

For the leftward component 4 ($\mu_4 = \pi$), the confidence and credible intervals of adults and infants do not overlap, which can also be observed in Figure B.6 by noting that this component has a different shape between Figures B.6c and B.6a. For the component weight α_4, adults have EM-estimate and 95% bootstrap confidence interval $\hat{\alpha}^{(EM)} = 0.465$ (0.443, 0.502) and posterior median and credible interval $\hat{\alpha}^{(MCMC)} = 0.542$ (0.431, 0.58), compared to infants which have $\hat{\alpha}^{(EM)} = 0.405$ (0.37, 0.455) and $\hat{\alpha}^{(MCMC)} = 0.472$ (0.28, 0.614).

For the circular standard deviation σ_{c4}, adults have $\hat{\sigma}_c^{(EM)} = 0.886$ (0.812, 0.964) and $\hat{\sigma}_c^{(MCMC)} = 0.995$ (0.786, 1.07), compared to infants which have $\hat{\sigma}_c^{(EM)} = 1.16$ (1.036, 1.258) and $\hat{\sigma}_c^{(MCMC)} = 1.161$ (0.749, 1.391). Therefore, infants seem to have a larger variance on this component than adults. From this, it can be concluded that the horizontal bias exists, and differs between adults and infants.

Hypothesis testing

Using the model comparison methods discussed in Section B.3.4, several models of interest can be compared using Bayesian hypothesis tests.

First, it is worthwile to investigate whether in general infants and adults differ. This can be done by comparing the model that is discussed in Section B.4.2, which allows separate parameters for infants and adults, to a model where both are given the same parameters (for which parameter estimates are not shown). For this model, the log Bayes Factor in favor of the model that has separate parameters is 52.7, which is associated with a posterior model

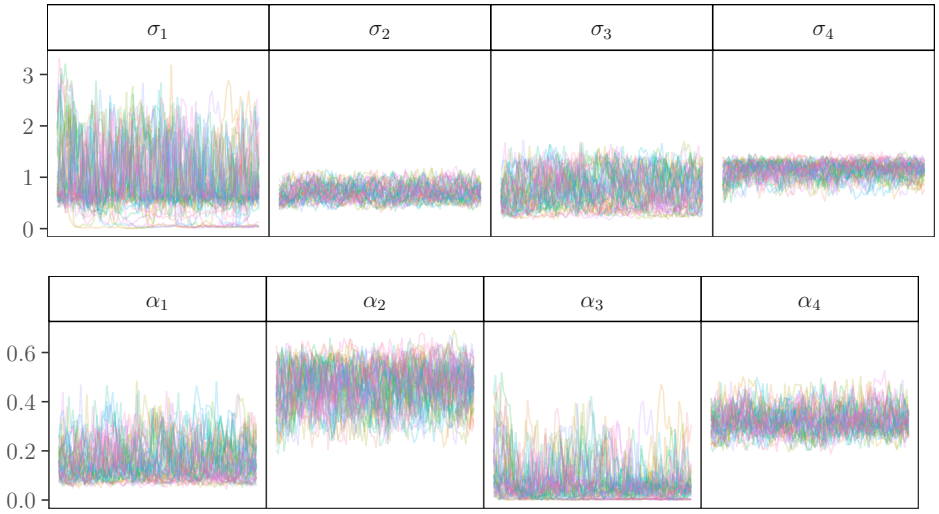

Figure B.7: Convergence plot for the infant data. The plot shows 46 chains of 1000 MCMC iterations, with a thinning factor of 50.

probability (assuming equal prior odds) in favor of separate parameters close to 100%. Therefore, we have separated the groups throughout.

Second, as can be seen in Figure B.6c, one may be unsure about the number of required components for infants. Although four components were assumed so far, three may suffice. Again, we find almost certain evidence, log Bayes Factor 70.7, posterior probability $\approx$ 100%, that the model with four components fits better than the model with only three components.

Finally, the assumption that the means can be fixed to the cardinal directions can be checked. To test whether this was a valid assumption, a model with free means is run for both adults and infants (parameter estimates not shown). This model is then compared to the model with fixed means from before, which gives a log Bayes factor of 61 in favor of free means. This suggests that the data can be fit better by allowing the means to be freely estimated. This could be understood as a systematic bias of the means away from the cardinal directions contained in the stimuli used. However, for the sake of simplicity, the means were kept fixed throughout this paper.

B.5 Discussion

In this paper, a new mixture model for flexible circular distributions was developed. It can be used to distinguish clusters in samples of directions, for

Table B.2: Free-viewing fit using the Power Batschelet mixture model, for adults (left) and infants (right). Mean directions were fixed at $\mu_1 = -\pi/2$ (upward), $\mu_2 = 0$ (rightward), $\mu_3 = \pi/2$ (downward), $\mu_4 = \pi$ (leftward).

		Adults						Infants					
		EM	Boot. CI		Bayes (MCMC)			EM	Boot. CI		Bayes (MCMC)		
		Est.	2.5%	97.5%	Median	2.5%	97.5%	Est.	2.5%	97.5%	Median	2.5%	97.5%
Up	κ_1	0.81	0.69	1.03	5.94	0.85	666.66	0.38	0.25	0.91	6.76	0.14	635.15
	λ_1	1.00	1.00	1.00	0.41	-0.53	0.97	-1.00	-1.00	0.17	-0.56	-0.97	0.55
	α_1	0.11	0.09	0.12	0.02	0.01	0.12	0.15	0.11	0.18	0.05	0.00	0.28
	σ_{c1}	1.54	1.37	1.64	0.32	0.09	1.46	1.96	1.46	2.13	0.68	0.03	2.33
Right	κ_2	3.05	2.61	3.50	2.46	2.09	3.39	2.34	1.90	3.75	2.22	1.49	3.78
	λ_2	0.67	0.56	0.78	0.77	0.58	0.91	0.72	0.40	0.90	0.67	0.38	0.93
	α_2	0.32	0.31	0.35	0.36	0.31	0.40	0.27	0.23	0.32	0.32	0.23	0.43
	σ_{c2}	0.48	0.42	0.58	0.62	0.44	0.76	0.65	0.43	0.84	0.69	0.43	1.05
Down	κ_3	1.93	1.65	3.34	4.33	1.51	30.56	1.41	1.21	1.94	2.14	0.90	18.24
	λ_3	0.76	0.44	0.90	0.41	-0.20	0.85	0.99	0.61	1.00	0.65	-0.09	0.96
	α_3	0.10	0.07	0.12	0.06	0.05	0.14	0.18	0.15	0.20	0.13	0.06	0.34
	σ_{c3}	0.80	0.47	0.95	0.38	0.23	1.01	1.12	0.80	1.23	0.73	0.25	1.42
Left	κ_4	1.84	1.70	1.97	1.62	1.50	2.02	1.34	1.18	1.49	1.28	0.98	2.06
	λ_4	0.96	0.88	1.00	0.97	0.87	1.00	0.98	0.82	1.00	0.88	0.61	0.99
	α_4	0.47	0.44	0.50	0.54	0.43	0.58	0.41	0.37	0.46	0.47	0.28	0.61
	σ_{c4}	0.89	0.81	0.96	1.00	0.79	1.07	1.16	1.04	1.26	1.16	0.75	1.39

example those obtained from saccade directions. The main contribution is the development of mixture models for circular data that allow for peaked and flat-topped shapes. In order to do this, a new family of distributions was introduced, the Power Batschelet distributions, that mimic the distributions developed in Jones & Pewsey (2012), but that enjoy more appealing computational properties.

The method developed here can be used as a method to investigate whether two sets of saccade directions differ from each other, as shown in Section B.4.2. This allows eye-tracking researchers to answer more complex questions about their saccade data, and draw inference where this was previously not possible.

Although developed in the context of saccade directions, the method has potentially much broader applications. For example, wind directions are commonly modeled with circular distributions (Bowers et al., 2000; Holzmann et al., 2006; Bao et al., 2010), and sometimes feature peaked distributions. Also, observed arrival times can sometimes be governed by an event occuring at a single time point, causing strongly peaked distributions as well. Also, the method is a strong contender for any form of non-parametric fit on a set of univariate circular data. In that case, the current method functions as a flexible parametric alternative to a fully non-parametric analysis. The mixture of Batschelet distributions then allows much more extensive interpretation and inference than a non-parametric analysis typically would, at a minor cost

of flexibility.

It should be noted that in general saccade data is time-series data where each observation is correlated with the previous observations. In the free-viewing paradigm, this autocorrelation is not of core interest, as the time series consist of only 3-5 saccades per viewed image. In general, fitting the saccade directions with a flexible model such as the one provided here while ignoring the time-series structure violates an assumption of the model. However, the time series structure of saccade directions usually does not follow a traditional autocorrelation structure, because, for example, reaching the end of a page results in negative autocorrelation. Therefore, this issue should be addressed separately. The current approach does allow a powerful parametric comparison of different groups of saccade direction data, even when ignoring the autocorrelation. For some applications however, interest might specifically lie in the autocorrelation structure, and for those settings different models might be preferred.

In future studies, it may be fruitful to model the saccade direction jointly with saccade length, instead of the saccade direction separately. One promising model that has not been applied to the field of eye-tracking is the Abe-Ley model for cylindrical data (Abe & Ley, 2017). In this model, saccades with larger length naturally have a higher (circular) concentration, a property which is commonly observed in vision research. However, the complex form of such models means that extensions such as mixtures are not available, although a hidden Markov model has been developed (Lagona et al., 2015).

Finally, it should be noted that methods developed here are made accessible to eye-tracking researchers through the easy-to-use R package `flexcircmix`. This means that the methods can be readily applied to new data, without requiring extensive technical knowledge. Hopefully, the methods developed in this paper will provide a valuable new direction for eye-tracking researchers to perform more valid parametric inference on the angles of saccades throughout a broad range of applications.

B.6 Acknowledgements

This work was supported by a —— grant awarded to —— from —— (——).

Appendix A

Bayesian inference for mixtures of von Mises distributions using the reversible jump MCMC sampler

A.1 Introduction

Circular data are data measured in angles or orientations in two-dimensional space. Examples include directions on a compass (0° - 360°), time of day (0 - 24 hours) or day of year (0 - 365 days). These data are encountered across behavioral research (Mechsner et al., 2001; Gurtman, 2009) and many other scientific disciplines.

Analysis of circular data requires special statistical methods due to the periodicity of the sample space. For example, the arithmetic mean of the two time points 00:30h and 23:30h would be 12:00h, while the circular mean is 00:00h, which is clearly a preferable central tendency in this case. Several books on circular statistics are available, in particular Pewsey et al. (2013), Mardia & Jupp (2009) and Fisher (1995).

This paper will focus on the modeling of multi-modal circular data with mixtures with an unknown number of components. Mixture models often assume the number of mixture components to be known, although this is rarely true in practice. As a solution, the number of mixture components is usually selected by comparing information criteria such as the AIC (Akaike, 1974) or BIC (Schwarz, 1978). Such an approach allows selection of a mixture model with the best-fitting number of components, but entirely ignores our uncertainty about the parameter determining the number of components.

A more natural and sophisticated approach is to treat the number of modes as unknown, and obtaining the uncertainty around the number of modes jointly with the rest of the analysis. The main contribution of this paper is to provide an algorithm to perform a fully Bayesian mixture model that correctly captures the uncertainty about the number of components, as well as showing its usefulness and interpretability with a real data example.

The motivating example for this paper is a data set on music listening behavior. The data was provided by music service `http://www.22tracks.com/`, and consists of the time of day (on the 24-hour clock) at which a user played a particular song. The songs that are being listened to are also categorized in genres such as 'Pop' or 'Deep House'. When a user visits the *22tracks* service, they are presented with a genre. The user can then choose to listen to this genre, select a different genre or stop using the service. Reducing the fraction of users that stop using the site is of direct interest to the music service. Currently, the initially presented genre is selected uniformly random over the genres. The aim of our analysis is to determine which genres are listened to most at certain times, so the most relevant genre at a given time can be presented. In addition, a model where parameters can be directly interpreted may allow us to understand what drives music listening behavior.

The base distribution for our circular mixture model will be the von Mises distribution, which is commonly used for analysis of circular data and can be considered the circular analogue of the Normal distribution. Von Mises mixture models with a fixed number of modes have been developed previously in a frequentist setting (A Mooney et al., 2003), for example using the Expectation Maximization (EM) algorithm (McLachlan & Krishnan, 2007; Banerjee et al., 2005). Bayesian analysis for this type of model can be performed through Markov chain Monte Carlo (MCMC) sampling (Tierney, 1994; Besag et al., 1995). In particular, the high-dimensional variant of this mixture model has seen some popularity due to several appealing applications such as text mining, which has led to an R package for this model (Hornik & Grün, 2014). Such high-dimensional circular mixtures use the von Mises-Fisher distribution on hyperspheres, with the von Mises as a special case. We will focus on the circular mixture model only.

The core difficulty in employing MCMC samplers in such applications is that the parameter space is of variable dimension. That is, if there are more components in the mixture model, there are more parameters. Therefore, the usual MCMC approaches do not provide a way to explore the whole parameter space, and we must use a solution such as Reversible jump MCMC (Green, 1995; Richardson & Green, 1997). In a reversible jump MCMC sampler, we allow moves between parameter spaces by use of a special case of the Metropolis-Hastings (MH) acceptance ratio (Hastings, 1970). This

paper provides a detailed account of the adaptation of a reversible jump sampler for von Mises mixtures.

Three major contributions are made to the field of mixture modeling for circular data. First, this paper presents the first application of the reversible jump sampler to this setting, which allows us to perform inference on the amount of components in the mixture model. Second, a novel split move, which makes use of the trigonometric properties of the von Mises distribution, allows the sampler to move across the parameter space efficiently. Lastly, a simulation study is performed to show that this method performs well in common research scenarios.

Several alternative approaches for Bayesian modeling of multi-modal circular data could be considered. Most are found in the field of Bayesian non-parametrics, such as Dirichlet process mixture models (Ghosh et al., 2003), log-spline distributions (Ferreira et al., 2008) or a family of densities based on non-negative trigonometric sums (Fernández-Durán & Mercedes Gregorio-Domínguez, 2016). Such approaches generally have the advantage of making fewer assumptions about the distribution of the data. However, none of these methods provide a way for direct inference on the number of subpopulations (ie. components) making up the mixture, and the parameters in the mixture model with unknown number of components are much more interpretable.

Therefore, the approach taken in this paper can be seen as a useful in-between step between mixture models with a fixed number of components and non-parametric approaches. Compared to fixed-component mixture models, our approach is more realistic in the uncertainty about the amount of components, allows performing inference about the number of components, but also enables leaving the number of components to be uncertain. In particular, while information criteria based methods also allow selection of the most likely number of components, our approach provides a posterior probability distribution around the number of components, and as such acknowledges that the selected number of components can be wrong. Compared to non-parametric approaches, our approach feature much more interpretable parameters and inference, at the cost of taking more assumptions about the shape of the distribution. Concluding, if the number of components is known or not of interest, a fixed-component mixture model can be preferred for simplicity, while if density estimation is the goal a fully non-parametric approach may be the best choice. If the number of components is not known, of interest, and interpretation of the parameters of subpopulations is of interest, our method aligns the best with these goals.

The paper is organized as follows. Section A.2 describes the model and chosen priors. Section A.3 contains the description and implementation of

each of the steps involved in sampling the model parameters. In Section A.4 the performance of the sampler is investigated in a simulation study. The sampler is applied to the *22tracks* data in Section A.5. Finally, the results are discussed in Section B.7.

A.2 Von Mises Mixture Model

In this section, the von Mises-based mixture model will be developed. First, its general form will be given. Second, the likelihoods necessary for inference are discussed. Third, priors for this model are shortly discussed.

A.2.1 Von Mises mixture density

The von Mises distribution is a symmetric, unimodal distribution commonly used in the analysis of circular data. Its density is given by

$$f_{VM}(\theta \mid \mu, \kappa) = \frac{1}{2\pi I_0(\kappa)} \exp(\kappa \cos(\theta - \mu)), \tag{A.1}$$

where $\theta \in [0, 2\pi)$ is an angle measured in radians, $\mu \in [0, 2\pi)$ is the mean direction, $\kappa \in [0, \infty)$ is a non-negative concentration parameter and $I_0(\cdot)$ is the modified Bessel function of the first kind and order zero. For an introduction into circular statistics, see (Mardia & Jupp, 2009).

When data consist of observations from multiple subpopulations for which the labels are not observed, the distribution of the pooled observations can be described by a mixture model. For example, times at which people listen to music are expected to coincide with daily events, such as dinner time or the daily commute, which are clustered around certain time points that show up as modes in the data set.

The density of the pooled observations can be expressed as a mixture

$$f(\theta \mid \boldsymbol{w}, \boldsymbol{\mu}, \boldsymbol{\kappa}) = \sum_{j=1}^{g} w_j f_{VM}(\theta \mid \mu_j, \kappa_j), \tag{A.2}$$

where $g \in \mathbb{N}^+$ is the number of components in the mixture, $\boldsymbol{\mu} = \{\mu_1, \ldots, \mu_g\}$ and $\boldsymbol{\kappa} = \{\kappa_1, \ldots, \kappa_g\}$ are vectors of distribution parameters of each von Mises component and weight vector $\boldsymbol{w} = \{w_1, \ldots, w_g\}$ contains the relative size of each component in the total sample. Weights, which are also sometimes called mixing probabilities, satisfy the usual constraints to lie on the simplex, that is $0 \leq w_j \leq 1$ and $\sum_{j=1}^{g} w_j = 1$.

A.2.2 Likelihood

For a dataset $\boldsymbol{\theta} = \{\theta_1, \ldots, \theta_N\}$ of observations from a mixture of von Mises components, the likelihood is

$$\mathcal{L}(\boldsymbol{w}, \boldsymbol{\mu}, \boldsymbol{\kappa}, g \mid \boldsymbol{\theta}) = \prod_{i=1}^{N} \sum_{j=1}^{g} w_j f_{VM}(\theta_i \mid \mu_j, \kappa_j), \tag{A.3}$$

where it should be noted that the number of components g is treated as an unknown parameter instead of fixed, and that the lengths of $\boldsymbol{\mu}, \boldsymbol{\kappa}$ and $\boldsymbol{w}$ depend on g.

In order to perform inference on ($\boldsymbol{w}$, $\boldsymbol{\mu}$, $\boldsymbol{\kappa}$, g), it will be convenient to include a latent vector $\boldsymbol{z} = \{z_1, \ldots, z_N\}$ that encodes the component to which observation θ_i is attributed. Parameters $z_1, \ldots, z_N$ are realizations of categorical random variable $Z_1, \ldots, Z_N$, such that

$$P(Z_i = j \mid \boldsymbol{w}) = w_j, \qquad (i = 1, \ldots, N; j = 1, \ldots, g). \tag{A.4}$$

The reason for introducing this parameter vector is that conditional on $\boldsymbol{Z}$, $\theta_1, \ldots, \theta_N$ are independent observations from their respective component

$$p(\theta_i \mid Z_i = j, \boldsymbol{\mu}, \boldsymbol{\kappa}) = f_{VM}(\theta_i \mid \mu_j, \kappa_j), \tag{A.5}$$

where inference for μ_j and κ_j is markedly easier than in the mixture likelihood in Equation A.3, because it can be done as if the model is simply a single von Mises component. The vector $\boldsymbol{z}$ is called the allocation vector and will be updated as part of the MCMC procedure. With this allocation vector, the expression for the likelihood of the parameters of each component is simply

$$\mathcal{L}(\mu_{z_i}, \kappa_{z_i} \mid \boldsymbol{\theta}, \boldsymbol{z}) = \prod_{i=1}^{N} f_{VM}(\theta_i \mid \mu_{z_i}, \kappa_{z_i}). \tag{A.6}$$

As per usual in the Bayesian framework, inference will be performed on the posterior distribution, which is given by

$$p(\boldsymbol{w}, \boldsymbol{\mu}, \boldsymbol{\kappa}, \boldsymbol{z} \mid \boldsymbol{\theta}, g) \propto p(\boldsymbol{w}, \boldsymbol{\mu}, \boldsymbol{\kappa}, \boldsymbol{z}, g) \mathcal{L}(\boldsymbol{w}, \boldsymbol{\mu}, \boldsymbol{\kappa}, \boldsymbol{z}, g \mid \boldsymbol{\theta}), \tag{A.7}$$

where the prior $p(\boldsymbol{w}, \boldsymbol{\mu}, \boldsymbol{\kappa}, \boldsymbol{z}, g)$ will be discussed next.

A.2.3 Prior distributions

Although informative priors could be used in practice, we will focus on providing uninformative priors for the parameters of the von Mises components

and their weights. The joint prior $p(\boldsymbol{w}, \boldsymbol{\mu}, \boldsymbol{\kappa}, g)$ is assumed to factor into several independent priors, which will be discussed in turn.

For the von Mises parameters μ_j and κ_j, a conjugate prior (Mardia & El-Atoum, 1976; Guttorp & Lockhart, 1988) is used, which is given uninformative prior hyperparameters. For μ_j, this is the circular uniform distribution, which we will write as $p(\mu_j) \sim \mathcal{U}(0, 2\pi)$, where $U(a, b)$ is the uniform distribution from a to b.

For κ_j this is a constant prior $p(\kappa_j) \propto 1$. Both priors represent a lack of knowledge about these parameters. A more informative prior for κ_j can also be set in the conjugate prior, for example if highly concentrated von Mises distributions are not expected to represent real subpopulations.

The prior for $\boldsymbol{w}$ is the Dirichlet distribution $p(\boldsymbol{w}) = \mathcal{D}(1, 1, \ldots, 1)$, which assigns equal probability to all combinations of weights.

The prior for the number of components g is chosen as $p(g) \propto \text{geom}(0.05)^N$ such that $p(g) \propto 0.05(1-0.05)^{gN}$. The geometric distribution is raised to the power N, the number of observations, as a method for penalizing complexity. While somewhat of a pragmatic choice, this prior performs well in practice. The prior prevents overfitting and can be interpreted as the belief that a parsimonious model is preferred, irrespective of the number of observations.

A.3 Reversible jump MCMC for von Mises Mixtures

Bayesian inference for the von Mises mixture model will proceed by sampling from the posterior in Equation A.7 using MCMC sampling. As mentioned, standard MCMC will not be able to deal with the changing dimensionality in the parameter space after g changes, and therefore we will resort to reversible jump MCMC to solve this issue.

The reversible jump MCMC algorithm consists of five move types. These moves can be divided into fixed-dimension move types and dimension changing move types. The fixed-dimension moves are the standard moves for MCMC on mixture models. They do not change the component count g and thus do not alter the dimensionality of the parameter space. These moves are

1. updating the weights $\boldsymbol{w}$;
2. updating component parameters ($\boldsymbol{\mu}$, $\boldsymbol{\kappa}$);
3. updating the allocation $\boldsymbol{z}$.

When g is known for a mixture of von Mises components, a sampler consisting of just these three moves would be sufficient.

In many cases however, g is not known and should be estimated as part of the MCMC procedure. This can be achieved by including two more move types, which are the reversible jump move types. They are

4. splitting a component in two, or combining two components;

5. the birth or death of an empty component.

Both of these move types change g by 1 and update the other parameters $(\boldsymbol{w}, \boldsymbol{\mu}, \boldsymbol{\kappa}, \boldsymbol{z})$ accordingly. In our implementation, the move types 1-5 are performed in order. One complete pass over each of these moves will be called an *iteration* and is the time step of the algorithm. The chosen implementations of these move types will be discussed in detail in the following sections.

A.3.1 Updating the weights w

Weights $\boldsymbol{w}$ can be drawn directly from their full conditional distribution $p(\boldsymbol{w} \mid \boldsymbol{\mu}, \boldsymbol{\kappa}, \boldsymbol{z}, g)$, which is Dirichlet and dependent only on the current allocation $\boldsymbol{z}$. It is given by

$$\boldsymbol{w} \mid \boldsymbol{z} \sim \mathcal{D}(n_1 + 1, ..., n_g + 1), \tag{A.8}$$

where n_j is the number of observations allocated to component j

$$n_j = \sum_{i=1}^{N} \mathbf{1}_{z_i = j}, \tag{A.9}$$

where $\mathbf{1}$ is an indicator function.

A.3.2 Updating component parameters μ and κ

The conditional posterior distribution of each μ_j is von Mises and given by

$$\mu_j \mid \kappa_j, \boldsymbol{\theta}_j \sim VM\left(\bar{\theta}_j, R_j \kappa_j\right), \tag{A.10}$$

where $\boldsymbol{\theta}_j$ is the vector of observations currently allocated to component j and $\bar{\theta}_j$ and R_j are the mean direction and the resultant length respectively, which can be computed as in (Mardia & Jupp, 2009, p. 15).

The conditional distribution of κ can be expressed as

$$f(\kappa_j \mid \mu_j, \boldsymbol{\theta}_j) \propto I_0(\kappa_j)^{-n_j} \exp\left\{R_j \kappa_j \cos\left(\mu_j - \bar{\theta}\right)\right\}. \tag{A.11}$$

It is not straightforward to sample from this distribution. The method proposed by Forbes & Mardia (2014) is applied, which uses a rejection sampler to produce a sample from the full conditional distribution.

A.3.3 Updating the allocation z

Allocation z_i for each observation is sampled based on the relative densities of the components. For observation i this is given by

$$P(Z_i = j \mid \theta_i, w_j, \mu_j, \kappa_j) = \frac{w_j f_{VM}(\theta_i \mid \mu_j, \kappa_j)}{\sum_{h=1}^{g} w_h f_{VM}(\theta_i \mid \mu_h, \kappa_h)}. \tag{A.12}$$

This is the categorical or 'multinouilli' distribution, and is simple to sample from.

A.3.4 Dimensionality changing moves

For the dimensionality changing moves we make use of reversible jump moves which are a special case of a Metropolis-Hastings step (Richardson & Green, 1997). The goal is to allow the sampler to move from a current state, which we'll denote by $x = (\boldsymbol{w}, \boldsymbol{\mu}, \boldsymbol{\kappa}, \boldsymbol{z})$, to another state x', which has a different number of dimensions than x.

This move is implemented by sampling a random vector $\boldsymbol{u}$ that is independent of x, the current state of the sampler. The proposal for a new state x' can then be expressed as an invertible function $x'(x, \boldsymbol{u})$, to be chosen later, which maps x and u jointly to a proposal x'. It is required that the move is designed as a pair, such that there also exists the reverse function $x(x', \boldsymbol{u})$, which is why the algorithm is called *reversible jump*. Essentially, we develop a bridge between two spaces of different dimension, and as a result are able to change the dimensionality.

Given a random vector u and the invertible function $x'(x, \boldsymbol{u})$, we can accept or reject the proposal x' using a Metropolis-Hastings (MH) acceptance ratio, which can be written as

$$\min\left\{1, \frac{p(x'|y)}{p(x|y)} \frac{r_m(x')}{r_m(x)q(\boldsymbol{u})} \left|\frac{\delta x'}{\delta(x, \boldsymbol{u})}\right|\right\}, \tag{A.13}$$

where $p(x' \mid y)/p(x \mid y)$ is the ordinary ratio of posterior probability of states x and x', $r_m(x)$ is the probabilty of choosing move type m from state x, and $q(\boldsymbol{u})$ is the density function of $\boldsymbol{u}$, and the final term $\left|\frac{\delta x'}{\delta(x, \boldsymbol{u})}\right|$ is the Jacobian that arises from the change of parameter space from $(x, \boldsymbol{u})$ to x'.

The reversible jump moves will dictate how to sample proposals for a new state x' given a vector $\boldsymbol{u}$, after which the proposal is accepted or rejected based on the MH ratio just described. The precise form of this MH ratio depends on the move type and the chosen function $x'(x, \boldsymbol{u})$. Developing the move types and their associated invertible functions represents a large chunk

of the work involved in implementing the reversible jump algorithm for a specific model. Next, some sensible choices for the von Mises model will be discussed.

Split or combine move

The split or combine move is designed as a reversible pair, as is required in the reversible jump framework. That is, any proposed split move is associated with a combine move that would undo it. A split move takes one component and replaces it with two new components. Conversely, a combine move joins two existing components into a single component.

Constructing split/combine proposals for reversible jump MCMC samplers can be done using moment matching (Brooks et al., 2003), where the moments of a combined component are defined to be the sum of the moments of the split components. In the case of von Mises components, this is not straightforward, because the second (linear) moment of a von Mises distribution is mathematically intractable. Rather, trigonometric moments can be used. The first trigonometric moments of a von Mises component with parameters μ and κ are given by $\alpha = E[\cos(\theta)] = \rho\cos(\mu)$ and $\beta = E[\sin(\theta)] = \rho\sin(\mu)$, where the mean resultant length is $\rho = A(\kappa) = I_1(\kappa)/I_0(\kappa)$ and $A(\kappa)$ can be approximated (Mardia & Jupp, 2009, p. 40).

To make sure that the trigonometric moments represent a valid von Mises distributions, the point described by (α, β) must lie on the unit disc, which means that $-1 \leq \alpha \leq 1$, $-1 \leq \beta \leq 1$, and most importantly

$$\sqrt{\alpha^2 + \beta^2} \leq 1. \tag{A.14}$$

This is important for the reversible jump algorithm, because whenever any dimensionality changing move occurs, any new component must also satisfy these constraints.

The constraint of mapping to valid von Mises components, along with the reversibility condition, limit the set of possible moves. However, any move that follows these limitations will be valid in the sense that it will correctly sample from the desired posterior. As long as the limitations are met, we are free to select move types based on computational efficiency, for example. Computational efficiency will be attained when the proposals are likely to be accepted, which in turn is more likely when the proposals are in some sense 'close' to the original components. This will lead the specific choices for the combine and split moves, which will be discussed next.

Combine move

In the combine move, two current components, say j_1 and j_2, are combined into a single new component j^*. The combine move can be obtained from a simple weighted sum of the trigonometric moments. That is, the new combined component has trigonometric moments that are a weighted average between the two components that it stems from.

The parameters of the new component are defined by their trigonometric moments and component weight, $(w_{j^*}, \alpha_{j^*}, \beta_{j^*})$, by computing

$$\begin{aligned} w_{j^*} &= w_{j_1} + w_{j_2}, \\ w_{j^*}\alpha_{j^*} &= w_{j_1}\alpha_{j_1} + w_{j_2}\alpha_{j_2}, \\ w_{j^*}\beta_{j^*} &= w_{j_1}\beta_{j_1} + w_{j_2}\beta_{j_2}. \end{aligned} \tag{A.15}$$

It can be shown that the $(w_{j^*}, \alpha_{j^*}, \beta_{j^*})$ correspond to a valid von Mises distribution and weight, due to the convexity of the unit disc (for $\alpha_{j^*}, \beta_{j^*}$) and the convexity of the unit interval for the weight w_{j^*}.

Split move

In the split move, we start from joint component j^* and split it into two components, j^1 and j^2. The split move must also conform to (A.15) to fulfill the requirement of reversibility, but we must be more careful than in the combine move to prevent the trigonometric moments falling outside the allowed range. We will solve this by proposing the split components from the largest possible disc that is centered at the trigonometric moments of j^*, while being covered by the unit disc. This last property ensures that all proposals are valid.

Next we will discuss how exactly we draw the proposals from within this disc. We can do this by drawing vector $\boldsymbol{u}$ from

$$u_1 \sim \mathcal{U}(0, 0.5) \qquad u_2 \sim \mathcal{U}(0, 2\pi) \qquad u_3 \sim \text{Beta}(2, 1), \tag{A.16}$$

where $\text{Beta}(a, b)$ is the beta distribution. After drawing this vector, we can obtain our split components by computing

$$\begin{aligned} \rho_{max} &= (1 - \rho_{j^*})u_3 \\ w_{j_1} &= w_{j^*}u_1 & w_{j_2} &= w_{j^*}(1 - u_1) \\ \alpha_{j_1} &= \rho_{j^*} - \cos(u_2)\rho_{max} & \alpha_{j_2} &= \rho_{j^*} + \cos(u_2)\rho_{max}w_{j_1}/w_{j_2}, \\ \beta_{j_1} &= \sin(u_2)\rho_{max}, & \beta_{j_2} &= -\sin(u_2)\rho_{max}w_{j_1}/w_{j_2}. \end{aligned} \tag{A.17}$$

As discussed, different choice are possible, but these were found to perform well in practice. To aid understanding, this procedure is given a visual representation in Figure A.1, which will be discussed step by step next.

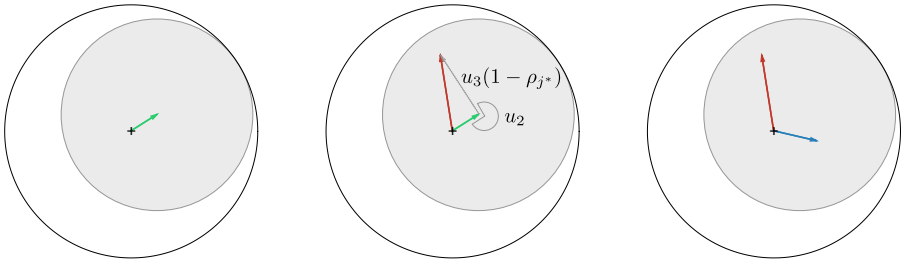

(a) Step 1 (b) Step 2 (c) Step 3

Figure A.1: Construction of split proposal. Step 1 illustrates the mean resultant vector for the von Mises component to be split. In Step 2, the first split component is determined as a function of random vector $\boldsymbol{u}$. Step 3 shows the first and second split component, where the second split component follows from the combination of trigonometric moments.

In step 1 (A.1a), the von Mises component j^* is represented by its trigonometric moments α_{j^*} and β_{j^*} as an arrow. The two new components' trigonometric moments must fall inside the unit circle, as to satisfy constraint (A.14). To do this, a disc with radius $1 - \rho_{j^*}$ centered at $(\alpha_{j^*}, \beta_{j^*})$ is indicated in grey in the figure, from which the split components will be sampled.

In step 2 (A.1b), the first new von Mises component j_1 is placed relative to the original component. The random direction u_2 determines in what direction the new trigonometric moment of j_1 will lie. The trigonometric moments of the proposal $(\alpha_{j_1}, \beta_{j_1})$ are then chosen to lie in this direction, a distance of $u_3(1 - \rho_{j^*})$ away from $(\alpha_{j^*}, \beta_{j^*})$.

Step 3 (A.1c) places the second new von Mises component. Given the original component j^* and the first new component j_1, the moments for the second component j_2 are placed. They are found in the opposite direction from $(\alpha_{j^*}, \beta_{j^*})$, that is $u_2 + \pi$. The distance is determined depending on the ratio of the two weights. This can be computed as given in (A.15).

The probability of performing a split move as opposed to a combine move $r_m(x)$ is set to $\frac{1}{2}$, independent of the current state of the MCMC sampler. It then follows that the probability of the corresponding combine move $r_m(x') = 1 - r_m(x) = \frac{1}{2}$ and their ratio $r_m(x')/r_m(x) = 1$. This can result in an attempted combine move when $g = 1$, which is immediately rejected.

The Jacobian for the split move is straightforward to derive, but long in

form and given by

$$\begin{aligned}\left|\frac{\delta x'}{\delta(x,u)}\right| =& \frac{(R_{j^*}-1)^2 R_{j^*} w_{j^*}(1-2u_1)^2 u_3}{u_1-1} \times \\ & \left(2(R_{j^*}-1)R_{j^*}\cos(u_2)u_3 + (1-2R_{j^*})u_3^2 + R_{j^*}^2(1+u_3^2)\right)^{-1/2} \times \\ & \left[(1-2R_{j^*})u_1^2u_3^2 + R_{j^*}^2(1-2u_1+u_1^2(1+u_3^2)) - \right. \\ & \left. 2(R_{j^*}-1)R_{j^*}\cos(u_2)(u_1-1)u_1u_3\right]^{-1/2}.\end{aligned}$$

The inverse of this Jacobian is used for the combine move.

Birth or death move

A birth move introduces a new component into the mixture, without assigning any observations to this component. Its inverse, a death move, removes a component that has no observations.

The proposal for a birth move consists of drawing parameters (w_{j^*}, μ_{j^*}, κ_{j^*}) for a new component. They are chosen from a proposal distribution as

$$v_{j^*} \sim \mathcal{U}(0,1) \qquad \mu_{j^*} \sim \mathcal{U}(0,2\pi) \qquad \kappa_{j^*} \sim \chi^2_{10}. \tag{A.18}$$

These parameters are then used to construct vector $\boldsymbol{u} = (v_{j^*}, \mu_{j^*}, \kappa_{j^*})$. The weights of the other components need to be rescaled such that the sum of weights remains 1. The new weights are given by $w'_j = w_j(1-v_{j^*})$, for $\{j \in 1,\ldots,g\}$.

Notably, as no observations are allocated to the newly created component, the likelihood of the data is unaltered by the move. Additionally, as with the split or combine move type, the probability of performing a birth move $r_m(x)$ is set equal to the probability of performing the corresponding death move $r_m(x')$, independent of the state of the MCMC sampler. Therefore, the acceptance probability (A.13) can be simplified to

$$\min\left\{1, \frac{p(x')}{p(x)}\frac{1}{q(u)}\left|\frac{\delta x'}{\delta(x,u)}\right|\right\}. \tag{A.19}$$

The Jacobian for a birth move is given by

$$\left|\frac{\delta x'}{\delta(x,u)}\right| = (1-w_{j^*})^g. \tag{A.20}$$

For a death move, vector $\boldsymbol{u}$ is given by the component parameters of the component that is removed j^*, $\boldsymbol{u} = (w_{j^*}, \mu_{j^*}, \kappa_{j^*})$. Its MH acceptance ratio is the inverse of the MH acceptance ratio of the corresponding birth move.

A.3.5 Label switching

When fitting a mixture model with a fixed number of components g, label switching (Jasra et al., 2005) can occur when, for example, the means of two components are close and by random chance switch order. This can also be seen as an identifiability problem. When applying a sampler that can jump between parameter spaces and change the number of components as part of the MCMC chain, label switching is very likely to occur, regardless of the distance between means, because split moves do not define an order for the created components.

A simple method of dealing with label switching is by imposing an identifiability constraint, for example by requiring the means to be ordered. This is a crude method that does not work in the case of circular data, since two means will always be ordered the same way on a circle.

A solution is provided by Stephens (2000) in the form of a post-processing step to define the most likely allocation of sampled parameters to individual components and does not rely on constraints. The second post-processing algorithm featured in the paper is applied to the samples belonging to each specific g separately.

A.4 Simulation study

A simulation study was performed to investigate the relative performance of the MCMC sampler in different scenarios. The sampler was implemented in R (R Core Team, 2015) using the `circular` package (Agostinelli & Lund, 2013). The source code has been made available at `https://github.com/pieterjongsma/circular-rjmcmc`.

A.4.1 Simulation scenarios

In order to assess the performance in a variety of settings, five true data generating processes were selected to represent either common or particularly difficult mixture datasets to fit. These scenarios are visualised in Figure A.2 and consist of (A.2a) a single von Mises component where $\mu_1 = 0$ and $\kappa_1 = 10$, (A.2b) two von Mises components where $\mu_1 = 0$, $\mu_2 = \pi$ and $\kappa_1 = \kappa_2 = 10$, (A.2c) two von Mises components where $\mu_1 = -\pi/6$, $\mu_2 = \pi/6$ and $\kappa_1 = \kappa_2 = 10$, (A.2d) three von Mises components where $\mu_1 = -\pi/3$, $\mu_2 = 0$, $\mu_3 = \pi/3$ and $\kappa_1 = \kappa_2 = \kappa_3 = 10$ and (A.2e) a uniform von Mises component ($\kappa = 0$). Each scenario is simulated with 50, 100, 250, 500, 1000, 2500 and 10,000 observations across 1000 replications.

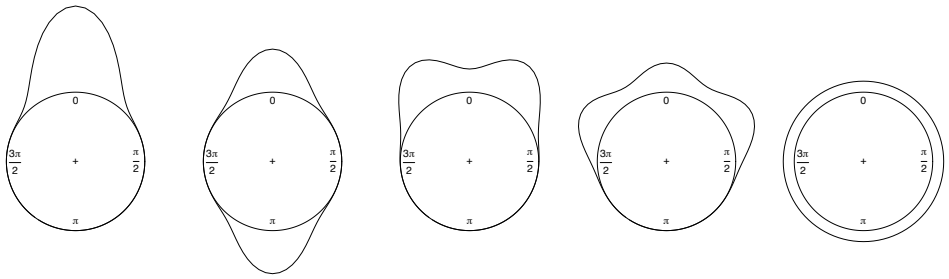

(a) (b) (c) (d) (e)

Figure A.2: Visualization of simulation scenarios used for investigating sampler performance.

A.4.2 Starting values

The MCMC sampler is initialized with a single component ($g = 1$) and parameters for the component drawn analogous to a birth move

$$w = 1 \qquad \mu \sim \mathcal{U}(0, 2\pi) \qquad \kappa \sim \chi^2_{10}. \tag{A.21}$$

The observations are all attributed to this single component by setting the allocation vector as $z_i = 1$ for $\{i \in 1, \ldots, N\}$.

A.4.3 Convergence

The convergence of a reversible jump MCMC algorithm is difficult to assess using conventional methods such as the inspection of the sampled values of a parameter. Due to the changing dimensionality, the posterior distributions of individual component parameters depend on the component count g. The chains for these components are expected to jump with every change of g and would therefore not provide a valid measure of convergence. Instead, the likelihood $p(x \mid \boldsymbol{\theta})$ is calculated for each iteration of the MCMC chain for which convergence of the posterior probability is assessed visually. All chains, regardless of starting value and variation in replicated data, converged within a burn-in of 10,000 iterations. After the burn-in, the next 5,000 iterations are retained and used to describe the posterior properties of the simulated dataset.

A.4.4 Results

For brevity, this section will be focused on the ability of the sampler to recover the number of components g correctly. In addition, performance of

model parameters will be assessed for a subset of simulations.

Number of components g

The results for the number of components g of the simulation study are summarized in Table A.1. It shows the fraction of replications in which the maximum a posteriori (MAP) estimate of g, g_{MAP}, which is the posterior mode, was equal to the simulated g, g_{TRUE}. Furthermore, the posterior distribution of g is given, averaged over all replications.

Results with few observations ($n = 50$) show high uncertainty about the number of components. For these replications, the mode of the posterior distribution for g was rarely equal to the simulated g. As expected, the estimation of g then improves with the number of observations. Most scenarios show a near 100% correct mode g_{MAP} at 1000 observations or more. One exception is scenario A.2b for $n = 10000$. Here, g is overestimated and accuracy is seemingly worse than at a smaller sample size. It should be noted that an overestimation of g does not necessarily indicate a problem with the MCMC method. A model with a higher number of components may have a higher likelihood of the data. The chosen prior for g is intended to counter this effect, such that the simpler model is favored. The prior is seemingly not powerful enough for scenario A.2b where $n = 1000$ or larger.

For the uniform scenario A.2e, the column $g_{MAP} = g_{TRUE}$, showing the correspondence between the mode of the posterior distribution and the simulated g, has been omitted. Although this data was simulated as a single component with $\kappa = 0$, the interpretation of 'true' g of this distribution is ambiguous. For larger datasets, the method favors a small number of components, as expected.

Parameter estimates

Results for the recovery of the von Mises parameters $\boldsymbol{\mu}$ and $\boldsymbol{\kappa}$, are summarized for scenario A.2d in Table A.2. To obtain these estimates, only the MCMC states with three components are retained, so that $g = 3$ as in the data generating process of scenario A.2d. For each simulated data set, MAP estimates for $\hat{\boldsymbol{\mu}}$ and $\hat{\boldsymbol{\kappa}}$, are computed by estimating the posterior modes from the MCMC sample. Then, these MAP estimates are averaged over all simulated datasets and presented.

The estimates of component parameters for scenario A.2d show that in general the method is able to recover the true parameter estimates without bias, even with small sample size ($n = 50$). The concentration parameter $\boldsymbol{\kappa}$ is overestimated with small samples, but estimates are reasonable for samples

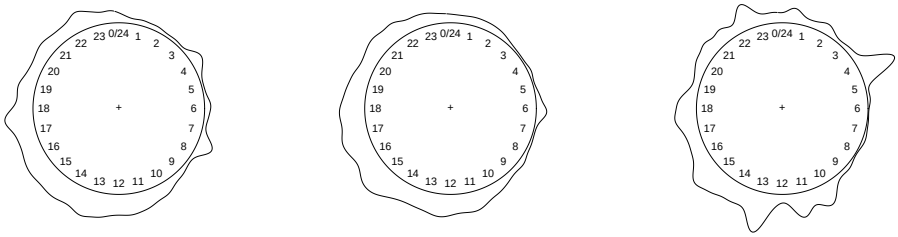

(a) Indie Electronic ($n = 11,393$)

(b) Relax ($n = 10,657$)

(c) Deep House ($n = 4,757$)

Figure A.3: Kernel density estimates of observations for analyzed *22tracks* genres, using a von Mises kernel with $\kappa = 200$. The period of the circle is 24 hours.

where $n \geq 500$. The concentration parameter of the central component, κ_2, is systematically underestimated in this scenario. Most likely, the central is assigned some observations that belong to its two neighbors, and as a result is estimated as less concentrated than the true data generating process.

A.5 Illustration

As a motivating example, we will apply the reversible jump MCMC sampler to a dataset of listening behavior, made available by *22tracks*. This data will first be described and visualized in Section A.5.1. Then, results from applying the sampler to the data are discussed in Section A.5.2.

A.5.1 Dataset

The data provided by *22tracks* contain metrics of all users of the service over the span of one week (January 4-10, 2016). The data consist of the time of day (00:00h to 23:59h) at which a user played a particular song, categorized by the genre this song was in. In this paper, a subset of the data is used as an illustration. These consist of all observations categorized under one of three genres that were selected arbitrarily. The genres are Indie Electronic, Relax and Deep House. Figure A.3 shows kernel density estimates of each genre. It can be seen that depending on the genre, the data features a different number of modes, although determining the precise number of modes is difficult without running the mixture model.

The first goal of this analysis is to estimate the genre that is most likely to be selected at any given time. Supposedly, users listen to the genres available on the *22tracks* service at different times of day. For example, Pop might be a genre that users listen to throughout the day while Deep House is preferred during the night. Quantifying this behavior is valuable for the music service, as it allows them to present the most appropriate genres to users when they visit the site at a particular time.

The second goal is to understand music listening behavior through the parameters of our mixture components, as the times at which we listen to music are a reflection of life in our society. The mixture components are then interpreted as a subpopulation of observations that correspond to a certain category of music listening, such as listening while working, during transit, or while dancing.

A.5.2 Results

We apply the mixture model to each genre separately, with starting values as described in Section A.4.2, using a burn-in of 10,000 iterations and retaining the next 100,000 iterations for inference. The posterior distributions for component count g are summarized in Table A.3. The posteriors are quite different, with the Deep House genre showing a notably higher estimated component count, which is in accordance with the data as displayed in Figure A.3.

To obtain estimates for the other parameters $\boldsymbol{w}$, $\boldsymbol{\mu}$ and $\boldsymbol{\kappa}$, only the samples for which $g = g_{MAP}$ are used. For Deep House, these are samples where $g = 6$, for Indie Electronic $g = 2$ and for Relax $g = 3$. The parameters have been summarized in Table A.4, ordered by the weights $\boldsymbol{w}$.

The Indie Electronic genre shows two broad components spanning most of the day. One is centered at the middle of the day (14:15h) and one is centered in the evening (21:13h), most likely corresponding to listening while working and listening at home during the evening. The components have a small concentration, suggesting only slight preference for these times. Such broad components are necessary, because listening occurs throughout the day. Similarly, the Relax genre is given three components with small concentration.

For the Deep House genre, six components provided the best fit. The first three components are broad and similar to the components found for the other genres. The central times are later in the day, as one might expect for this type of music. The sampler was also able to detect and fit the strong concentrations of observations at 10:41h, 04:27h and 12:58h. It is unlikely that these patterns have been created by actual users. More likely, they

indicate a special attribute of the data. For example, a computer bot instead of an actual person could have triggered a large amount of plays in a short time span. Although this does not tell us anything about the behavior of actual users, it is still an interesting property that the sampler detects quite well. In fact, such a component has direct financial implications for this business, as such plays can be rejected to save costs.

Compared to a kernel density model, this provides a much simpler and more interpretable summary of the data. The posterior distribution also provides uncertainty around all of these estimates, although these are not shown here for brevity.

A.6 Discussion

We have presented a method for Bayesian inference of von Mises mixture distribution. Previous work has assumed the number of components to be known, which is an assumption we have relaxed by employing the reversible jump MCMC algorithm. The main contributions included a novel set of dimensionality changing moves based on the trigonometric properties of the von Mises distribution. In addition, the performance of the method was investigated in a simulation study. Generally, the method performed well. An illustration was provided on music listening behavior, showing the interpretation of this method.

Results of the simulation study showed that the estimation of the number of components g was accurate for the majority of the simulated sample sizes, so the proposed split and combine moves successfully move between parameter spaces. In one scenario (A.2b), g is overestimated at a very large sample count ($n = 10000$). In this case the proposed prior for g appears insufficient. A different choice of prior might be able to counter this effect and seems a topic for further investigation. It should be noted that although undesirable, an overfitted mixture is not necessarily problematic in application. The estimation of parameters $\boldsymbol{w}$, $\boldsymbol{\mu}$ and $\boldsymbol{\kappa}$ of the individual components is not directly affected and these parameters remain interpretable. Furthermore, the component weights allow us to gauge the relative importance of each component.

Application to the *22tracks* data provides an example for the interpretation of reversible jump MCMC sampler output. It should be noted that the observation counts in the *22tracks* data were higher than what showed the most accurate estimation of the simulated component count in the simulation study and as such we did not infer much from the estimated g. Because the parametric von Mises model is easy to interpret, one can compare the

results with intuition. The estimated component parameters $\boldsymbol{\mu}$ and $\boldsymbol{\kappa}$ in the provided example seem reasonable as they indicate listening to occur during daytime and in the evening.

In conclusion, the method presented in this paper provide a reversible jump MCMC sampler that is shown to perform well on simulated data as well as a real world example.

Table A.1: Simulation results for each of the scenarios in Figure A.2 with sample sizes ranging from $n = 50$ to $n = 10000$. Each row represents 1000 replications. The fraction of replications where the estimated g was equal to the simulated g is given under $g_{MAP} = g_{TRUE}$. In addition, the posterior distribution $p(g \mid \theta)$ is given as the average over all replications.

			$p(g \mid \boldsymbol{\theta})$				
Scenario	n	$g_{MAP} = g_{TRUE}$	$g = 1$	$g = 2$	$g = 3$	$g = 4$	$g \geq 5$
A.2a	50	0.40	0.29	0.29	0.21	0.12	0.10
	100	0.73	0.54	0.32	0.11	0.03	0.00
	250	0.88	0.69	0.27	0.04	0.00	0.00
	500	0.94	0.72	0.25	0.03	0.00	0.00
	1000	0.96	0.76	0.22	0.02	0.00	0.00
	2500	0.99	0.82	0.17	0.01	0.00	0.00
	10000	1.00	0.85	0.14	0.01	0.00	0.00
A.2b	50	0.12	0.00	0.10	0.15	0.16	0.59
	100	0.66	0.00	0.50	0.31	0.12	0.06
	250	0.91	0.00	0.81	0.18	0.01	0.00
	500	0.88	0.00	0.77	0.21	0.01	0.00
	1000	0.81	0.00	0.71	0.27	0.02	0.00
	2500	0.71	0.00	0.63	0.34	0.03	0.00
	10000	0.58	0.00	0.54	0.44	0.02	0.00
A.2c	50	0.30	0.05	0.23	0.29	0.21	0.22
	100	0.66	0.08	0.51	0.30	0.09	0.03
	250	0.93	0.03	0.83	0.13	0.01	0.00
	500	0.97	0.01	0.85	0.13	0.01	0.00
	1000	0.98	0.00	0.86	0.13	0.01	0.00
	2500	0.98	0.00	0.89	0.11	0.00	0.00
	10000	1.00	0.00	0.94	0.06	0.00	0.00
A.2d	50	0.30	0.01	0.11	0.22	0.22	0.44
	100	0.60	0.01	0.25	0.45	0.21	0.08
	250	0.84	0.00	0.15	0.78	0.07	0.00
	500	0.96	0.00	0.04	0.91	0.06	0.00
	1000	0.97	0.00	0.02	0.94	0.04	0.00
	2500	0.97	0.00	0.02	0.95	0.03	0.00
	10000	0.98	0.00	0.01	0.98	0.01	0.00
A.2e	50		0.01	0.03	0.05	0.07	0.84
	100		0.15	0.25	0.25	0.17	0.18
	250		0.34	0.37	0.20	0.07	0.02
	500		0.36	0.38	0.19	0.06	0.01
	1000		0.37	0.37	0.19	0.05	0.01
	2500		0.37	0.38	0.19	0.05	0.01
	10000		0.37	0.37	0.21	0.04	0.01

Table A.2: Parameter estimates for scenario A.2d with parameters $\mu_1 = -1.05$, $\mu_2 = 0$, $\mu_3 = 1.05$ and $\kappa_1 = \kappa_2 = \kappa_3 = 10$.

n	$\hat{\mu}_1$	$\hat{\mu}_2$	$\hat{\mu}_3$	$\hat{\kappa}_1$	$\hat{\kappa}_2$	$\hat{\kappa}_3$
50	-0.99	0.01	1.02	183.7	82.0	192.9
100	-1.04	0.00	1.07	161.8	62.6	133.9
250	-1.05	-0.01	1.05	31.6	34.7	17.8
500	-1.05	0.00	1.06	11.9	8.0	10.6
1000	-1.05	0.00	1.05	10.7	8.2	10.5
2500	-1.04	0.01	1.04	10.0	9.7	10.1
10000	-1.04	0.00	1.04	10.0	9.7	10.0

Table A.3: Posterior probability of component counts $p(g)$ for selected *22tracks* genres.

	g							
Genre	1	2	3	4	5	6	7	8
Indie Electronic	0.01	0.52	0.36	0.10	0.01	0.00	0.00	0.00
Relax	0.00	0.25	0.55	0.18	0.02	0.00	0.00	0.00
Deep House	0.00	0.00	0.00	0.02	0.30	0.37	0.28	0.03

Table A.4: Estimated component parameters for individual genres in *22tracks* data. LB and UB indicate the lower and upper bound of the 95% density of the data density of this von Mises component. Components have been ordered according to their respective weights.

					95% density	
Genre	j	$\hat{w}_j$	$\hat{\mu}_j$	$\hat{\kappa}_j$	LB	UB
Indie Electronic	1	0.72	3.73 (14:15h)	0.89	1.04 (03:58h)	0.15 (00:33h)
	2	0.28	5.55 (21:13h)	0.72	2.77 (10:36h)	2.05 (07:50h)
Relax	1	0.54	4.11 (15:43h)	1.20	1.63 (06:15h)	0.31 (01:11h)
	2	0.33	5.49 (20:59h)	0.85	2.78 (10:37h)	1.93 (07:22h)
	3	0.13	3.09 (11:49h)	1.75	1.10 (04:12h)	5.09 (19:27h)
Deep House	1	0.30	3.99 (15:15h)	2.07	2.25 (08:35h)	5.74 (21:55h)
	2	0.28	6.04 (23:04h)	1.64	3.95 (15:05h)	1.85 (07:03h)
	3	0.17	5.13 (19:36h)	1.59	2.99 (11:27h)	0.98 (03:45h)
	4	0.10	2.79 (10:41h)	33.81	2.45 (09:23h)	3.13 (11:59h)
	5	0.08	1.16 (04:27h)	635.81	1.09 (04:09h)	1.24 (04:45h)
	6	0.07	3.40 (12:58h)	648.16	3.32 (12:41h)	3.47 (13:16h)

References

Agostinelli, C., & Lund, U. (2013). R package `circular`: Circular statistics (version 0.4-7) [Computer software manual]. CA: Department of Environmental Sciences, Informatics and Statistics, Ca' Foscari University, Venice, Italy. UL: Department of Statistics, California Polytechnic State University, San Luis Obispo, California, USA. Retrieved from https://r-forge.r-project.org/projects/circular/

Akaike, H. (1974). A new look at the statistical model identification. *IEEE transactions on automatic control*, *19*(6), 716–723.

A Mooney, J., Helms, P. J., & Jolliffe, I. T. (2003, January). Fitting mixtures of von Mises distributions: a case study involving sudden infant death syndrome. *Computational Statistics & Data Analysis*, *41*(3-4), 505–513.

Banerjee, A., Dhillon, I. S., Ghosh, J., & Sra, S. (2005). Clustering on the Unit Hypersphere using von Mises-Fisher Distributions. *Journal of machine Learning research*, *6*(Sep), 1345–1382.

Besag, J., Green, P., Higdon, D., & Mengersen, K. (1995, February). Bayesian computation and stochastic systems. *Statistical science*, *10*(1), 3–41.

Brooks, S. P., Giudici, P., & Roberts, G. O. (2003). Efficient construction of reversible-jump Markov chain Monte Carlo proposal distributions. *Journal of the Royal Statistical Society: Series B (Statistical Methodology)*, *65*(1), 3–55.

Fernández-Durán, J. J., & Mercedes Gregorio-Domínguez, M. (2016, February). Bayesian analysis of circular distributions based on non-negative trigonometric sums. *Journal of Statistical Computation and Simulation*, *86*(16), 3175–3187.

Ferreira, J. T. A. S., Juárez, M. A., & Steel, M. F. J. (2008, June). Directional log-spline distributions. *Bayesian Analysis*, *3*(2), 297–316.

Fisher, N. I. (1995). *Statistical analysis of circular data*. Cambridge: Cambridge University Press.

Forbes, P. G. M., & Mardia, K. V. (2014, June). A fast algorithm for sampling from the posterior of a von Mises distribution. *Journal of Statistical Computation and Simulation*, *85*(13), 2693–2701.

Ghosh, K., Jammalamadaka, R., & Tiwari, R. (2003, February). Semiparametric Bayesian Techniques for Problems in Circular Data. *Journal of Applied Statistics*, *30*(2), 145–161.

Green, P. J. (1995, December). Reversible jump Markov chain Monte Carlo computation and Bayesian model determination. *Biometrika*, *82*(4), 711–732.

Gurtman, M. B. (2009, July). Exploring Personality with the Interpersonal Circumplex. *Social and Personality Psychology Compass*, *3*(4), 601–619.

Guttorp, P., & Lockhart, R. A. (1988). Finding the location of a signal: A bayesian analysis. *Journal of the American Statistical Association*, *83*(402), 322–330.

Hastings, W. K. (1970, April). Monte Carlo sampling methods using Markov chains and their applications. *Biometrika*, *57*(1), 97–109.

Hornik, K., & Grün, B. (2014). movmf: An r package for fitting mixtures of von mises-fisher distributions. *Journal of Statistical Software*, *58*(10), 1–31.

Jasra, A., Holmes, C. C., & Stephens, D. A. (2005, February). Markov chain Monte Carlo methods and the label switching problem in Bayesian mixture modeling. *Statistical science*, *20*(1), 50–67.

Mardia, K. V., & El-Atoum, S. (1976). Bayesian inference for the von mises-fisher distribution. *Biometrika*, *63*(1), 203–206.

Mardia, K. V., & Jupp, P. E. (2009). *Directional Statistics*. Wiley.

McLachlan, G., & Krishnan, T. (2007). *The EM algorithm and extensions*. John Wiley & Sons.

Mechsner, F., Kerzel, D., Knoblich, G., & Prinz, W. (2001, November). Perceptual basis of bimanual coordination. *Nature*, *414*(6859), 69–73.

Pewsey, A., Neuhäuser, M., & Ruxton, G. D. (2013). *Circular statistics in r*. Oxford University Press.

R Core Team. (2015). R: A language and environment for statistical computing [Computer software manual]. Vienna, Austria. Retrieved from https://www.R-project.org/

Richardson, S., & Green, P. (1997). On Bayesian Analysis of Mixtures with Unknown Number of Components. *Journal of the Royal Statistical Society: Series B (Statistical Methodology)*, *59*(4), 731–792.

Schwarz, G. (1978, March). Estimating the Dimension of a Model. *The Annals of Statistics*, *6*(2), 461–464.

Stephens, M. (2000, January). Dealing with label switching in mixture models. *Journal of the Royal Statistical Society: Series B (Statistical Methodology)*, *62*(4), 795–809.

Tierney, L. (1994, December). Markov chains for exploring posterior distributions. *The Annals of Statistics*, *22*(4), 1701–1728.

Appendix B

Dealing With Partially Observed Crime Times

B.1 Introduction

Crime analysis is concerned with understanding and predicting crime by evaluating core aspects of crimes such as their location, time, targets, offenders and the availability of guardians. When tasked with understanding or predicting whether a certain crime is likely to occur, one must know where the crime is to occur, but also at what time of the day. Burglaries, for example, are less likely to occur in the evening. Temporal variation, such as the hour of day, contributes more to the overall variation in crime likelihood than any other type of variation (Felson & Poulsen, 2003). However, in the crime analysis literature the temporal dimension is routinely ignored (Ratcliffe & McCullagh, 1998; Ratcliffe, 2000).

A central difficulty of the temporal dimension is that most crime times are not directly observed. That is, when a crime is recorded, the victim is often uncertain of when the crime occured exactly, but is only able to say that the crime happened after start time s and before some end time e. Therefore, one is left with a set of intervals of time (s, e) in which the crime occurred. Figure B.1 shows three examples of such intervals. This type of crime time data where the exact time is not known is called *aoristic data*, with the interval (s, e) called an *aoristic interval*. Using such data severely complicates crime time analysis: if only the start times are used, the analysis is biased towards estimating crimes as happening too early, while using the end times gives estimates that are too late.

A more sophisticated approach to deal with aoristic data is what Ashby & Bowers (2013) call *aoristic analysis* (Ratcliffe & McCullagh, 1998; Ratcliffe,

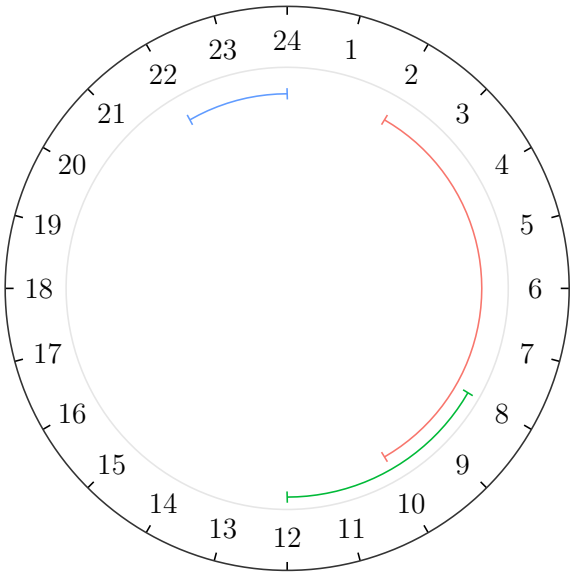

Figure B.1: Example of three aoristic intervals representing possible crime times, which are 2 AM - 10 AM (red), 8 AM - 12 AM (green), and 10 PM - 12 PM (blue).

2000). This method consists of giving each observation a total weight of 1, and spreading this weight out over the length of the interval. Thus, for a crime that took place in the interval 15:00 - 18:00, the hours in this interval each get a weight of 1/3 from this observation. Therefore, the more certainty that a crime occured within a certain hour, the more probability is assigned to it. Then, the weights of all aoristic intervals are averaged within some chosen unit of time (e.g. an hour) to get an estimate of the proportion of crimes occuring during that unit of time. Because the weight is called the *aoristic fraction*, we will refer to this approach as the *aoristic fraction method* to distinguish it from other aoristic data analysis methods. Details for the aoristic fraction method are given in Section B.3.

The goal in aoristic analyses is to obtain an estimated *crime time density*, that is, a mathematical function $\hat{p}(t)$ that takes in an interval of time and returns the proportion of crimes that will happen in that interval. If the estimate is good, we know well when crimes will happen. It should be noted that we can find estimated crime time densities at an aggregate level, or if additional predicting covariates are available, the estimated crime time density conditional on these covariates. This last approach is particularly valuable for purposes of imputing the crime time, so that it can be used in further analysis.

From a statistical point of view, this crime time density is an estimate of a probability density function. In fact, the hope of any aoristic analysis is to approach the true probability density function of crime times, so we can evaluate any aoristic method by seeing whether it comes close to the true crime time density.

Currently available methods, such as the one described by Ashby & Bowers (2013), have several major drawbacks. The drawbacks we will address here are that the currently available methods (a) systematically overrepresent the variance of the data, (b) are not built on a solid statistical foundation so that they do not provide valid statistical inference about the true distribution of crime times, (c) do not take into account model uncertainty caused by small samples, (d) can not be embedded in a larger statistical model, (e) split time in categories which leads to arbitrary choices, and (f) do not allow mixing aoristic data with data where times are directly observed. These drawbacks limit both predictive performance as well as the use of these models for understanding patterns in crime. In this work, methods will be developed which are easier to use, built on a more solid statistical foundation, and which can be embedded in a larger model. This method is rooted in circular statistics, which is the branch of statistics that deals with periodical sample spaces, such as the 24-hour clock in this case. It should be noted that all examples and discussion will be based on aoristic data on the 24-hour clock, but all methods are equally applicable to other time periods, such as weeks, months and years.

Throughout this paper, these drawbacks will be expanded on and addressed. The rest of this paper will be structured as follows. In Section B.2, a general introduction to aoristic data will be given. The Aoristic Fraction method and its drawbacks will be addressed in Section B.3. Section B.4 will provide a way to estimate parametric statistical models using aoristic data, while Section B.5 will add a non-parametric Bayesian method to these approaches, which is more realistic for multimodal crime time data. Section B.6 will show how this method can be applied to several problems in crime time analysis. Finally, B.7 has some concluding remarks.

B.2 Aoristic data

Aoristic data are temporal data that contain intervals (s, e) instead of having all observed time points. Such data arises in crime analysis when crimes happen while the victim is not present. For some types of crime close to all records are aoristic, such as for the bike thefts analyzed in Ashby & Bowers (2013) or property theft, such as burglaries. For other crimes, a combination

of directly observed times (e.g. caught red-handed) and aoristic intervals is observed. This mixed data type can be a problem for some aoristic analysis methods, such as the aoristic fraction method described in the next section.

Importantly, aoristic data or temporal data refers here to the time of the day, the day of the week, month, or year. To be precise, this is the cyclic, or periodical, aspect of time. Time can also be viewed linearly, for example by making statements about crime increasing in a certain area over time, or using a time series model for the changing frequency of crime, or including year as a covariate in a model for crime. Such analyses can be combined with the aoristic methods under consideration, but are not the focus of this work.

The main issue of observing intervals of time instead of directly observing time points is that descriptive or inferential analysis methods are generally developed for directly observed data, so they do not allow intervals as inputs. Therefore, the aoristic data must be dealt with, either through a pragmatic solution or a specialized analysis method for it.

Simple ways to deal with aoristic data include ignoring the aoristic data, taking only the start points of the intervals, the end points, mid points, or a random point in the interval, which are compared in Ashby & Bowers (2013). Removing all aoristic intervals from the data set is wasteful and often leaves us with little to no data. Using start times of the interval will clearly cause us to expect crime earlier than it really happens, while taking the end times of the interval will lead to estimates that are too late. Taking the mid-points is a better solution, but this means that we allege to know the true crime time, and as such overestimates our certainty in our analyses. Sampling a random point (uniformly) in the interval is the most valid amongst these pragmatic options, but can cause the results to depend on the random sampling. Therefore, the aforementioned aoristic fraction method is often recommended, which will be examined in the following section.

The aoristic data problem can also be seen as a missing data problem, where the crime times are not completely missing but rather partially observed. In this view, the random sampling approach essentially amounts to single imputation of missing data with the distribution of the data uniform in the interval. Single imputation is generally not recommended (Van Buuren, 2018). Commonly used missing data analysis methods use multiple imputations, and do not impute a data point uniformly from its possible places, but use the rest of the data to estimate the distribution of the missing data points, and draw imputations from this distribution. A multiple imputation approach could be a possible solution for aoristic data, but it difficult to define the crime time density within an aoristic interval based on the other aoristic intervals. Therefore, we will focus on other solutions.

Before we continue with an investigation of aoristic analysis methods, it

is helpful to consider two ways in which aoristic data makes it more difficult to learn about the true crime time density.

First, the uncertainty about the location of the true crime time in the interval also means increased uncertainty in any statistical model that incorporates it. Therefore, making decisions using aoristic data requires a larger sample size than using known times. However, in this case it is still possible to create aoristic analysis methods that do not introduce any systematic bias in the estimated crime time density.

However, a systematic unobserved preference within the interval can cause bias which can not be solved, although this has not yet been investigated in previous work on aoristic analysis. To see this, note that the true crime time may have a tendency to be located near either the beginning or the end of the interval. For example, if offenders observe their victims, and strike when they leave their property, true crime times will have a tendency to occur in the beginning of the interval. If the unobserved true crime time is t_{actual}, then we can also think about the start time s as the true value minus some difference, or $s = t_{\text{actual}} - \delta^l$, and the end time e as the true time plus some difference, $e = t_{\text{actual}} + \delta^u$. Note that the differences δ^l and δ^u are also unobserved (unless they are zero). If for some interval δ^l is larger than δ^u or vice versa, there is no problem because these will cancel out on average. However, if one is larger than another on average over the whole dataset, then any estimate of t_{actual} is systematically biased with no way for the crime analyst to detect this. From the missing data viewpoint, this is similar to the concept of missing not at random (MNAR), in that there is no information in our current dataset that can solve this issue. The only solution is to introduce outside information into the analysis, such as prior knowledge about the intervals or a sufficiently sized known-time dataset. Due to this difficulty, throughout this work we will follow other work on aoristic analysis in taking the assumption that δ^l and δ^u have the same average, that is, the true crime time is equally likely to be near the start or the end of the interval.

As a final unrelated note, temporal data (including aoristic data) is usually treated by splitting times into broad categories, such as hours ('15:00 - 16:00'), three or four groups (such as 'evening') (Pereira et al., 2016) or dichotomous splits ('5 AM - 5 PM') (Felson & Poulsen, 2003). While easy to perform, categorization requires the crime analyst to choose the amount of categories and where to place cutpoints, a choice which can influence the resulting conclusions. In addition, categorization treats adjacent categories, say '15:00 - 16:00' and '16:00 - 17:00', as being just as distant as, say, '15:00 - 16:00' and '02:00 - 03:00'. Certainly, we should be able to 'borrow information' from adjacent categories, which is especially relevant if there is limited data. In fact, from a statistical viewpoint, we can. Therefore, we will em-

ploy continuous methods throughout, because they do not pose signficant additional challenge in either statistical or computational methods.

B.3 Aoristic Fraction method

The aoristic fraction method is a descriptive method for aoristic data discussed in Ratcliffe & McCullagh (1998), which is similar various other methods that have been described over time (Gottlieb et al., 1994; Rayment, 1995; Brown, 1998). It can be described as a circular histogram that is created from aoristic intervals. While the random point method would sample a value from the uniform distribution within each interval (s, e), the aoristic fraction method keeps this uniform distribution and treats it as a building block for the histogram.

The aoristic fraction method uses the aoristic function, which is a function that captures the information in the data, as an approximation of the crime time density. The final analysis takes the form of a plot of this function, either directly on a 24-hour clock such as one displayed in Figure B.2, which shows both the observed aoristic intervals and the resulting aoristic function, or on a map such as generated by the `R` package `aoristic` (Kikuchi, 2015). To compute the aoristic function, for each observation i we take the interval (s_i, e_i) and compute the length of the interval $e_i - s_i$. Then we give all values within the observed interval weight $\frac{1}{e_i - s_i}$, so that shorter intervals have more weight. Finally, we sum these weights up for all observed intervals to obtain the estimated crime time density. Mathematically, we can write this function at time t as

$$\hat{p}_{AF}(t) = \frac{1}{n} \sum_{i=1}^{n} \frac{I(e_i < t < s_i)}{e_i - s_i} \tag{B.1}$$

where $I(e_i < t < s_i)$ an indicator function, which is 1 if t is in aoristic interval i, and 0 otherwise.

The aoristic function serves as estimate of the probability density at each time point of a crime occuring. That is, if the true crime times are distributed such that a crime at time point t has probability density $p(t)$, then the aoristic fraction method is an estimate of this, which we called $\hat{p}_{AF}(t)$. This estimate can then be used to make decisions, perhaps by calculating the expected percentage of crimes that will occur within a certain time frame. For example, the proportion of crimes expected to occur between 18:00 and 19:00 is $\hat{p}(18 < t < 19) = \int_{18}^{19} \hat{p}_{AF}(t)dt = 0.069$, so 6.9%. This type of information is directly useful in crime prevention, such as in police resource allocation through the timing of police shifts.

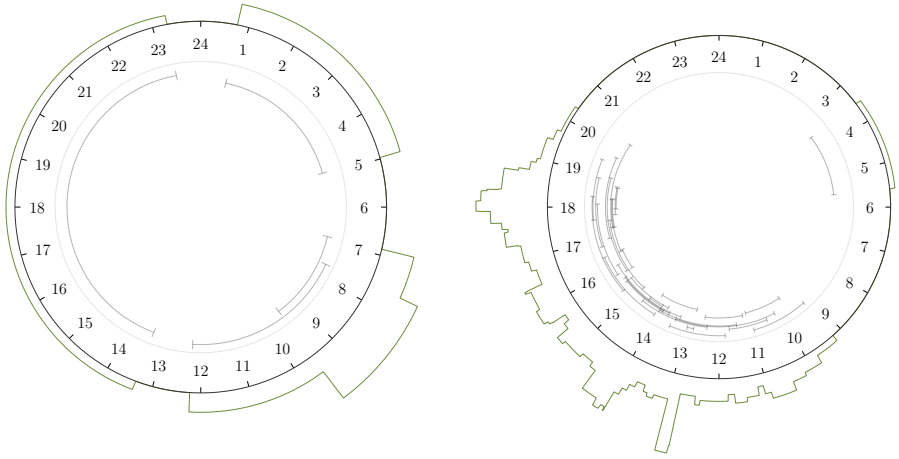

(a) (b)

Figure B.2: Two examples of observed aoristic intervals (grey, inside circle) and the output of the aoristic fraction method (green, outside circle) denoting the estimate of the crime time density. Left, a small data with four observations. Right, a more realistic dataset with 30 observed intervals.

While this method has several appealing properties, a major problem of the aoristic fraction method is that it systematically overestimates the variance of the crime time density. This means that any estimate derived from these methods is systematically biased towards crime times that are more spread out over the 24-hour clock. Here, this will be explained through an example, but this fact can also be proven mathematically, which is done in Appendix .3.

Suppose there is a neighbourhood where burglaries mostly take place in the afternoon, say, between 11:00 and 16:00. However, we are not able to observe the crime times as the victims are almost never present. Victims will provide us with the start time s they left their premises, for example leaving for work, and the end time e when they returned. For illustration, we have sampled true crime times and intervals, computed the aoristic function and have plotted these together in Figure B.3. Due to the fact that most work schedules are similar, we will obtain a large amount of observations that have intervals roughly similar to (8:00, 19:00). However, this means that the aoristic fraction method will give a large amount of weight to the time frames 8:00 - 11:00 and 16:00 - 19:00, which there were very few true crime times in that region.

A final way to think of the aoristic function is that if we represent each

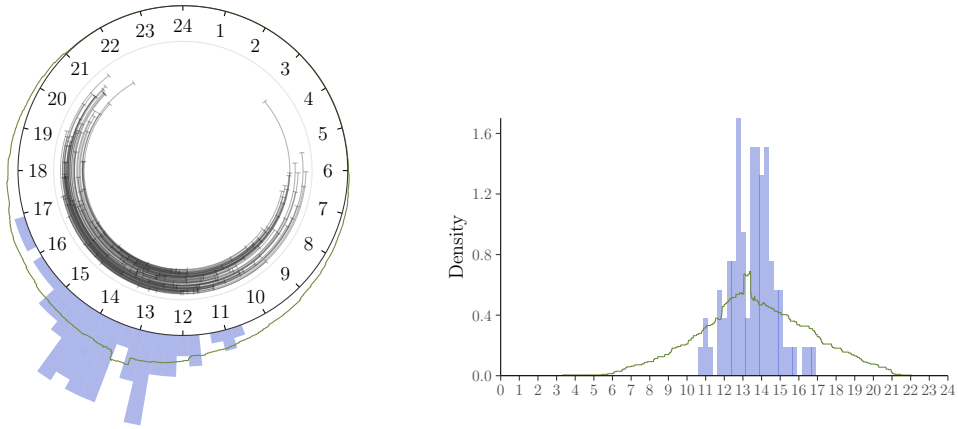

(a) (b)

Figure B.3: Example of how the aoristic fraction method overestimates the variance. The simulated true crime times are displayed as the blue histogram, while the approximation to this distribution is plotted as the dark green aoristic function.

aoristic interval by the uniform distribution on that interval, the aoristic function is the average of these uniform distributions at some time point t. This implies that we know nothing about where in the interval the data point is most likely to lie. That is, we do not think any point in the interval is more likely than another. However, the whole point of analyzing the dataset is to decide which crime times are more likely than others, and we are usually able to do this. Therefore, the uniform distribution on the aoristic interval is at odds with what we purport to do in our analysis.

Concluding, the aoristic fraction method is an appealing descriptive method, because its plot shows at a glance what the data looks like, but it does not allow us to infer the true crime time density. While descriptive statistics tells us something about the data, inferential statistics attempt to estimate the form of the true data generating process, which is generally the ultimate goal of crime analysis and prediction. The shortcomings of the descriptive aoristic fraction method motivate us to develop an inferential analysis method which treats the aoristic intervals as a missing data problem. That is, the true crime times are unknown, but we will try to use as much information as possible to understand where in the interval the true crime time is most likely to be.

B.4 Statistical models for aoristic data

In this section, inferential statistical methods will be developed for aoristic data. A crime analyst is using data to learn something about the world, and draws conclusions based on some statistical model. Initially, we are uncertain about the parameters in this statistical model, but as more data comes in we learn more about the parameters of the model and estimate them with more certainty.

In order to perform statistical inference on aoristic data, we need to set up some statistical model to learn, as well as some way to learn about them. In the next section we will shortly recap statistical models for temporal data, and in the section thereafter we will present a method to deal with the aoristic property of the data.

B.4.1 Circular data models

Statistical models for circular data, such as the temporal data under consideration here, have been developed in the field of circular statistics (Fisher, 1995; Mardia & Jupp, 2000; Pewsey et al., 2013). Circular data can consist of measurements in angles, directions, or times on the 24-hour clock, for example. This type of data can be found throughout discliplines, such as life sciences (Mardia, 2011), behavioural biology (Bulbert et al., 2015), cognitive psychology (Kaas & Van Mier, 2006), bioinformatics (Mardia et al., 2008), political science (J. Gill & Hangartner, 2010) and environmental sciences (Lagona, 2016; Lagona et al., 2015; Arnold & SenGupta, 2006). Circular data differ from linear data in the sense that circular data are measured in a periodical sample space. For example, an angle of 1° is quite close to an angle 359°, although linear intuition suggests otherwise. Similarly, times on the 24-hour clock have 23:59 and 0:01 being close to one another, while the numerical representation suggests otherwise. As a result, models for circular data must be different from linear models, such as the Normal distribution.

A natural analogue of the Normal distribution for circular data is the von Mises distribution (Von Mises, 1918), which can be written as the probability density

$$p(t \mid \mu, \kappa) = \frac{1}{2\pi I_0(\kappa)} \exp\left\{\kappa \cos(t - \mu)\right\}, \tag{B.2}$$

where t is a circular observation, such as a crime time, μ is the mean direction parameter, κ is a concentration parameter, and $I_0(\cdot)$ is the modified Bessel function of the first kind and order zero. This is a unimodal, symmetric model for circular data which will be used as a building block for more complex models throughout this work.

In order to perform statistical inference, we use the data to estimate population values for μ and κ. In addition, we are always interested in quantifying the uncertainty in our estimates (caused by our limited sample size), which might be given as a standard error in frequentist inference or as the posterior distribution in Bayesian inference. Either way, in order to do this, the likelihood function is used, which will be discussed in the following section.

B.4.2 Aoristic Likelihood

The information contained in the data is usually entered into the statistical model through the likelihood function. The likelihood function of the von Mises distribution can be specified as

$$L(\boldsymbol{\phi} \mid \boldsymbol{t}) = \prod_{i=1}^{n} p(t_i \mid \mu, \kappa), \tag{B.3}$$

where μ and κ are the aforementioned parameters of the von Mises distribution, and $p(t_i \mid \mu, \kappa)$ is the von Mises density given in B.2, which could also be replaced by any other density if we so desire. Usually, we would algebraically or numerically optimize this likelihood function to obtain maximum likelihood estimates (MLEs), which can be plugged into the von Mises density to obtain an estimate of the crime time density. However, this formulation supposes all crime times are directly observed.

In order to adapt the likelihood for aoristic data, some ideas from the survival analysis literature can be used. In survival analysis, data are usually *right-censored*, where it is known that an event takes place after a certain time, but not exactly when. Aoristic data, then, is *interval-censored*, where an event has taken place after a certain time, as well as before some later time, but where in this is interval the event took place is not known. Interval-censored data analysis is considered in medical statistics (Klein et al., 2013), and two specialized books exist as well (Sun, 2007; Chen et al., 2012).

Based on theory for interval-censored data, we can define an aoristic ver-

sion of the likelihood of the von Mises distribution, by writing

$$L(\mu, \kappa \mid \boldsymbol{t}_a) = \prod_{i=1}^{n} \int_{s_i}^{e_i} \frac{p(t \mid \mu, \kappa)}{e_i - s_i} dt \tag{B.4}$$

$$= \prod_{i=1}^{n} \frac{1}{e_i - s_i} \int_{s_i}^{e_i} p(t \mid \mu, \kappa) dt \tag{B.5}$$

$$= \prod_{i=1}^{n} \frac{F(e_i \mid \mu, \kappa) - F(s_i \mid \mu, \kappa)}{e_i - s_i}, \tag{B.6}$$

where $F(t \mid \mu, \kappa)$ is the cumulative distribution function (CDF) of the von Mises distribution. The computation of this aoristic likelihood is somewhat more complicated, but still feasible. To get estimates for μ and κ, this aoristic likelihood is optimized numerically to get maximum likelihood estimates. This approach can be simplified somewhat by filling in the unbiased estimator for μ which is given in .3.2, so that the aoristic likelihood only needs to be optimized for κ. It should be noted that if a different circular data model is desired, one can simply use the desired distribution in place of the cumulative distribution function of the von Mises distribution.

This aoristic likelihood correctly takes into account the uncertainty introduced by the aoristic intervals, but does not overestimate the spread of the crime time density as the aoristic fraction method does. This is shown in Figure B.4, where it can be seen that estimated crime time density from the aoristic likelihood (red) can correctly recover the true distribution of crime times (blue histogram), while the aoristic fraction method (green) fails. Note that the blue histogram containing the true burglary times is never observed, as we only obtain aoristic intervals. Still, the aoristic likelihood recovers the shape of the true crime time distribution.

Besides maximum likelihood estimates, one might be interested in obtaining an uncertainty around these estimates, perhaps in the form of a confidence interval or credible interval. Often, these can be obtained by deriving standard errors, but this is difficult due to the mathematical form of the aoristic likelihood. Therefore, one must resort to resampling methods, such as bootstrapping (Davison & Hinkley, 1997), or Bayesian approaches such as MCMC sampling to obtain the uncertainty around the maximum likelihood estimates.

We implemented bootstrapping using the R package `boot` (Canty & Ripley, 2017). The final results give an estimated mean of 13:16, with bootstrap confidence interval (CI) computed as (13:12, 13:21). Throughout the paper, we will write give bootstrap confidence intervals between parentheses after a maximum likelihood estimate, ie. MLE (Lower Bound, Upper Bound). The

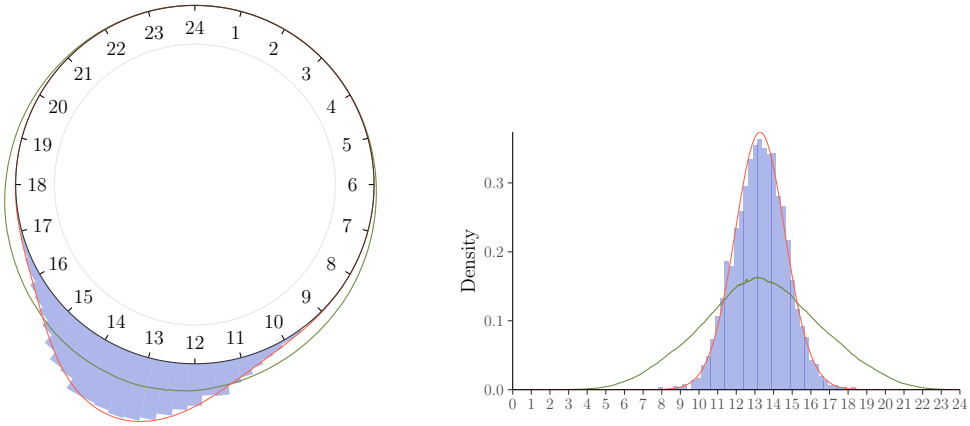

(a) (b)

Figure B.4: Example of how the von Mises model estimated by the aoristic likelihood (red) correctly reconstructs the true distribution of the crime times (blue histogram), while the aoristic fraction method (green) does not.

concentration parameter has an estimated value of 8.16 (7.64, 8.75). The true values under which the data was sampled are a true mean direction of 13:15 and a true concentration parameter of 8, so even though the data was made aoristic, the aoristic likelihood approach is able to precisely recover the true values using aoristic data.

B.4.3 Data augmentation

The aoristic likelihood approach is the most appealing method for most simple applications such as fitting a single unimodal distribution on a set of aoristic intervals. However, to compute our uncertainty in these estimates (such as through standard errors), or to incorporate this into more complex models, it can be beneficial to employ data augmentation strategies, such as for the nonparametric models discussed in the following section. Data augmentation is also the standard way to deal with missing data in Bayesian inference (Gelman et al., 2003).

Data augmentation strategies (Tanner & Wong, 1987; Gelfand & Smith, 1990; Van Dyk & Meng, 2001) make use of the fact that a statistical model implies a certain probability density $p(t \mid \boldsymbol{\phi})$ for any crime time t. Therefore, if we have our statistical model, we could sample the aoristic crime times from their intervals according to this probability density, which is the cur-

rent estimated crime time density. For example, in the burglary example, the sampled values for each aoristic interval could come from a von Mises distribution truncated at the ends of the interval (for details of two ways to do this, see Appendix .5). The issue with this strategy is that the statistical model can only be estimated if the data are imputed, but the data are imputed using the statistical model, leading to circular reasoning. Therefore, such an approach usually involves some sort of iterative method, starting with the crime times uniformly sampled in the aoristic intervals, then estimating the statistical model, sampling the crime times again according to the new model, estimating the model again with the new data points, and so on until some sort of convergence.

The advantage of the data augmentation approach is that in each iteration, estimating the statistical model can be performed with off-the-shelf algorithms made for directly observed data. The disadvantage of this approach is that the resulting algorithm will require some sort of iterative updating, which can require more computational effort, as well as depending on random sampling. It is therefore recommended to use data augmentation only when necessary due to the computational complexity of a chosen model, such as in the following section.

B.5 Nonparametric models

While the aoristic likelihood approach works well for somewhat simple models, crime time data often displays more complex patterns which are not captured by such models. Crime is governed by a dynamic complex system, society, where many unobserved and unknown factors contribute to why a crime occurs at exactly a certain time at exactly a certain place. As a result, crime times might not follow a simple unimodal distribution. For example, burglaries are known to occur either while victims are away during the day, or are asleep during the night, which would be a multimodal distribution. In addition, crime time densities are often skewed or violate distributional assumptions in some other way.

If the crime time density does not follow the distributional assumptions of the von Mises distribution, for example, these crime times might be a good fit for a nonparametric statistical model that does not make any assumption on the shape of the data distribution. Nonparametric models for interval censored data were first investigated in Turnbull (1974, 1976), but such models are not applicable to aoristic data. Therefore, we will apply Dirichlet process mixture models, which will be discussed next.

B.5.1 Dirichlet Process Mixture models

Among the most appealing nonparametric models are Dirichlet process mixture (DPM) models (Ferguson, 1973; Antoniak, 1974; Neal, 2000) found in the field of Bayesian nonparametrics (Hjort et al., 2010). For an introduction, see Gelman et al. (2003, ch. 23). DPM models are very flexible statistical models that are able to capture any underlying true distribution. Due to the increasing feasibility of computation for DPM models, they have seen an enormous increase in popularity over the last 20 years. Therefore, we believe that they represent a very promising approach for crime time modeling. A technical treatment of DPM models is beyond the scope of this paper, but we will recap some of its relevant properties here.

First, Dirichlet process models can fit any data distribution. This means that whether the true crime time density is multimodal, peaked, flat, or irregularly distributed in some other way, the DPM model will be able to learn this pattern after enough data, and thus give a good estimate of the true crime time density. Conceptually, this is true because the DPM model defines a prior over all possible probability distributions on the circle. Therefore, fear that our chosen statistical model does not fit the data is much less of a concern for such models. This is a property that this method shares with the aoristic fraction method, but without the attached issues discussed in Section B.3.

Second, among the most appealing properties of the DPM model for crime time analysis is that we can not only compute an estimate of the probability of a crime happening in any desired time interval, but moreover we can compute the uncertainty around this estimate. For example, after running the DPM model, we might say the estimated probability of a crime happening between 13:17 and 14:04 is 8.4%. This is already very useful, but the model also provides us a 95% credible interval, which might be, say, $(0.4\%, 19.4\%)$. Because this interval is quite wide, we can conclude that more data are required to give a more precise estimate, but that the true probability of crime happening in this interval is unlikely to be larger than 19.4%. This is important, because it allows us to know when our predictions are unreliable because we have based them on too little data.

Third, because the DPM model is still a statistical model, it can be extended and connected to other statistical models. For example, DPM models can be embedded in hierarchical model (Teh et al., 2005), dynamic models (Ren et al., 2008), spatial models (Duan et al., 2007) or regression models (Chib & Greenberg, 2010). This would not be possible with the aoristic fraction method, for instance. Temporal and spatial analyses of crime are often said to be too separated in crime analysis (Grubesic & Mack, 2008),

which we could address by developing a statistical model for the temporal aspects.

The DPM model takes the form of a mixture model with a varying number of components. As a result, we must choose some base distribution which serves as a building block for the DPM model. The base distribution is often chosen for computational convenience, because the resulting DPM is so flexible that it is not very sensitive to the choice of base distribution. More important is that the base distribution must be assigned a prior, as in any Bayesian analysis. This prior can indeed influence the resulting analysis if the sample size is small, but reasonable choices are available.

Dirichlet processes have been employed for circular data in a handful of papers, but none of them have treated aoristic data. Hernandez-Stumpfhauser et al. (2016) develops a Dirichlet process using the projected Normal distribution as the base distribution and applies this to small area estimation. McVinish & Mengersen (2008) develop a Dirichlet process model based on triangular distributions on the circle. DPM models have also been used to overcome problems in circular regression (Ghosh et al., 2003; George & Ghosh, 2006). Several other papers in this field have approached this in varying ways (Nuñez-Antonio et al., 2015).

We will use the von Mises distribution as the base distribution, with an uninformative prior on the parameters. Details of the model are given in Appendix .4. The computation of DPM models tends to be relatively computationally intensive, and still requires us to choose a solution for the aoristic property of our data. Two approaches for computation of our DPM model with aoristic data will be discussed next.

Augmented sampler

The main problem to deal with when applying the DPM model is the fact that there are aoristic observations. If there were no aoristic observations, then a von Mises based Dirichlet Process could be performed. Therefore Dirichlet process models for interval-censored data were first investigated in the successive substitution sampling of Doss (1994), which represents an application of the data augmentation strategy as discussed in Section B.4.3.

A technical issue arises here that is unique to aoristic data. Usually, data augmentation strategies for censored observations sample values by direct rejection. That is, a candidate is sampled from the full distribution, and if it falls in the required interval, it is accepted. If not, the process is repeated until acceptance. However, aoristic data might include both large and small intervals. If an aoristic interval is small, the probability of acceptance can also become very small, so a large number of candidates must be sampled

before acceptance. In such cases, an alternative envelope rejection sampling method is used. Therefore, the sampling algorithm is chosen adaptively. That is, the rejection probability is estimated, and if it is too small (for example acceptance probability below 10%), we will use the envelope rejection sampler. For details, see Appendix .5.

Marginal sampler

An alternative to the augmented sampler is to use the aoristic likelihood discussed in Section B.4.2 directly. It can simply be substituted in wherever the likelihood is used in the DPM computation. The downside here compared to the augmented sampler is each iteration of the algorithm takes a significantly larger amount of time. The upside is that the marginal sampler requires fewer random sampling steps and allows a larger set of priors than the augmented sampler. For most situations however, the augmented sampler will perform better and should be used.

B.6 Applications

This section will provide several applications of our method. Apart from results that directly stem from our approaches to estimating the crime time density, we will also show several further calculations that can be made which may be of interest. It should be noted that all of these analyses can simply be performed using the `R` package aoristicinference.

B.6.1 Ashby & Bowers data

In Ashby & Bowers (2013), the authors exemplify the aoristic fraction method by aoristic data obtained on bike theft in London. This paper provides a fantastic example dataset, because the authors have painstakingly gone through CCTV footage of the subway station under consideration to determine the true crime times for each of the police reports. This means that this dataset has the rare property that it is both ecologically valid, as well as having the true crime time t_{actual} available. Therefore, this dataset is an excellent opportunity to compare different methods.

The data consists of 242 aoristic intervals, each with an attached t_{actual}. The data are broadly unimodal, with most bike thefts taking place in the afternoon. The aoristic intervals are quite large, in this case, with a mean of 8.93 hours. Some intervals were larger than 24 hours, which are removed for this illustration, along with instances where t_{actual} was outside the aoristic interval (which occurs most likely due to reporting errors by the victim).

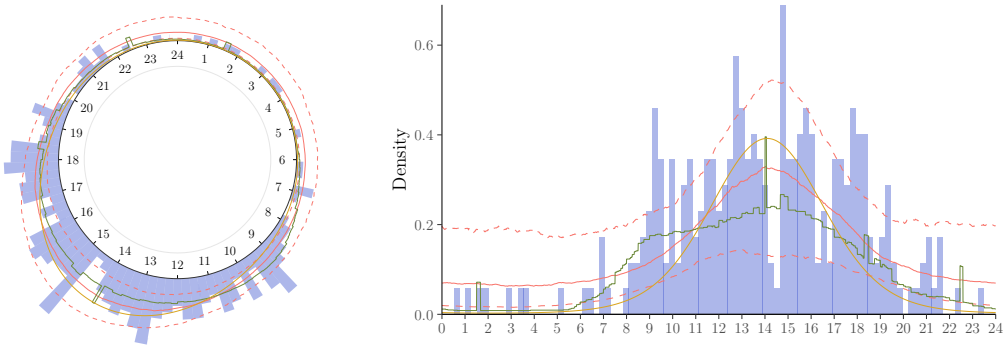

(a) (b)

Figure B.5: Three different models run on the data of Ashby & Bowers (2013). The 242 aoristic intervals are not displayed, but the true theft times are displayed as the blue histogram. The estimated crime time densities, which attempt to fit this histogram, are the aoristic fraction method (green), the maximum likelihood estimate of a von Mises distribution fit with the Aoristic Likelihood (yellow), and the Dirichlet Process Mixture model and its credible interval (red solid line, with 80% credible interval red and dashed).

It should be noted that the original dataset contains 263 observations, of which 21 crime times were known precisely due to being caught in the act, for instance. These were not analyzed previously, but both the aoristic likelihood method and the DPM model can use a mix of known times and aoristic data.

The results for the three methods considered in Sections B.3, B.4 and B.5 are displayed in Figure B.5. Because the data are mostly unimodal, the three methods can be seen to be broadly in agreement. All three options give a unimodal estimated crime time density, although the aoristic fraction method gives a more jagged estimate of the crime time density, as well as having a higher variance. The aoristic likelihood estimates the mean at 14:27 (13:48, 15:10), with concentration 2.15 (1.77, 2.67). In the fit of the DPM model it can be seen that an uncertainty around the crime time density is also provided, which would become smaller if more data would be obtained.

An advantage of the DPM model, as mentioned previously, is that it is possible to compute the proportion of crimes happen within a certain time frame along with its uncertainty. In particular, Ashby & Bowers (2013) focus on the proportion of crime times occuring during each of three police shifts: (7:00 - 15:00), (15:00 - 23:00), and (23:00 - 07:00). During the morning shift,

the model suggests estimates 40.4% of the bike thefts to occur during it, with a credible interval (CI) of (19.5%, 58.8%). The evening shift expects to obtain 35.7% with CI (17.5%, 59.4%), with the night shift is estimated to have 16.5% with CI (2.7%, 46.2%). Although it is clear that most bike thefts at this location occur during the morning and evening shift, the main conclusion to be drawn from this analysis is the uncertainty in our conclusions from the model is much larger than previous analyses have made it out to be. The cause for this can be found in the fact that the aoristic intervals provide less information than precise times, so the 'effective sample size' is much lower than the 242 observations we appeared to have.

B.6.2 Montgomery Crime data

The city of Montgomery is among several cities to publish open data of crimes in the city that includes a start and end date. This dataset was obtained from the Montgomery Open Crime Data website. The dataset contains 44299 observations of crimes in Montgomery observed in the years 2016 - 2018. Many crime types are provided, but we will focus on two types of property crime, theft from building and burglary, as these are the most interesting aoristic data points. Crimes missing start or end times are removed, while those with start and end times that exactly equal or up to 2 minutesn apart are treated as observed crime times. All others are treated as aoristic.

For this type of data, the Aoristic Fraction approach is a good way to obtain an initial descriptive analysis of the data. Figure B.6 shows the results of all three methods for the two crime types in the Montgomery data. Note that a true evaluation of which approach performs best here is not possible as the true crime times are not known.

'Theft from building', defined[1] as *'A theft from within a building which is either open to the general public or where the offender has legal access'*, is broadly unimodal, with a peak around 15:00. All three methods perform reasonably well. The aoristic likelihood method is able to fully capture the shape of this distribution, with an estimated mean direction of 15:30 (15:20, 15:40), with concentration 1.12 (1.07, 1.17). The DPM model fits the data slightly better, and is fairly certain about the distribution due to the size of the dataset.

For 'burglary', defined[2] as *'The unlawful entry into a building or other structure with the intent to commit a felony or a theft'*, the distribution is bimodal, with one peak in the middle of the night (around 3:00), and another

[1] https://ucr.fbi.gov/nibrs/2011/resources/nibrs-offense-definitions
[2] https://ucr.fbi.gov/nibrs/2011/resources/nibrs-offense-definitions

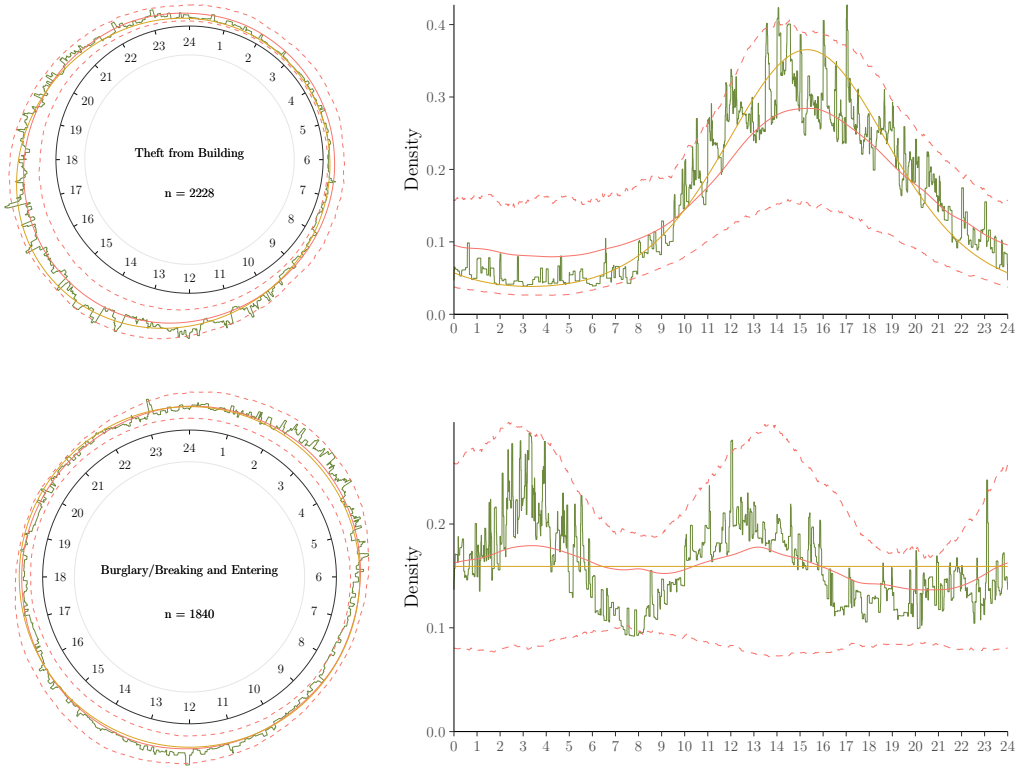

Figure B.6: The three methods discussed in this paper applied to two crime types, theft from building and burglary. The methods displayed are the aoristic fraction method (green), the maximum likelihood estimate of a von Mises distribution fit with the Aoristic Likelihood (yellow), and the Dirichlet Process Mixture model and its credible interval (red solid line, with 80% credible interval red and dashed).

around lunchtime at 13:00. These times correspond to times when properties are most likely left unattended. In this case, the aoristic likelihood fails to fit the data well because it attempts to fit a unimodal density to the bimodal dataset, and as a result gives a uniform result, with concentration 0 (0, 0.07). The DPM model still captures the distribution adequately.

B.6.3 Montly crime time trends

The DPM model can also provide inference for any function of the parameters of the model, which allows a wealth of further analyses. As an example, we show how to investigate seasonal changes in crime times. First, we run the

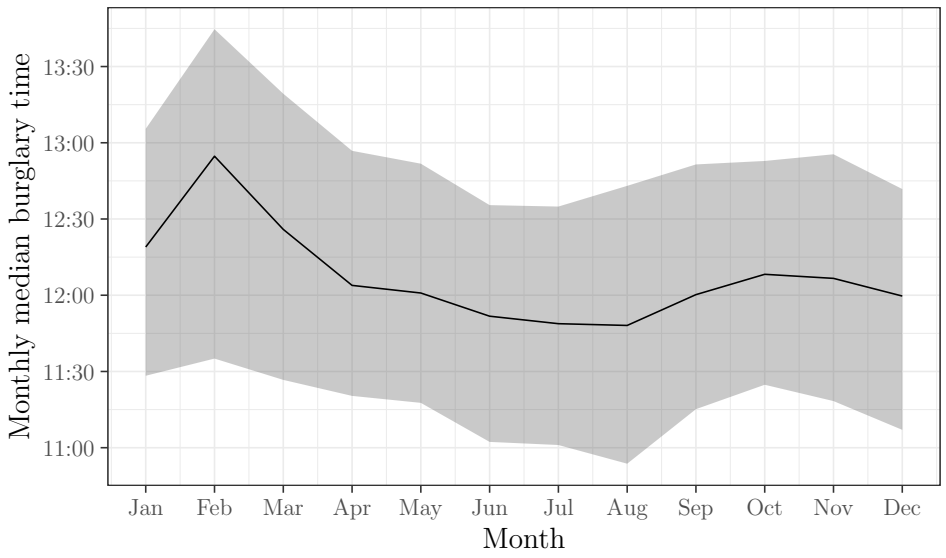

Figure B.7: Median burglary time from Dirichlet Process Model plotted as it changes per month (black line), and its confidence interval (grey area).

DPM model separately for each month, giving a non-parametric fit along with the uncertainty around this fit. Second, we compute the mean direction of the resulting crime time density for 1000 MCMC samples from the DPM model, giving us an estimate of the mean direction for this month as well as the uncertainty around it. Then, this is plotted in Figure B.7, where the black line provides the estimated mean crime time for each month, and the grey area provides the uncertainty around this, which was obtained as a credible interval from the mean direction in each of the MCMC samples. From it, we can conclude that there seems to be a general trend of slightly earlier burglary times during the summer, although the uncertainty around this trend is still fairly large.

B.7 Discussion

In this paper, we have developed novel methods for dealing with aoristic data in crime analysis and beyond. Three methods were presented. The aoristic fraction method is a descriptive method for which major downsides have been established, primarily a systematic overestimation of the variance of the crime time density. We have shown how the aoristic likelihood method provides a solid method for fitting unimodal crime times, using all information contained in the aoristic data.

The Dirichlet Process Mixture model provides a natural extension of these models, allowing us to fit any crime time distribution regardless of the number of modes or the shape of the distribution. This is an appealing property that this model shares with the aoristic fraction method, but as opposed to that method the DPM model is built on a solid statistical foundation. This provides the DPM three main advantages. First, it uses all information in the data. Second, it provides measures of uncertainty in our model and conclusions. Third, it can be extended and connected to other statistical models.

Choosing between aoristic likelihood methods and nonparametric approaches is a choice made dependent on the specific crime type under investigation. Some crime types are fit well with a symmetric unimodal model, and for these, the aoristic likelihood approach is simpler, faster, more interpretable and easier. However, if the crime time density for this crime type is bimodal or otherwise differently distributed, the DPM model provides an extremely flexible extension that is able to adapt to any shape of the data distribution.

A major hurdle in employing aoristic analyses is the complexity of implementing the computational methods, so that crime analysts are usually not inclined to incorporate aoristic analyses in their workflow, as evidenced by several authors mentioning the importance of aoristic methods without implementing any. To address this, analyses in this work have been implemented in an easy to use `R` package, aoristicinference. It provides introductions and user guides, so that users not familiar with the details of the statistical methods in this work should also be able to use the methods.

A strongly related method to the aoristic fraction method is what is called *Interstitial Crime Analysis* (ICA) (A. Gill et al., 2014). Interstitial Crime Anaysis is a technique not for unknown time but unknown location. For example, Newton et al. (2014) use this technique to estimate the proportion of thefts that occurs between any two metro stations of the London Underground. From a statistical perspective, this method suffers from the same problems as the aoristic fraction method. In fact, Appendix .3.1 is a proof of why the variance will be systematically overestimated, with the minor difference that ICA is usually done on a categorical sample space. Therefore, a future investigation into an "Interstitial Likelihood" could prove fruitful.

A limitation of any aoristic analysis method is that if the true crime times are systematically more likely situated toward the start or end of the intervals, our analysis will be biased. This is strongly related to the assumption of independence of the intervals and the true crime times. That is, in reality the intervals can depend on the crime time, for example if an offender waits until they see their chosen victim leave their house. This could also

happen if offenders and victims both follow a fixed pattern, for example if burglaries are usually in the afternoon, while the victims are always gone during working hours, and thus provide intervals close to working hours. It is impossible to infer such behaviours from a fully aoristic dataset, akin to the problem of Missing Not At Random (MNAR) missing data. However, one might attempt to test this assumption if a sufficiently sized known-time dataset is available. Then, it could be checked whether the known-time and aorisitic datasets produce differrent crime time densities. If so, we are indeed violating our assumptions. So long as this is not the case, our method extracts the most information from a set of (partly) aoristic data, given the constraints we have.

With these tools for addressing aoristic data, future work should focus on combining these methods with spatial analyses, in particular point process models as in Wang & Gelfand (2014). A combined spatio-temporal model that uses aoristic data to their fullest extent would provide a powerful tool for understanding both when and where crimes occur, as well as for predictive policing.

B.8 Acknowledgements

This work was supported by a —— grant awarded to —— from —— (——).

The authors are grateful to Matthew Ashby for providing the data from Ashby & Bowers (2013).

Appendix A

Appendix

.1 Conditional distribution of β_0

Here, it will be shown that β_0 conditionally has the von Mises distribution, that is

$$L(\beta_0 \mid \kappa, \boldsymbol{\delta}, \boldsymbol{\beta}, \boldsymbol{\theta}, \boldsymbol{X}, \boldsymbol{d}) \propto \mathcal{VM}(\beta_0 \mid \bar{\psi}, R_\psi \kappa). \tag{1}$$

The proof for the conditional distribution of β_0 in the GLM closely follows the derivation for the distribution of the mean direction μ of the von Mises distribution, which shows that $L(\mu \mid \kappa, \boldsymbol{\theta}) \propto \mathcal{VM}(\mu \mid \bar{\theta}, R_\theta \kappa)$.

The conditional likelihood of β_0 is given by

$$\begin{aligned} L(\beta_0 \mid \kappa, \boldsymbol{\delta}, \boldsymbol{\beta}, \boldsymbol{\theta}, \boldsymbol{X}, \boldsymbol{d}) &\propto \exp\left\{ \kappa \sum_{i=1}^{n} \cos\left[\theta_i - (\beta_0 + \boldsymbol{\delta}^T \boldsymbol{d}_i + g(\boldsymbol{\beta}^T \boldsymbol{x}_i))\right] \right\} \\ &= \exp\left\{ \kappa \sum_{i=1}^{n} \cos\left[\beta_0 - (\theta_i - \boldsymbol{\delta}^T \boldsymbol{d}_i - g(\boldsymbol{\beta}^T \boldsymbol{x}_i))\right] \right\}. \end{aligned}$$

We know that for any angle $\psi_i, i = 1, \ldots, n$,

$$C_\psi = \sum_{i=1}^{n} \cos(\psi_i), \quad S_\psi = \sum_{i=1}^{n} \sin(\psi_i), \quad R_\psi = \sqrt{C_\psi^2 + S_\psi^2},$$

$$\text{and} \quad \frac{C_\psi}{R_\psi} = \cos\bar{\psi}, \quad \frac{S_\psi}{R_\psi} = \sin\bar{\psi}, \quad \text{where} \quad \bar{\psi} = \operatorname{atan2}(S_\psi, C_\psi).$$

Thus, setting angle $\psi_i = \theta_i - \boldsymbol{\delta}^T \boldsymbol{d}_i - g(\boldsymbol{\beta}^T \boldsymbol{x}_i)$,

$$
\begin{aligned}
L(\beta_0 \mid \kappa, \boldsymbol{\delta}, \boldsymbol{\beta}, \boldsymbol{\theta}, \boldsymbol{X}, \boldsymbol{d}) &\propto \exp\left\{\kappa \sum_{i=1}^{n} \cos(\beta_0 - \psi_i)\right\} \\
&= \exp\left\{\kappa \left[\cos\beta_0 \sum_{i=1}^{n} \cos\psi_i + \sin\beta_0 \sum_{i=1}^{n} \sin\psi_i\right]\right\} \\
&= \exp\left\{R_\psi \kappa \left[\cos\beta_0 \frac{C_\psi}{R_\psi} + \sin\beta_0 \frac{S_\psi}{R_\psi}\right]\right\} \\
&= \exp\left\{R_\psi \kappa \left[\cos\beta_0 \cos\bar{\psi} + \sin\beta_0 \sin\bar{\psi}\right]\right\} \\
&= \exp\left\{R_\psi \kappa \cos\left(\beta_0 - \bar{\psi}\right)\right\} \\
&\propto \mathcal{VM}(\beta_0 \mid \bar{\psi}, R_\psi \kappa).
\end{aligned}
$$

.2 Properties of the Power Batschelet Distribution

The probability density function of the Power Batschelet distribution is defined as

$$f_{PB}(\theta \mid \mu, \kappa, \lambda) = [K^*_{\kappa,\lambda}]^{-1} \exp\{\kappa \cos t^*_\lambda(\theta - \mu)\}, \tag{2}$$

where

$$t^*_\lambda(\theta) = \text{sign}(\theta)\pi \left(\frac{|\theta|}{\pi}\right)^{\gamma(\lambda)}, \tag{3}$$

with $\gamma(\lambda) = \frac{1-c\lambda}{1+c\lambda}$, where $c = 0.4052284$ and the inverse of the normalizing constant being

$$K^*_{\kappa,\lambda} = \int_{-\pi}^{\pi} \exp\{\kappa \cos t^*_\lambda(\theta - \mu)\} d\theta, \tag{4}$$

which is usually numerically integrated.

Note that for any symmetric base density, such as the von Mises used in this case, the sign(θ) in Equation 3 is optional, because $f_{PB}((\theta - \mu) \mid \mu, \kappa, \lambda) = f_{PB}(-(\theta - \mu) \mid \mu, \kappa, \lambda)$.

The log-likelihood is

$$\ell(\mu, \kappa, \lambda \mid \boldsymbol{\theta}) = -\log[K^*_{\kappa,\lambda}] + \kappa \sum_{i=1}^{n} \cos t^*_\lambda(\theta_i - \mu), \tag{5}$$

so that, assuming $\theta_i \neq \mu \ \forall \ i \in 1, \ldots, n$, the score functions are

$$\frac{\partial \ell(\mu, \kappa, \lambda \mid \boldsymbol{\theta})}{\partial \mu} = \kappa \pi^{1-\gamma(\lambda)} \gamma(\lambda) \sum_{i=1}^{n} |\theta_i - \mu|^{\gamma(\lambda)-1} \sin t_\lambda^*(\theta_i - \mu) \tag{6}$$

$$\frac{\partial \ell(\mu, \kappa, \lambda \mid \boldsymbol{\theta})}{\partial \kappa} = -\left[K_{\kappa,\lambda}^*\right]^{-1} \int_{-\pi}^{\pi} \cos t_\lambda^*(\theta) e^{\kappa \cos t_\lambda^*(\theta)} d\theta + \sum_{i=1}^{n} \cos t_\lambda^*(\theta_i - \mu) \tag{7}$$

$$\frac{\partial \ell(\mu, \kappa, \lambda \mid \boldsymbol{\theta})}{\partial \lambda} = -\left[K_{\kappa,\lambda}^*\right]^{-1} \int_{-\pi}^{\pi} h(\theta, \mu, \kappa, \lambda) e^{\kappa \cos t_\lambda^*(\theta)} d\theta + \sum_{i=1}^{n} h(\theta_i, \mu, \kappa, \lambda) \tag{8}$$

where

$$h(\theta, \mu, \kappa, \lambda) = \frac{\partial \kappa \cos t_\lambda^*(\theta - \mu)}{\partial \lambda} = \frac{\kappa \gamma'(\lambda) |\theta - \mu|^{\gamma(\lambda)}}{\pi^{\gamma(\lambda)-1}} \sin\left(\frac{|\theta - \mu|^{\gamma(\lambda)}}{\pi^{\gamma(\lambda)-1}}\right) \log\left(\frac{\pi}{|\theta - \mu|}\right) \tag{9}$$

where $\gamma'(\lambda) = \frac{2c}{(1+c\lambda)}$. Due to the form of the score functions, as well as the condition that $\theta_i \neq \mu \ \forall \ i \in 1, \ldots, n$, it is clear that the Hessian and Fisher Information will not be easy to work with. Therefore, it is preferred to work directly with the log-likelihood.

.3 Proof of variance overestimation using the aoristic fraction method

The fact that the variance of the data in density estimation methods such as the aoristic fraction method can be proven mathematically. First, for familiarity, this will be done for the linear case, where the data lies on the real line. Second, we will show the same proof for circular interval censored data, such as aoristic data.

.3.1 Data on the real line

Here, we will show that for data on the real line using a density estimate based on the interval-censored histogram (ICH) method, essentially the linear analogue of the aoristic fraction method, leads to an overestimate of the variance in the linear case.

Let $X \in \mathbb{R}$ be a random variable with some unknown distribution, but where $E[X] = \mu$ and $\text{Var}[X] = \sigma^2$. This X is not directly observed, but rather we observe an interval (a, b), knowing $a \leq x \leq b$. We can expand the

bounds as $a = x - \delta_i^l$ and $b = x + \delta_i^u$, where δ_i^l is the distance between the start of the interval and the unobserved true x, and δ_i^u the distance further from x to the end of the interval. Note that δ_i^l and δ_i^u are random variables themselves, with unknown distribution. A core assumption that we will make is that δ_i^l and δ_i^u have the same distribution. Then, we also assume that the expected difference between x and an interval bound is $E[\delta_i^l] = E[\delta_i^l] > 0$. That is, the data are actually censored. As a result, $E[\delta_i^u - \delta_i^l] = 0$.

The procedure under investigation is to estimate the unknown density $p(x)$ by the interval-censored histogram, which is an average of uniform distributions for each interval, that is

$$\hat{p}_{ICH}(x) = \frac{1}{n} \sum_{i=1}^{n} \frac{I(a_i < x < b_i)}{b_i - a_i},$$

where $I(\cdot)$ is the indicator function. The question we will evaluate is whether the variance of this density, which we will call $\hat{\sigma}^2_{ICH}$, overestimates the true variance σ^2 of X. Thus, the question is whether $E[\hat{\sigma}^2_{ICH}] > \sigma^2$.

First, we will need the expectation to produce an estimate of the variance. Note that our estimate of the expected value of X using the ICH density is

$$\begin{aligned}
\hat{\mu} &= \int_{\mathbb{R}} x \; \hat{p}_{ICH}(x) dx && (10)\\
&= \int_{\mathbb{R}} x \frac{1}{n} \sum_{i=1}^{n} \frac{I(a_i < x < b_i)}{b_i - a_i} dx && (11)\\
&= \frac{1}{n} \sum_{i=1}^{n} \int_{a_i}^{b_i} x dx = \frac{1}{n} \sum_{i=1}^{n} \frac{b_i - a_i}{2} && (12)\\
&= \frac{1}{n} \sum_{i=1}^{n} x_i + \frac{\delta_i^u - \delta_i^l}{2}, && (13)
\end{aligned}$$

where the last form is not observed, but helps us realise that if we take the expectation of the unknown interval lengths, $\frac{E[\delta_i^u] - E[\delta_i^l]}{2} = 0$. Then, $\hat{\mu} = \bar{x} = \frac{1}{n} \sum_{i=1}^{n} x_i$. So, if δ_i^l and δ_i^u have the same expectation, the estimate $\hat{\mu}$ is an unbiased estimator of μ.

For simplicity, we will assume that the data are centered so that $\hat{\mu} = 0$.

Then, we can create an unbiased estimator of σ^2 by

$$\hat{\sigma}^2_{ICH} = \left(1 - \frac{1}{n}\right) \mathrm{Var}[X] = \left(1 - \frac{1}{n}\right) E[X^2] \tag{14}$$

$$= \int_{\mathbb{R}} x^2 \frac{1}{n-1} \sum_{i=1}^{n} \frac{I(a_i < x < b_i)}{b_i - a_i} dx \tag{15}$$

$$= \frac{1}{n-1} \sum_{i=1}^{n} \frac{1}{3} \frac{b_i^3 - a_i^3}{b_i - a_i} = \frac{1}{3} \frac{1}{n-1} \sum_{i=1}^{n} a_i^2 + a_i b_i + b_i^2 \tag{16}$$

Then, expanding the bounds, and taking the expectation over δ_i^l and δ_i^u,

$$E_{\delta_i^l}[E_{\delta_i^u}[\hat{\sigma}^2_{ICH}]] = E_{\delta_i^l}\left[E_{\delta_i^u}\left[\frac{1}{3}\frac{1}{n-1}\sum_{i=1}^{n} 3x_i^2 - 2\delta_i^l x_i + {\delta_i^l}^2 + \delta_i^u x_i - \delta_i^l \delta_i^u + 2\delta_i^u x_i + {\delta_i^u}^2\right]\right] \tag{17}$$

$$= \frac{1}{3}\left\{\frac{1}{n-1}\sum_{i=1}^{n} 3x_i^2 + E_{\delta_i^l}\left[E_{\delta_i^u}\left[{\delta_i^l}^2 + {\delta_i^u}^2 - \delta_i^l \delta_i^u\right]\right]\right\} \tag{18}$$

$$= \left\{\frac{1}{n-1}\sum_{i=1}^{n} x_i^2\right\} + \frac{1}{3}\left\{\frac{1}{n-1}\sum_{i=1}^{n} E_{\delta_i^l}\left[E_{\delta_i^u}\left[{\delta_i^l}^2 + {\delta_i^u}^2 - \delta_i^l \delta_i^u\right]\right]\right\}. \tag{19}$$

We can recognize that $\frac{1}{n-1}\sum_{i=1}^{n} x_i^2$ is simply an unbiased estimator of the variance. Therefore, taking the expectation over x,

$$E_x[E_{\delta_i^l}[E_{\delta_i^u}[\hat{\sigma}^2_{ICH}]]] = E_x\left[\frac{1}{n-1}\sum_{i=1}^{n} x_i^2\right] + \frac{1}{3}\left\{\frac{1}{n-1}\sum_{i=1}^{n} E_{\delta_i^l}\left[E_{\delta_i^u}\left[{\delta_i^l}^2 + {\delta_i^u}^2 - \delta_i^l \delta_i^u\right]\right]\right\} \tag{20}$$

$$= \sigma^2 + \frac{1}{3}\left\{\frac{1}{n-1}\sum_{i=1}^{n} E_{\delta_i^l}\left[E_{\delta_i^u}\left[{\delta_i^l}^2 + {\delta_i^u}^2 - \delta_i^l \delta_i^u\right]\right]\right\} \tag{21}$$

However, note that ${\delta_i^l}^2 + {\delta_i^u}^2 - \delta_i^l \delta_i^u \geq 0$, with equality if and only if $\delta_i^l = \delta_i^u = 0$, which would mean there was no interval-censoring. Because the second term is positive, we have that the variance is overestimated by $\hat{\sigma}^2_{ICH}$, that is, it is biased upwards. From this last equation, it is clear that the upwards bias depends on the distribution of δ_i^l and δ_i^u. Specifically, the bias is $E[\hat{\sigma}^2_{ICH} - \sigma] = \frac{1}{3}\left\{\frac{1}{n-1}\sum_{i=1}^{n} E_{\delta_i^l}\left[E_{\delta_i^u}\left[{\delta_i^l}^2 + {\delta_i^u}^2 - \delta_i^l \delta_i^u\right]\right]\right\}$.

.3.2 Aoristic data

In the circular case, let $\theta \in [0, 2\pi)$ be a circular random variable, which again is not directly observed, but rather only up to an interval $a_i \leq \theta \leq b_i$, with again $a = \theta - \delta_i^l$ and $b = \theta + \delta_i^u$. This time, the intervals are assumed to be bounded on the semicircle, that is $\delta_i^l \in [0, \pi)$, and $\delta_i^u \in [0, \pi)$. Again, assume that δ_i^l and δ_i^u have some unknown distribution.

The distribution of θ is unknown, but let's assume it has a population mean direction μ. An unbiased estimator of μ is given by $\bar{\theta} = \text{atan2}(\sum_{i=1}^n \sin(\theta_i), \sum_{i=1}^n \cos(\theta_i))$ (Mardia & Jupp, 2000). For aoristic data, an unbiased estimator of μ is

$$\tilde{\theta} = \text{atan2}\left(\sum_{i=1}^n \sin(a_i) + \sin(b_i), \sum_{i=1}^n \cos(a_i) + \cos(b_i)\right). \tag{22}$$

This is equal to taking the mean direction of the midpoints of the aorisitic intervals. To show that this is unbiased, taking the expectation over the distribution of δ_i^l and δ_i^u, we obtain

$$E_{\delta_i^l, \delta_i^u}\left[\sum_{i=1}^n \cos(a_i) + \cos(b_i)\right] = \sum_{i=1}^n \cos(\theta_i) E_{\delta_i^l, \delta_i^u}\left[\cos(\delta_i^l) + \cos(\delta_i^u)\right] \tag{23}$$

$$E_{\delta_i^l, \delta_i^u}\left[\sum_{i=1}^n \sin(a_i) + \sin(b_i)\right] = \sum_{i=1}^n \sin(\theta_i) E_{\delta_i^l, \delta_i^u}\left[\cos(\delta_i^l) + \cos(\delta_i^u)\right]. \tag{24}$$

Note that this last term $E_{\delta_i^l, \delta_i^u}\left[\cos(\delta_i^l) + \cos(\delta_i^u)\right]$ is the same for both components. Also, for any constant $q > 0$ we have $\text{atan2}(qs, qc) = \text{atan2}(s, c)$. So, if we set $q = E_{\delta_i^l, \delta_i^u}\left[\cos(\delta_i^l) + \cos(\delta_i^u)\right] > 0$, we can see $\text{atan2}(q \sum_{i=1}^n \sin(\theta_i), q \sum_{i=1}^n \cos(\theta_i)) = \bar{\theta}$, which is an unbiased estimator of μ.

The population variance is given by $1 - \rho$, where $\rho = \int_0^{2\pi} \cos(\theta - \mu) p(\theta) d\theta$ is the population resultant length. If we center data by subtracting the mean direction estimate $\tilde{\theta}$ such that the mean direction is zero, then we simply have $\rho = \int_0^{2\pi} \cos\theta p(\theta) d\theta$, with an unbiased estimator being $\frac{1}{n} \sum_{i=1}^n \cos\theta_i$.

The aoristic fraction method leads us to estimate the resultant length as

$$\hat{\rho}_{AF} = \int_0^{2\pi} \cos\theta \ \hat{p}_{AF}(\theta) d\theta \tag{25}$$

$$= \int_0^{2\pi} \cos\theta \frac{1}{n} \sum_{i=1}^{n} \frac{I(a_i < x < b_i)}{b_i - a_i} d\theta \tag{26}$$

$$= \frac{1}{n} \sum_{i=1}^{n} \frac{1}{b_i - a_i} \int_{a_i}^{b_i} \cos\theta d\theta \tag{27}$$

$$= \frac{1}{n} \sum_{i=1}^{n} \frac{\sin b_i - \sin a_i}{b_i - a_i} \tag{28}$$

$$= \frac{1}{n} \sum_{i=1}^{n} \frac{\sin(\theta_i + \delta_i^u) - \sin(\theta_i - \delta_i^l)}{b_i - a_i} \tag{29}$$

$$= \frac{1}{n} \sum_{i=1}^{n} \frac{\sin\theta_i \cos\delta_i^u + \cos\theta_i \sin\delta_i^u - \sin\theta_i \cos\delta_i^l + \cos\theta_i \sin\delta_i^l}{b_i - a_i}. \tag{30}$$

Then, taking the expectation over θ, δ_i^l and δ_i^u, recalling $E[\sin\theta] = 0$, this gives

$$E[\hat{\rho}_{AF}] = \frac{1}{n} \sum_{i=1}^{n} \frac{E[\sin\theta_i]E[\cos\delta_i^u] + E[\cos\theta_i]E[\sin\delta_i^u] - E[\sin\theta_i]E[\cos\delta_i^l] + E[\cos\theta_i]E[\sin\delta_i^l]}{E[\delta_i^l] + E[\delta_i^u]} \tag{31}$$

$$= \frac{1}{n} \sum_{i=1}^{n} \frac{E[\cos\theta_i]E[\sin\delta_i^u] + E[\cos\theta_i]E[\sin\delta_i^l]}{E[\delta_i^l] + E[\delta_i^u]} \tag{32}$$

$$= \frac{1}{n} \sum_{i=1}^{n} \rho \frac{E[\sin\delta_i^l] + E[\sin\delta_i^u]}{E[\delta_i^l] + E[\delta_i^u]}. \tag{33}$$

Then, set the distributions of δ_i^l and δ_i^u equal again to the distribution of some δ, to get

$$E[\hat{\rho}_{AF}] = \frac{1}{n} \sum_{i=1}^{n} \rho \frac{E[\sin\delta_i]}{E[\delta_i]}. \tag{34}$$

Finally, if $0 < \delta < \pi$, that is, there is interval censoring, we know that $\sin\delta < \delta$, so $\frac{E[\sin\delta_i]}{E[\delta_i]} < 1$, and the bias is

$$E[\hat{\rho}_{AF} - \rho] = \frac{1}{n} \sum_{i=1}^{n} \rho \frac{E[\sin\delta_i]}{E[\delta_i]} - \rho = \left(\frac{1}{n} \sum_{i=1}^{n} \frac{E[\sin\delta_i]}{E[\delta_i]} - 1 \right) \rho < 0. \tag{35}$$

Therefore, the estimate of the resultant length given by the aoristic fraction method $\hat{\rho}_{AF}$ is biased downwards, so that the circular variance $1 - \hat{\rho}_{AF}$ is biased upwards.

.4 Von Mises based Dirichlet Process Mixture model

We propose to use a von Mises based Dirichlet Process mixture (DPM) model. The von Mises DPM model on circular observation $\theta_i \in [0, 2\pi)$ can be written as

$$\theta_i \mid (\mu_i, \kappa_i) \sim \mathcal{M}(\mu_i, \kappa_i) \tag{36}$$
$$(\mu_i, \kappa_i) \mid G \sim G \tag{37}$$
$$G \sim \mathrm{DP}(P_0, \alpha). \tag{38}$$

The base distribution P_0 is the conjugate prior for the von Mises distribution, that is

$$p(\mu, \kappa \mid \mu_0, R_0, n_0) \propto [I_0(\kappa)]^{-n_0} \exp\left\{R_0 \kappa \cos(\mu - \mu_0)\right\}, \tag{39}$$

where μ_0 is the prior mean, R_0 is the prior resultant length, and n_0 is somewhat like a prior sample size.

Because this prior is conjugate, the posterior has the same form, which is

$$p(\mu, \kappa \mid \mu_n, R_n, m) \propto [I_0(\kappa)]^{-m} \exp\left\{R_n \kappa \cos(\mu - \mu_n)\right\}, \tag{40}$$

where, setting $S_n = \sum_{i=1}^{n} \sin(\theta_i) + R_0 \sin(\mu_0)$ and $C_n = \sum_{i=1}^{n} \cos(\theta_i) + R_0 \cos(\mu_0)$, the posterior mean direction is $\mu_n = \mathrm{atan2}\,(S_n, C_n)$, the posterior resultant length is given by $R_n = \sqrt{C_n^2 + S_n^2}$, and the posterior sample size is $m = n + n_0$.

For computation, we also require the prior predictive distribution of a data point $\tilde{y}$. It is given by

$$p(\tilde{y} \mid \mu_0, R_0, n_0) = \int_0^{\infty} \int_0^{2\pi} p(\mu, \kappa \mid \mu_0, R_0, n_0) \mathcal{M}(\tilde{y} \mid \mu, \kappa) d\mu d\kappa \tag{41}$$
$$= \frac{1}{C} \frac{1}{(2\pi)^{n_0}} \int_0^{\infty} \frac{I_0(R_p \kappa)}{I_0(\kappa)^{n_p}} d\kappa \tag{42}$$

where $p(\mu, \kappa \mid \mu_0, R_0, n_0)$ is the base distribution P_0, $\mathcal{M}(\tilde{y} \mid \mu, \kappa)$ is the probability density function of the von Mises distribution, $R_p = \sqrt{\left(\cos \tilde{y} + R_0 \cos \mu_0\right)^2 + \left(\sin \tilde{y} + R_0 \sin \mu_0\right)^2}$, $n_p = n_0 + 1$, and

$$C = (2\pi)^{1-n_0} \int_0^{\infty} \frac{I_0(R_0 \kappa)}{I_0(\kappa)^{n_0}} d\kappa \tag{43}$$

is the normalizing constant of the base distribution P_0.

To obtain a Dirichlet process that is uninformative with regards to the mean direction, we must take $R_0 = 0$ so that the terms with μ_0 disappear in the posterior computations. If we want a non-informative prior to limit the influence of the prior, this suggests setting $R_0 = 0$, $n_0 = 1$, and μ_0 any value, as it is irrelevant now. The downside of such an approach is that it puts most weight on components that have low concentration, an issue which is addressed in Appendix .6.

Computation was implemented using the R package dirichletprocess (J. Ross & Markwick, 2018), to which methods for circular data and aoristic data were contributed. This package uses the Gibbs sampling schemes from Neal (2000).

.5 Rejection sampling aoristic data

A computational issue arises in rejection sampling for aoristic data because it will tend to contain both very small and larger intervals. Usually, data augmentation will use direct rejection sampling, such as in Doss (1994). This direct rejection algorithm will attempt to sample a value t from interval (a, b) which has distribution $p(t \mid \boldsymbol{\phi}, a, b) \propto p(t \mid \boldsymbol{\phi})I(a < t < b)$, where $\boldsymbol{\phi}$ are the parametrs of the distribution and $I(\cdot)$ is the indicator function. This algorithm can be summarized as follows.

1. Sample a value $t^* \sim p(t \mid \boldsymbol{\phi})$.
2. If $a < t < b$, set $t = t^*$. Otherwise, go back to step 1.

However, if we have a very small interval, say (17:18, 17:21), the algorithm will perform have very low acceptance probability and thus perform badly. This is because the acceptance probability of the direct rejection algorithm is $\int_a^b p(t \mid \boldsymbol{\phi})dt$ which can be quite small for small intervals.

An alternative is to use envelope rejection sampling (Gilks & Wild, 1992), which can be summarized as follows.

1. Compute the maximum value of the distribution $p(t \mid \boldsymbol{\phi})$ within the interval, that is $m = \max_{t:a<t<b} p(t \mid \boldsymbol{\phi})$.
2. Sample a value $t^* \sim U[a, b]$, that is from the uniform distribution between a and b.
3. Sample $u \sim U[0, 1]$. If $um < p(t^* \mid \boldsymbol{\phi})$, set $t = t^*$. Otherwise, go back to step 2.

This algorithm has rejection probability $m(b-a) - \int_a^b p(t \mid \boldsymbol{\phi})dt$. This should make it clear that the envelope rejection and direct rejection will often perform differently in terms of acceptance probability.

For this reason, we employ a adaptive strategy for the sampling. A final issue is that the acceptance probability is generally not available in closed form and costly to compute. Therefore, we approximate the distribution by a Normal distribution. For the von Mises distribution with mean direction μ and concentration κ, we can approximate it by a Normal distribution $N(\mu, \frac{1}{\kappa})$. If the approximated acceptance probability for direct rejection is smaller than some number, say 10%, we switch to the envelope rejection strategy.

.6 Prior independent of μ_0

In the Dirichlet Process, we have $\{\mu, \kappa\} \sim DP(\alpha P_0)$. The base measure P_0 is the conjugate prior for the von Mises distribution, that is

$$p(\mu, \kappa \mid \mu_0, R_0, n_0) \propto [I_0(\kappa)]^{-n_0} \exp\{R_0 \kappa \cos(\mu - \mu_0)\}. \tag{44}$$

As R_0 gets closer to n_0, more weight is given to higher κ, so more concentrated components, in the direction of μ_0. Note that the prior mean direction μ_0 is irrelevant if $R_0 = 0$, so a common prior undecided about μ_0 has $R_0 = 0, n_0 = 1$.

However, we would like to put prior mass on more concentrated components, while remaining undecided on μ_0. A prior with this property can be obtained by integrating out μ_0, which results in the prior

$$p(\mu, \kappa \mid R_0, n_0) \propto \int_0^{2\pi} [I_0(\kappa)]^{-n_0} \exp\{R_0 \kappa \cos(\mu - \mu_0)\} \, d\mu_0 = \frac{I_0(R_0 \kappa)}{I_0(\kappa)^{n_0}}. \tag{45}$$

This prior, however, will lead to heavily increased computational burden, because it is no longer conjugate.

To regain conjugacy, the sampler can be augmented by taking $\mu_0 \sim U(0, 2\pi)$, so $p(\mu_0) = 1/(2\pi)$. Then, sampling μ_0 each time, the base measure, averaged over μ_0, will be

$$\begin{aligned} E_{\mu_0}[p(\mu, \kappa \mid \mu_0, R_0, n_0)] &= \int_0^{2\pi} p(\mu, \kappa \mid \mu_0, R_0, n_0) p(\mu_0) d\mu_0 && (46) \\ &= \int_0^{2\pi} [I_0(\kappa)]^{-n_0} \exp\{R_0 \kappa \cos(\mu - \mu_0)\} \frac{1}{2\pi} d\mu_0 && (47) \\ &\propto p(\mu, \kappa \mid R_0, n_0). && (48) \end{aligned}$$

This last one is exactly as required. Therefore, the μ_0 can be simply randomly sampled uniformly over the circle in each iteration, and filled into the conjugate model.

An alternative is to marginalize the posterior summary statistics μ_n, R_n, m over the uniform distribution on μ_0. We obtain $E_{\mu_0}[\mu_n] = \bar{\theta}$, and $E_{\mu_0}[m] = n + n_0$, with R_n being the average distance of the points on a circle with center $(\sum_{i=1}^n \cos(\theta_i), \sum_{i=1}^n \sin(\theta_i))$ and radius R_0. This is given by

$$\begin{aligned} E_{\mu_0}[R_n] &= \frac{1}{2\pi} \int_0^{2\pi} \sqrt{R_0^2 + R^2 + 2 R_0 R \cos(t)} dt && (49) \\ &= \frac{2[R_0 + R]}{\pi} E_2\left(\frac{2\sqrt{R_0 R}}{R_0 + R}\right) && (50) \end{aligned}$$

where R is the resultant length of the data, and $E_2(\cdot)$ is the complete elliptic integral of the second kind. There is no closed form available for this last integral, but efficient algorithms are available.

A final option is introduce a data dependence in the prior by setting $\mu_0 = \bar{\theta}$ if there is data, and $\mu_0 \sim U[0, 2\pi)$ if there is not. This prior can be set in terms of posterior parameters μ_n, R_n, m because if $\mu_0 = \bar{\theta}$, we have $\mu_n = \bar{\theta}$, $R_n = R_0 + R$, and $m = n_0 + n$. The data dependence in this prior is sometimes seen as problematic in the Bayesian community (Darnieder, 2011), but the ease of use by setting this in the posterior parameters and conjugacy while allowing for more concentrated priors makes it an appealing alternative.

References

Abe, T., & Ley, C. (2017). A tractable, parsimonious and flexible model for cylindrical data, with applications. *Econometrics and Statistics*, *4*, 91–104.

Abe, T., Shimizu, K., & Pewsey, A. (2010). Symmetric unimodal models for directional data motivated by inverse stereographic projection. *Journal of the Japan Statistical Society*, *40*(1), 45–61.

Ajne, B. (1968). A simple test for uniformity of a circular distribution. *Biometrika*, *55*(2), 343–354.

Akaike, H. (1987). Factor analysis and aic. In *Selected papers of hirotugu akaike* (pp. 371–386). Springer.

Antoniak, C. E. (1974). Mixtures of Dirichlet processes with applications to Bayesian nonparametric problems. *The Annals of Statistics*, 1152–1174.

Ardia, D., Baştürk, N., Hoogerheide, L., & Van Dijk, H. K. (2012). A comparative study of monte carlo methods for efficient evaluation of marginal likelihood. *Computational Statistics & Data Analysis*, *56*(11), 3398–3414.

Arnold, B. C., & SenGupta, A. (2006). Recent advances in the analyses of directional data in ecological and environmental sciences. *Environmental and Ecological Statistics*, *13*(3), 253–256.

Artes, R. (2008). Hypothesis tests for covariance analysis models for circular data. *Communications in Statistics - Theory and Methods*, *37*(10), 1632–1640.

Ashby, M. P. J., & Bowers, K. J. (2013). A comparison of methods for temporal analysis of aoristic crime. *Crime Science*, *2*(1), 1.

Aslin, R. N. (2007). What's in a look? *Developmental Science*, *10*(1), 48–53.

Baayen, C., & Klugkist, I. (2014). Evaluating order-constrained hypotheses for circular data from a between-within subjects design. *Psychological Methods*, *19*(3), 398.

Baayen, C., Klugkist, I., & Mechsner, F. (2012). A test of order-constrained hypotheses for circular data with applications to human movement science. *Journal of Motor Behavior*, *44*(5), 351–363.

Bao, L., Gneiting, T., Grimit, E. P., Guttorp, P., & Raftery, A. E. (2010). Bias correction and Bayesian model averaging for ensemble forecasts of surface wind direction. *Monthly Weather Review*, *138*(5), 1811–1821.

Batschelet, E. (1981). Circular statistics in biology. *Academic Press, London*, *111*, 388.

Best, D. J., & Fisher, N. I. (1979). Efficient simulation of the von Mises distribution. *Applied Statistics*, *28*, 152–157.

Bhattacharya, S., & Sengupta, A. (2009). Bayesian analysis of semiparametric linear-circular models. *Journal of Agricultural, Biological, and Environmental Statistics*, *14*(1), 33–65.

Bhattacharya, S., & SenGupta, A. (2009). Bayesian inference for circular distributions with unknown normalising constants. *Journal of Statistical Planning and Inference*, *139*(12), 4179–4192.

Bhattacharyya, G. K., & Johnson, R. A. (1969). On hodges's bivariate sign test and a test for uniformity of a circular distribution. *Biometrika*, *56*(2), 446–449.

Bogdan, M., Bogdan, K., & Futschik, A. (2002). A data driven smooth test for circular uniformity. *Annals of the Institute of Statistical Mathematics*, *54*(1), 29–44.

Bowers, J., Morton, I., & Mould, G. (2000). Directional statistics of the wind and waves. *Applied Ocean Research*, *22*(1), 13–30.

Brazier, K. T. S. (1994). Confidence intervals from the rayleigh test. *Monthly Notices of the Royal Astronomical Society*, *268*(3), 709–712.

Brown, D. E. (1998). The regional crime analysis program (recap): a framework for mining data to catch criminals. In *Systems, man, and cybernetics, 1998. 1998 ieee international conference on* (Vol. 3, pp. 2848–2853).

Bulbert, M. W., Page, R. A., & Bernal, X. E. (2015). Danger comes from all fronts: predator-dependent escape tactics of túngara frogs. *PloS one*, *10*(4), e0120546.

Canty, A., & Ripley, B. D. (2017). boot: Bootstrap r (s-plus) functions [Computer software manual]. (R package version 1.3-20)

Carpenter, B., Gelman, A., Hoffman, M. D., Lee, D., Goodrich, B., Betancourt, M., ... Riddell, A. (2017). Stan: A probabilistic programming language. *Journal of Statistical Software*, *76*(1).

Chen, D.-G., Sun, J., & Peace, K. E. (2012). *Interval-censored time-to-event data: Methods and applications*. Chapman and Hall/CRC.

Chib, S. (1995). Marginal likelihood from the gibbs output. *Journal of the American Statistical Association*, *90*(432), 1313–1321.

Chib, S., & Greenberg, E. (1995). Understanding the metropolis-hastings algorithm. *The American Statistician*, *49*(4), 327–335.

Chib, S., & Greenberg, E. (2010). Additive cubic spline regression with Dirichlet process mixture errors. *Journal of Econometrics*, *156*(2), 322–336.

Coles, S. (1998). Inference for circular distributions and processes. *Statistics and Computing*, *8*(2), 105–113.

Consonni, G., Veronese, P., et al. (2008). Compatibility of prior specifications across linear models. *Statistical Science*, *23*(3), 332–353.

Damien, P., & Walker, S. (1999). A full Bayesian analysis of circular data using the von Mises distribution. *Canadian Journal of Statistics*, *27*(2), 291–298.

Darnieder, W. F. (2011). *Bayesian methods for data-dependent priors* (Unpublished doctoral dissertation). The Ohio State University.

Davison, A. C., & Hinkley, D. V. (1997). *Bootstrap methods and their applications*. Cambridge: Cambridge University Press. Retrieved from http://statwww.epfl.ch/davison/BMA/ (ISBN 0-521-57391-2)

Dickey, J. M., Lientz, B. P., et al. (1970). The weighted likelihood ratio, sharp hypotheses about chances, the order of a Markov chain. *The Annals of Mathematical Statistics*, *41*(1), 214–226.

Diebolt, J., & Ip, E. H. S. (1996). Stochastic EM: method and application. In *Markov chain Monte Carlo in practice* (pp. 259–273). Springer.

Di Marzio, M., Panzera, A., & Taylor, C. C. (2009). Local polynomial regression for circular predictors. *Statistics & Probability Letters*, *79*(19), 2066–2075.

Di Marzio, M., Panzera, A., & Taylor, C. C. (2013). Non-parametric regression for circular responses. *Scandinavian Journal of Statistics*, *40*(2), 238–255.

Doss, H. (1994). Bayesian nonparametric estimation for incomplete data via successive substitution sampling. *The Annals of Statistics*, 1763–1786.

Duan, J. A., Guindani, M., & Gelfand, A. E. (2007). Generalized spatial Dirichlet process models. *Biometrika*, *94*(4), 809–825.

Eddelbuettel, D., & François, R. (2011). Rcpp: Seamless R and C++ integration. *Journal of Statistical Software*, *40*(8), 1–18. Retrieved from http://www.jstatsoft.org/v40/i08/

Efron, B., & Tibshirani, R. J. (1994). *An introduction to the bootstrap*. CRC press.

Engbert, R., Trukenbrod, H. A., Barthelmé, S., & Wichmann, F. A. (2015). Spatial statistics and attentional dynamics in scene viewing. *Journal of Vision*, *15*(1), 14–14.

Everitt, B. S. (2004). Mixture distributions—i. *Encyclopedia of Statistical Sciences*, *7*.

Felson, M., & Poulsen, E. (2003). Simple indicators of crime by time of day. *International Journal of Forecasting*, *19*(4), 595–601.

Ferguson, T. S. (1973). A Bayesian analysis of some nonparametric problems. *The Annals of Statistics*, 209–230.

Fernández-Durán, J. J., & Mercedes Gregorio-Domínguez, M. (2016). Bayesian analysis of circular distributions based on non-negative trigonometric sums. *Journal of Statistical Computation and Simulation*, 1–13.

Ferrari, C. (2009). *The wrapping approach for circular data Bayesian modeling* (Unpublished doctoral dissertation).

Ferreira, J. T. A. S., Juárez, M. A., Steel, M. F. J., et al. (2008). Directional log-spline distributions. *Bayesian Analysis*, *3*(2), 297–316.

Fisher, N. I. (1995). *Statistical analysis of circular data*. Cambridge: Cambridge University Press.

Fisher, N. I., & Lee, A. J. (1992). Regression models for an angular response. *Biometrics*, 665–677.

Forbes, P. G. M., & Mardia, K. V. (2015). A fast algorithm for sampling from the posterior of a von Mises distribution. *Journal of Statistical Computation and Simulation*, *85*(13), 2693–2701.

Foulsham, T., Gray, A., Nasiopoulos, E., & Kingstone, A. (2013). Leftward biases in picture scanning and line bisection: A gaze-contingent window study. *Vision Research*, *78*, 14–25.

Foulsham, T., Kingstone, A., & Underwood, G. (2008). Turning the world around: Patterns in saccade direction vary with picture orientation. *Vision Research*, *48*(17), 1777–1790.

Friel, N., & Wyse, J. (2012). Estimating the evidence–a review. *Statistica Neerlandica*, *66*(3), 288–308.

Frühwirth-Schnatter, S. (2006). *Finite mixture and Markov switching models*. Springer Science & Business Media.

Gelfand, A. E., & Smith, A. F. M. (1990). Sampling-based approaches to calculating marginal densities. *Journal of the American Statistical Association*, *85*(410), 398–409.

Gelman, A., Carlin, J. B., Stern, H. S., & Rubin, D. B. (2003). *Bayesian data analysis*. CRC press.

Gelman, A., & Shalizi, C. R. (2013). Philosophy and the practice of Bayesian statistics. *British Journal of Mathematical and Statistical Psychology*, *66*(1), 8–38.

George, B. J., & Ghosh, K. (2006). A semiparametric Bayesian model for circular-linear regression. *Communications in Statistics: Simulation and Computation*, *35*(4), 911–923.

Geyer, C. J., & Thompson, E. A. (1992). Constrained monte carlo maximum likelihood for dependent data. *Journal of the Royal Statistical Society. Series B (Methodological)*, 657–699.

Ghosh, K., Jammalamadaka, R., & Tiwari, R. (2003). Semiparametric Bayesian techniques for problems in circular data. *Journal of Applied Statistics*, *30*(2), 145–161.

Gilks, W. R., Richardson, S., & Spiegelhalter, D. (1995). *Markov chain Monte Carlo in practice*. CRC press.

Gilks, W. R., & Wild, P. (1992). Adaptive rejection sampling for gibbs sampling. *Applied Statistics*, 337–348.

Gill, A., Partridge, H., & Newton, A. D. (2014). Interstitial crime analysis. *JDi Brief*.

Gill, J., & Hangartner, D. (2010). Circular data in political science and how to handle it. *Political Analysis*, *18*(3), 316–336.

Gottlieb, S., Arenberg, S. I., Singh, R., et al. (1994). *Crime analysis: From first report to final arrest*. Alpha Publishing Montclair, CA.

Gronau, Q. F., Sarafoglou, A., Matzke, D., Ly, A., Boehm, U., Marsman, M., ... Steingroever, H. (2017). A tutorial on bridge sampling. *Journal of Mathematical Psychology*, *81*, 80–97.

Grubesic, T. H., & Mack, E. A. (2008). Spatio-temporal interaction of urban crime. *Journal of Quantitative Criminology*, *24*(3), 285–306.

Gurtman, M. B. (2009). Exploring personality with the interpersonal circumplex. *Social and Personality Psychology Compass*, *3*(4), 601–619.

Gurtman, M. B., & Pincus, A. L. (2003). The circumplex model: Methods and research applications. *Handbook of Psychology*.

Guttorp, P., & Lockhart, R. A. (1988). Finding the location of a signal: A Bayesian analysis. *Journal of the American Statistical Association*, *83*(402), 322–330.

Hall, P., Watson, G. S., & Cabrera, J. (1987). Kernel density estimation with spherical data. *Biometrika*, *74*(4), 751–762.

Hastings, W. K. (1970). Monte Carlo sampling methods using Markov chains and their applications. *Biometrika*, *57*(1), 97–109.

Henderson, J. M. (2003). Human gaze control during real-world scene perception. *Trends in Cognitive Sciences*, *7*(11), 498–504.

Hermans, M., & Rasson, J. P. (1985). A new sobolev test for uniformity on the circle. *Biometrika*, *72*(3), 698–702.

Hernandez-Stumpfhauser, D., Breidt, F. J., & Opsomer, J. D. (2016). Hierarchical Bayesian small area estimation for circular data. *Canadian Journal of Statistics*, *44*(4), 416–430.

Hjort, N. L., Holmes, C., Müller, P., & Walker, S. G. (2010). *Bayesian nonparametrics* (Vol. 28). Cambridge University Press.

Hodges, J. L. (1955). A bivariate sign test. *The Annals of Mathematical Statistics*, *26*(3), 523–527.

Hoijtink, H. (2011). *Informative hypotheses: Theory and practice for behavioral and social scientists*. CRC Press.

Hoijtink, H., Klugkist, I., & Boelen, P. (2008). *Bayesian evaluation of informative hypotheses*. Springer Science & Business Media.

Holzmann, H., Munk, A., Suster, M., & Zucchini, W. (2006). Hidden Markov models for circular and linear-circular time series. *Environmental and Ecological Statistics*, *13*(3), 325–347.

Hornik, K., & Grün, B. (2013). On conjugate families and Jeffreys priors for von Mises–fisher distributions. *Journal of Statistical Planning and Inference*, *143*(5), 992–999.

Hornik, K., & Grün, B. (2014). movmf: An r package for fitting mixtures of von Mises-fisher distributions. *Journal of Statistical Software*, *58*(10), 1–31.

Itti, L., & Koch, C. (2001). Computational modelling of visual attention. *Nature Reviews Neuroscience*, *2*(3), 194–203.

J. Ross, G., & Markwick, D. (2018). dirichletprocess: Build Dirichlet process objects for Bayesian modelling [Computer software manual]. Retrieved from https://github.com/dm13450/dirichletprocess (R package version 0.2.1.900)

Jammalamadaka, S. R., & Sengupta, A. (2001). *Topics in circular statistics* (Vol. 5). World Scientific.

Jasra, A., Holmes, C. C., & Stephens, D. A. (2005). Markov chain Monte Carlo methods and the label switching problem in Bayesian mixture modeling. *Statistical Science*, 50–67.

Jeffreys, H. (1961). *Theory of probability*. Oxford: Clarendon Press.

Jones, M. C., & Pewsey, A. (2005). A family of symmetric distributions on the circle. *Journal of the American Statistical Association*, *100*(472), 1422–1428.

Jones, M. C., & Pewsey, A. (2012). Inverse Batschelet distributions for circular data. *Biometrics*, *68*(1), 183–193.

Kaas, A. L., & Van Mier, H. I. (2006). Haptic spatial matching in near peripersonal space. *Experimental Brain Research*, *170*(3), 403–413.

Kass, R. E., & Raftery, A. E. (1995). Bayes factors. *Journal of the American Statistical Association*, *90*(430), 773–795.

Kikuchi, G. (2015). Package 'aoristic'.

Klein, J. P., Van Houwelingen, H. C., Ibrahim, J. G., & Scheike, T. H. (2013). *Handbook of survival analysis*. Chapman and Hall/CRC.

Klugkist, I., Laudy, O., & Hoijtink, H. (2005). Inequality constrained analysis of variance: a Bayesian approach. *Psychological Methods*, *10*(4), 477.

Kuiper, N. H. (1960). Tests concerning random points on a circle. In *Indagationes mathematicae (proceedings)* (Vol. 63, pp. 38–47).

Lagona, F. (2016). Regression analysis of correlated circular data based on the multivariate von Mises distribution. *Environmental and Ecological Statistics*, *23*(1), 89–113.

Lagona, F., Picone, M., Maruotti, A., & Cosoli, S. (2015). A hidden Markov approach to the analysis of space–time environmental data with linear and circular components. *Stochastic Environmental Research and Risk Assessment*, *29*(2), 397–409.

Landler, L., Ruxton, G. D., & Malkemper, E. P. (2018). Circular data in biology: advice for effectively implementing statistical procedures. *Behavioral Ecology and Sociobiology*, *72*(8), 128.

Laubscher, N. F., & Rudolph, G. J. (1968). *A distribution arising from random points on the circumfence of a circle*. National Research Institute for Mathematical Sciences (South Africa).

Leary, T. (1957). *Interpersonal diagnosis of personality*. New York: Ronald Press.

Le Meur, O., & Coutrot, A. (2016). Introducing context-dependent and spatially-variant viewing biases in saccadic models. *Vision Research*, *121*, 72–84.

Liang, F., Paulo, R., Molina, G., Clyde, M. A., & Berger, J. O. (2012). Mixtures of g priors for Bayesian variable selection. *Journal of the American Statistical Association*.

Mardia, K. V. (2011). How new shape analysis and directional statistics are advancing modern life-sciences. In *Int. statistical inst.: Proc. 58th world statistical congress.*

Mardia, K. V., & El-Atoum, S. (1976). Bayesian inference for the von Mises-fisher distribution. *Biometrika*, *63*(1), 203–206.

Mardia, K. V., Hughes, G., Taylor, C. C., & Singh, H. (2008). A multivariate von Mises distribution with applications to bioinformatics. *Canadian Journal of Statistics*, *36*(1), 99–109.

Mardia, K. V., & Jupp, P. E. (1999). *Directional statistics*. New York: Wiley.

Mardia, K. V., & Jupp, P. E. (2000). *Directional statistics* (Vol. 494). John Wiley & Sons.

Mardia, K. V., & Voss, J. (2014). Some fundamental properties of a multivariate von Mises distribution. *Communications in Statistics-Theory and Methods*, *43*(6), 1132–1144.

Maruotti, A. (2016). Analyzing longitudinal circular data by Projected Normal models: a semi-parametric approach based on finite mixture models. *Environmental and Ecological Statistics*, 1–21.

McLachlan, G., & Peel, D. (2004). *Finite mixture models*. John Wiley & Sons.

McVinish, R., & Mengersen, K. (2008). Semiparametric Bayesian circular statistics. *Computational Statistics & Data Analysis*, *52*(10), 4722–4730.

Mechsner, F., Kerzel, D., Knoblich, G., & Prinz, W. (2001). Perceptual basis of bimanual coordination. *Nature*, *414*(6859), 69–73.

Mechsner, F., Stenneken, P., Cole, J., Aschersleben, G., & Prinz, W. (2007). Bimanual circling in deafferented patients: Evidence for a role of visual forward models. *Journal of neuropsychology*, *1*(2), 259–282.

Meng, X.-L., & Wong, W. H. (1996). Simulating ratios of normalizing constants via a simple identity: a theoretical exploration. *Statistica Sinica*, 831–860.

Metropolis, N., Rosenbluth, A. W., Rosenbluth, M. N., Teller, A. H., & Teller, E. (1953). Equation of state calculations by fast computing machines. *The Journal of Chemical Physics*, *21*(6), 1087–1092.

Morey, R. D., Romeijn, J.-W., & Rouder, J. N. (2013). The humble Bayesian: model checking from a fully Bayesian perspective. *British Journal of Mathematical and Statistical Psychology*, *66*(1), 68–75.

Najemnik, J., & Geisler, W. S. (2008). Eye movement statistics in humans are consistent with an optimal search strategy. *Journal of Vision*, *8*(3), 4–4.

Neal, R. M. (2000). Markov chain sampling methods for Dirichlet process mixture models. *Journal of Computational and Graphical Statistics*, *9*(2), 249–265.

Nelder, J. A., & Mead, R. (1965). A simplex method for function minimization. *The Computer Journal*, *7*(4), 308–313.

Newton, A. D., Partridge, H., & Gill, A. (2014). Above and below: measuring crime risk in and around underground mass transit systems. *Crime Science*, *3*(1), 1.

Nielsen, S. F., et al. (2000). The stochastic em algorithm: estimation and asymptotic results. *Bernoulli*, *6*(3), 457–489.

Nuñez-Antonio, G., Ausín, M. C., & Wiper, M. P. (2015). Bayesian nonparametric models of circular variables based on Dirichlet process mixtures of normal distributions. *Journal of Agricultural, Biological, and Environmental Statistics*, *20*(1), 47–64.

Nuñez-Antonio, G., & Gutiérrez-Peña, E. (2014). A Bayesian model for longitudinal circular data based on the Projected Normal distribution. *Computational Statistics & Data Analysis*, *71*, 506–519.

Nuñez-Antonio, G., Gutiérrez-Peña, E., & Escarela, G. (2011). A Bayesian regression model for circular data based on the Projected Normal distribution. *Statistical Modelling*, *11*(3), 185–201.

O'Hagan, A., & Forster, J. J. (2004). *Kendall's advanced theory of statistics, volume 2b: Bayesian inference* (Vol. 2). Arnold.

Oliveira, M., Crujeiras, R., & Rodríguez-Casal, A. (2014). Npcirc: An r package for nonparametric circular methods. *Journal of Statistical Software*, *61*(1), 1–26. Retrieved from https://www.jstatsoft.org/index.php/jss/article/view/v061i09 doi: 10.18637/jss.v061.i09

Oliveira, M., Crujeiras, R. M., & Rodríguez-Casal, A. (2012). A plug-in rule for bandwidth selection in circular density estimation. *Computational Statistics & Data Analysis*, *56*(12), 3898–3908.

Pereira, D. V., Andresen, M. A., & Mota, C. M. (2016). A temporal and spatial analysis of homicides. *Journal of Environmental Psychology*, *46*, 116–124.

Pewsey, A., Neuhäuser, M., & Ruxton, G. D. (2013). *Circular statistics in r*. Oxford University Press.

Pewsey, A., Shimizu, K., & de la Cruz, R. (2011). On an extension of the von Mises distribution due to Batschelet. *Journal of Applied Statistics*, *38*(5), 1073–1085.

Postma, A., Zuidhoek, S., Noordzij, M. L., & Kappers, A. M. L. (2008). Keep an eye on your hands: on the role of visual mechanisms in processing of haptic space. *Cognitive Processing*, *9*(1), 63–68.

Pycke, J.-R. (2010). Some tests for uniformity of circular distributions powerful against multimodal alternatives. *Canadian Journal of Statistics*, *38*(1), 80–96.

R Core Team. (2016). R: A language and environment for statistical computing [Computer software manual]. Vienna, Austria. Retrieved from https://www.R-project.org/

Rao, J. S. (1976). Some tests based on arc-lengths for the circle. *Sankhyā: The Indian Journal of Statistics, Series B*, 329–338.

Ratcliffe, J. H. (2000). Aoristic analysis: the spatial interpretation of unspecific temporal events. *International Journal of Geographical Information Science*, *14*(7), 669–679.

Ratcliffe, J. H., & McCullagh, M. J. (1998). Aoristic crime analysis. *International Journal of Geographical Information Science*, *12*(7), 751–764.

Ravindran, P., & Ghosh, S. K. (2011). Bayesian analysis of circular data using wrapped distributions. *Journal of Statistical Theory and Practice*, *5*(4), 547–561.

Rayment, M. R. (1995). Spatial and temporal crime analysis techniques. *Vancouver Police Department Technical Memorandum*.

Rayner, K. (2009). Eye movements and attention in reading, scene perception, and visual search. *The Quarterly Journal of Experimental Psychology*, *62*(8), 1457–1506.

Ren, L., Dunson, D. B., & Carin, L. (2008). The dynamic hierarchical Dirichlet process. In *Proceedings of the 25th international conference on machine learning* (pp. 824–831).

Richardson, S., & Green, P. J. (1997). On Bayesian analysis of mixtures with an unknown number of components (with discussion). *Journal of the Royal Statistical Society: series B (statistical methodology)*, *59*(4), 731–792.

Rueda, C., Fernández, M. A., & Peddada, S. D. (2009). Estimation of parameters subject to order restrictions on a circle with application to estimation of phase angles of cell cycle genes. *Journal of the American Statistical Association*, *104*(485), 338–347.

Schmidt-Koenig, K. (1963). On the role of the loft, the distance and site of release in pigeon homing (the" cross-loft experiment"). *The Biological Bulletin*, *125*(1), 154–164.

Schwarz, G., et al. (1978). Estimating the dimension of a model. *The Annals of Statistics*, *6*(2), 461–464.

Spiegelhalter, D. J., Best, N. G., Carlin, B. P., & Van Der Linde, A. (2002). Bayesian measures of model complexity and fit. *Journal of the Royal Statistical Society: Series B (Statistical Methodology)*, *64*(4), 583–639.

Stan Development Team. (2017). *Stan modeling language users guide and reference manual.* Retrieved from http://mc-stan.org/ (Version 2.17.0)

Stephens, M. (2000, January). Dealing with label switching in mixture models. *Journal of the Royal Statistical Society: Series B (Statistical Methodology)*, *62*(4), 795–809.

Stone, C. J., Hansen, M. H., Kooperberg, C., Truong, Y. K., et al. (1997). Polynomial splines and their tensor products in extended linear modeling: 1994 wald memorial lecture. *The Annals of Statistics*, *25*(4), 1371–1470.

Sun, J. (2007). *The statistical analysis of interval-censored failure time data.* Springer Science & Business Media.

Tanner, M. A., & Wong, W. H. (1987). The calculation of posterior distributions by data augmentation. *Journal of the American Statistical Association*, *82*(398), 528–540.

Tatler, B. W., Brockmole, J. R., & Carpenter, R. H. S. (2017). Latest: A model of saccadic decisions in space and time. *Psychological Review*, *124*(3), 267.

Tatler, B. W., & Vincent, B. T. (2009). The prominence of behavioural biases in eye guidance. *Visual Cognition*, *17*(6-7), 1029–1054.

Teh, Y. W., Jordan, M. I., Beal, M. J., & Blei, D. M. (2005). Sharing clusters among related groups: Hierarchical Dirichlet processes. In *Advances in neural information processing systems* (pp. 1385–1392).

Teicher, H. (1963). Identifiability of finite mixtures. *The Annals of Mathematical Statistics*, 1265–1269.

Turnbull, B. W. (1974). Nonparametric estimation of a survivorship function with doubly censored data. *Journal of the American Statistical Association*, *69*(345), 169–173.

Turnbull, B. W. (1976). The empirical distribution function with arbitrarily grouped, censored and truncated data. *Journal of the Royal Statistical Society. Series B (Methodological)*, 290–295.

Van Buuren, S. (2018). *Flexible imputation of missing data*. Chapman and Hall/CRC.

van Dijk, R., Kappers, A. M. L., & Postma, A. (2013). Superior spatial touch: improved haptic orientation processing in deaf individuals. *Experimental Brain Research*, *230*(3), 283–289.

Van Dyk, D. A., & Meng, X.-L. (2001). The art of data augmentation. *Journal of Computational and Graphical Statistics*, *10*(1), 1–50.

Van Renswoude, D. R., Johnson, S. P., Raijmakers, M. E. J., & Visser, I. (2016). Do infants have the horizontal bias? *Infant Behavior and Development*, *44*, 38–48.

Von Mises, R. (1918). Uber die ganzzahligkeit der atomgewichte und verwandte fragen. *Phys. Z*, *19*, 490–500.

Wagenmakers, E.-J., Lodewyckx, T., Kuriyal, H., & Grasman, R. (2010). Bayesian hypothesis testing for psychologists: A tutorial on the savage–dickey method. *Cognitive Psychology*, *60*(3), 158–189.

Wagenmakers, E.-J., & Waldorp, L. (2006). Editors' introduction. *Journal of Mathematical Psychology*, *50*(2), 99 - 100. Retrieved from http://www.sciencedirect.com/science/article/pii/S0022249606000022 (Special Issue on Model Selection: Theoretical Developments and Applications) doi: https://doi.org/10.1016/j.jmp.2005.01.005

Wang, F., & Gelfand, A. E. (2014). Modeling space and space-time directional data using projected gaussian processes. *Journal of the American Statistical Association*, *109*(508), 1565–1580.

Watanabe, S. (2010). Asymptotic equivalence of Bayes cross validation and widely applicable information criterion in singular learning theory. *Journal of Machine Learning Research*, *11*(Dec), 3571–3594.

Watson, G. S. (1961). Goodness-of-fit tests on a circle. *Biometrika*, *48*(1/2), 109–114.

Watson, G. S., & Williams, E. J. (1956). On the construction of significance tests on the circle and the sphere. *Biometrika*, *43*(3/4), 344–352.

Wetzels, R., Grasman, R. P. P. P., & Wagenmakers, E.-J. (2010). An encompassing prior generalization of the savage–dickey density ratio. *Computational Statistics & Data Analysis*, *54*(9), 2094–2102.

Zellner, A. (1986). Bayesian estimation and prediction using asymmetric loss functions. *Journal of the American Statistical Association*, *81*(394), 446–451.